Copyright
by
Rafael Eduardo Pérez Hernández
2020

The Thesis Committee for Rafael Eduardo Pérez Hernández
Certifies that this is the approved version of the following Thesis:

Simulations of Fluid Invasion During Fracturing in Unconventional Reservoirs

APPROVED BY
SUPERVISING COMMITTEE:

David DiCarlo, Supervisor

Kamy Sepehrnoori

Simulations of Fluid Invasion During Fracturing in Unconventional Reservoirs

by

Rafael Eduardo Pérez Hernández

Thesis

Presented to the Faculty of the Graduate School of
The University of Texas at Austin
in Partial Fulfillment
of the Requirements
for the Degree of

Master of Science in Engineering

The University of Texas at Austin
December 2020

Dedication

To my parents **Olga** and **Reyes**, my sisters **Lina** and **Paula**, my grandparents **Paulina** and **Fernando**, and my beloved wife **Alexandra.**

Acknowledgements

I would like to express my sincere gratitude to my supervisor Dr. David DiCarlo, his guidance and wisdom to conduct this research, as well as his confidence in my work were the fuel to complete this new stage in my life. Also, I am grateful for the priceless knowledge I received in his classes and in our work together these years. His patience and support are incomparable. My coach in Academia.

I am deeply grateful with Dr. Kamy Sepehrnoori, since the first days in PGE his guidance, enthusiasm and dedication to the students made me understand why we have the best graduated program in the world. Also, I want to say thank you for taking the time to be the reader of this thesis, a big privilege for me.

I do not have enough words for my wife Alexandra, her love always endorses and propels every project we start. Without her presence in my life, it would not be possible fulfil any goal. My eternal gratitude to the light of my life, my soulmate, the energy that moves every moment of my life, thank you (and Venecia) to be here to complete this dream.

Dr. Xiao Luo, I would like to thank you for your support during the master program. The knowledge and expertise in all the aspects of this thesis was a key factor to conduct and successfully finish this research.

The University of Texas at Austin, I only have words of gratitude. I am the happiest person in the world for this for this once in life opportunity. During these years at Austin I met extraordinary people that I would like to thank: Leo, Ruben, Camilo, Laura, and Javier only gratitude; Dr. Sarah Strigler her outstanding effort on writing class will never be forget, and Amy Stewart her work as graduated coordinator is indelible.

ECOPETROL S.A., thank you for believing in the people, and building the future of Colombian energy with knowledge and human development. Special thanks to the scholarship Committee and my leaders, John Alexander Pinto Góngora and Mauricio Orlando Herrera Polanía for making possible this dream.

Abstract

Simulations of Fluid Invasion During Fracturing in Unconventional Reservoirs

Rafael Eduardo Pérez Hernández, M.S.E.
The University of Texas at Austin, 2020

Supervisor: David DiCarlo

Unconventional reservoirs have become relevant as a new source of hydrocarbon reserves over the last years. The application hydraulic fracturing is needed to grant hydrocarbon production due to unconventional rocks lack of permeability. The fluids used in the fracturing leak-off into the rock matrix affecting potentially fracture geometry, and hydrocarbon production. Consequently, the understanding of fluid leak-off at laboratory and field scale is a key factor to choose the most suitable stimulation fluid. This work is divided in two parts: The first section is related to the simulation of the laboratory leak-off test behavior. The second section analyses reservoir fluid invasion phenomena, and the validation of previously proposed general leak-off model.

The first part of the thesis presents the simulation of the laboratory invasion test performed by Luo (2020), determining the key rock-fluid parameters like porosity, permeability, fluid properties and flow models that suit this specific porous media problem on the simulator. The simulation matching was performed over three different invasion cases: water, gas, and foam invasion (combination) using a 10 millidarcy core and considering two constant pressure boundary conditions at the injection and production sides. In the last part of the laboratory approach, the matched cases were run over permeability sensitivities to determined leak-off dependencies. Finally, the simulation results show a differing dependency for water ($k^{0.75}$), and gas cases ($k^{1.25}$), both diverging from the general leak off model statements ($k^{0.5}$).

The second part shows the leak-off reservoir approach, where the simulation parameters were set to mimic reservoir conditions. Three different invasion process were simulated in a 100 nanodarcy core including: gas invasion, water invasion, and foam invasion (combination). The results matched the expected square root of time behavior for all fluids stated in general leak-off model, differing from the linear behavior seen in the core gas invasion simulations. Moreover, several sensitivities were performed to understand the dependencies related to permeability, delta pressure, gas viscosity and oil compressibility, refuting the expected reservoir behavior explored in the general leak-off model. Finally, the sensitivities allow the determination of new corroborated proportionalities and suggested a more accurate model over the established reservoir conditions.

Table of Contents

List of Tables xii

List of Figures xiii

Chapter 1: Introduction 1

1.1. Problem statement 1

1.2. research objectives 2

1.3. Thesis Development 2

Chapter 2: Literature Review 4

Fluid Leak-off 4

2.1. Reservoir Zone Leak-off Approach 7

2.2. Leak-off Combined Mechanisms 8

2.3. General Leak-off Model 9

2.4. Newer Considerations 9

Chapter 3: Finite Core Invasion Test Simulation Matching 11

3.1. Laboratory Test Description 11

3.2. Simulation Process 15

3.2.1. Numerical Parameters 16

3.2.2. Reservoir Parameters 17

3.2.2.1. Wells 17

3.2.2.3. Fluid Properties 18

3.2.2.4. Porosity and Permeability 19

3.2.2.5. Rock-Fluid Interactions 19

3.3. Water Invasion Test Simulation 21

3.4. Gas Invasion Test Simulation 24
3.5. Foam Invasion Test Simulation (water and gas combination)................ 27
3.6. Summary 32
Chapter 4: Finite Core - Low to Ultra Low Permeability 33
4.1. Water Invasion Results 33
4.2. Gas Invasion Results 38
4.3. Foam Invasion Results 42
4.4. Leak-off Dependencies 45
4.5. Summary 48
Chapter 5: Reservoir Leak-off Simulation 49
5.1. Field Conditions 49
5.2. Core Scale Determination 50
5.3. Water Invasion 56
5.4. Gas Invasion 59
5.5. Foam Invasion (Combination) 62
5.6. Summary 66
Chapter 6: Semi-Infinite Core Leak-off Dependencies 68
6.1. Permeability Dependencies 68
6.2. Pressure Dependencies 74
6.2.1. Single Gas Invasion Viscosity Dependencies 82
6.2.2. Oil Compressibility Dependencies 84
6.3. Summarized leak-off dependencies 85
6.3.1. Single water Dependencies 87

        - 6.3.1.1. Permeability 87
        - 6.3.1.2. Pressure 88
        - 6.3.1.3. Oil compressibility 89
    - 6.3.2. Single Gas Dependencies..90
        - 6.3.2.1. Permeability 90
        - 6.3.2.2. Pressure 91
        - 6.3.2.3. Viscosity..92
        - 6.3.2.4. Oil compressibility 93
- 6.4. Summary..94

Chapter 7: Summary, Conclusions and Future Work 95

- 7.1. Summary..95
- 7.2. Conclusions...96
- 7.3. Future work..97

References...98

List of Tables

Table 1: Oil-Gas PVT properties. 18
Table 2: Water PVT properties. 19
Table 3: Finite core time and permeability dependencies. 48
Table 4: Semi-infinite core simulation parameters. 50
Table 5: Leak-off dependencies for combined (water and gas simultaneously) and single-phase invasion. For every injection case the following dependencies were determined: time, permeability, pressure, gas viscosity and oil compressibility. dependencies. 86

List of Figures

Figure 1: Experimental fluid los control curve for dynamic fluid-loss experiment (Williams, 1970). 6

Figure 2: Laboratory test Scheme: A) Single phase Invasion, B) Two phase Invasion (Luo, 2020). 12

Figure 3: Water Invasion into an oil-saturated core, the test was performed injecting water with a pressure of 620 psi in the pressurized core at 600 psi. The CT scan was used to measure fluid saturation at 4.25, 21.03, 30.42, 50.33, 70.25, and 118 minutes after the test started. The experimental results: A) Shows a pressure drop averaging 20 psi along the test validating the constant pressure displacement, B) Shows saturation profile measured with the CT scan to determine the fluid invasion length along the test (Luo, 2020). 13

Figure 4: Gas Invasion into an oil-saturated core, the test was performed injecting gas with a pressure of 620 psi in the pressurized core at 600 psi. The CT scan was used to measure fluid saturation at 1.75, 7.58, 14.75, 20.75, 27.23, and 32.33 minutes after the test started. The experimental results: A) Shows a pressure drop averaging 20 psi along the test validating the constant pressure displacement, B) Shows saturation profile measured with the CT scan to determine the fluid invasion length along the test (Luo, 2020). 13

Figure 5: Foam Invasion into an oil-saturated core, the test was performed injecting foam (gas and water combination) with a pressure of 650 psi in the pressurized core at 600 psi. The CT scan was used to measure fluid saturations at 5, 16, 27.5, 40, and 60 minutes after the test started. The experimental results: A) Shows a pressure drop averaging 50 psi along the test validating the constant pressure displacement, B) Shows saturation water profile measured with the CT scan to determine the fluid invasion length along the test, C) Shows gas saturation profile measured with the CT scan to determine the fluid invasion length along the test (Luo, 2020). 14

Figure 6: Dimensional model. Finite core test simulation. 16

Figure 7: Finite core Pressure-Temperature boundary conditions. Injection pressure: 620 psi (single water or gas invasion), 650 psi (simultaneous water and gas invasion). Constant 80°F temperature along the 10 md 28 centimeters core. 18

Figure 8: Simulated oil-water relative permeability curve. 20

Figure 9: Simulated gas-oil relative permeability curve. 20

Figure 10: Three-phase isoperms used in the foam (combination) simulation. 21

Figure 11: Laboratory water saturation profile. Simulated water Profile (left), Measured water-profile (right) (Luo, 2020). Single water invasion simulated test. 22

Figure 12: Cumulative water Invasion vs Time. Simulated Cumulative water (left), Measured Cum Water (right) (Luo, 2020). Single water invasion simulated test. 22

Figure 13: Water pressure profile. Single water invasion simulated on 10md; initial pressure of 600 psi. The water was injected at constant pressure of 620 psi along the simulated invasion. The shown values were picked at a simulated time of 30, 60 and 120 minutes. 23

Figure 14: Laboratory gas saturation profile. Simulated gas profile (left), Measured gas profile (right) (Luo, 2020). 25

Figure 15: Laboratory gas invaded volume vs time. Simulated gas invaded volume (left), Measured gas invaded volume (right) (Luo, 2020). 25

Figure 16: Gas pressure profile. Single gas invasion simulated on 10md; initial pressure of 600 psi. The gas was injected at constant pressure of 620 psi along the simulated invasion. The shown values were picked at a simulated time of 30, 60, and 120 minutes. 26

Figure 17: Laboratory water saturation profile. A) Simulated water combined profile, B) Measured water combined profile (Luo, 2020). 28

Figure 18: Laboratory gas saturation profile. A) Simulated gas combined profile, B) Measured gas combined profile (Luo, 2020). 28

Figure 19: Cumulative volumes. Water cumulative volume comparison between single invasion and foam invasion. Simultaneous gas and water invasion (foam) simulation on 10 md core. Injection pressure 650 psi, reservoir pressure 600 psi. Volume at reservoir conditions. 29

Figure 20: Cumulative volumes. Gas cumulative volume comparison between single invasion and foam invasion. Simultaneous gas and water invasion (foam) simulation on 10md core. Injection pressure 650 psi, reservoir pressure 600 psi. Volume at reservoir conditions. 29

Figure 21: Foam pressure profiles. Simultaneous gas and water invasion (foam) simulated on 10md core; initial pressure of 600 psi. The gas and water were injected at constant pressure of 650 psi along the simulated invasion. The shown values were pick at a simulated time of 15, 30, and 60 minutes. 30

Figure 22: Water saturation profiles. Single water invasion simulated on 10md (top) and 1md (bottom) core; initial pressure of 600 psi. The water was injected at constant pressure of 620 psi along the simulated invasion. The shown values were pick at a simulated time of 30, 70 and 118 minutes. 34

Figure 23: Water Pressure profiles. Single water invasion simulated on 10md (top) and 1md (bottom) core; initial pressure of 600 psi. The water was injected at constant pressure of 620 psi along the simulated invasion. The shown values were pick at a simulated time of 30, 60 and 120 minutes. 35

Figure 24: Cumulative volumes. Single water invasion simulated on 10md (top left), 1md (top right), 10µd (bottom left) and 100nd (bottom right) cores; initial pressure of 600 psi. The water was injected at constant pressure of 620 psi along the simulated invasion. The simulated invasion time was 120 minutes. 36

Figure 25: Gas saturation profiles. Single water invasion simulated on 10md (top) and 1md cores (bottom); initial pressure 600 psi. The gas was injected at constant pressure of 620 psi along the simulated invasion. The shown values were pick at a simulated time of 8, 21 and 33 minutes.....................38

Figure 26: Gas pressure profiles. Single gas invasion simulated on 10md (top) and 1md core (bottom); initial pressure of 600 psi. The gas was injected at constant pressure of 620 psi along the simulated invasion. The shown values were pick at a simulated time of 30, 60 and 120 minutes..................39

Figure 27: Cumulative gas volumes. Single gas invasion simulated on 10md, 1md, 10μd and 100nd cores; initial pressure of 600 psi. The gas was injected at constant pressure of 620 psi along the simulated invasion. The total simulated invasion time was 120 minutes. 40

Figure 28: Cumulative water volumes. Simultaneous water and gas invasion simulated on 10md, 1md, 10μd and 100nd cores; initial pressure of 600 psi. The water fluids were injected at constant pressure of 650 psi along the simulated invasion. The simulated invasion time was 120 minutes. 42

Figure 29: Cumulative water volumes. Simultaneous water and gas invasion simulated on 10md, 1md, 10μd and 100nd cores; initial pressure of 600 psi. The water fluids were injected at constant pressure of 650 psi along the simulated invasion. The simulated invasion time was 120 minutes. 43

Figure 30: Invasion length versus Permeability plot. Single gas invasion, water invasion, and simultaneous water and gas invasion were simulated in a 10md to 100nd cores with initial pressure of 600 psi. The fluids were injected at constant pressure of 620 psi (single invasion), and 650 psi (combined invasion) along the simulated invasion. The show values were pick at a simulated time of 10 minutes..45

Figure 31: Invasion length versus Permeability plot. Single gas invasion, water invasion, and simultaneous water and gas invasion were simulated in a 10md to 100nd cores with an initial pressure of 600 psi. The fluids were injected at constant pressure of 620 psi (single invasion), and 650 psi (combined invasion) along the simulated invasion. The show values were pick at a simulated time of 10 minutes..46

Figure 32: One dimensional semi-infinite problem. Schematic representation of the time dependent problem...50

Figure 33: Semi-infinite behavior core lengths. Needed Core lengths for permeabilities ranging from 10md to 100nd cores were found using penetration thickness equation...54

Figure 34: Analytical versus numerical solution for one phase problem. Numerical and analytical solution profiles are compared at 10, 60, and 90 minutes on a 100 nanodarcy 20 centimeters reservoir. Injection pressure: 4,500 psi, reservoir pressure 3,000 psi...55

Figure 35: Water Saturation and pressure profiles. One-centimeter zooms over single water invasion simulated in a 100nd reservoir; initial pressure of 3,000 psi. The water was injected at constant pressure of 4,500 psi along the simulated invasion. The shown values were pick at a simulated time of 10, 30, 60 and 120 minutes..56

Figure 36: Pressure profile. Single water invasion simulation; 20 centimeters 100 nD reservoir. Injection pressure 4,500 psi, reservoir pressure 3,000 psi. The shown values were pick at a simulated time of 10, 30, 60 and 120 minutes...57

Figure 37: Water cumulative invaded volume. Single water invasion simulation on 100nd reservoir. Injection pressure 4,500 psi, reservoir pressure 3,000 psi. Volume at reservoir conditions. 58

Figure 38: Gas Saturation and pressure profiles. One-centimeter zooms over single gas invasion simulated in a 100nd reservoir; initial pressure of 3,000 psi. The gas was injected at constant pressure of 4,500 psi along the simulated invasion. The shown values were pick at a simulated time of 10, 30, 60 and 120 minutes. 59

Figure 39: Gas pressure profile. Single gas invasion simulation; 20 centimeters 100 nD core. Injection pressure 4,500 psi, reservoir pressure 3,000 psi. The shown values were pick at a simulated time of 5, 10, 30, 60 and 120 minutes. 60

Figure 40: Gas cumulative volume. Single gas invasion simulation on 100nd core. Injection pressure 4,500 psi, reservoir pressure 3,000 psi. Volume at reservoir conditions. 61

Figure 41: Pressure profile. Simultaneous gas and water invasion simulation; 20 centimeters 100 nD core. Injection pressure 4,500 psi, reservoir pressure 3,000 psi. The shown values were pick at a simulated time of 5, 10, 30, 60 and 120 minutes. 62

Figure 42: Water Saturation and pressure profiles. One-centimeter zooms over water phase on simultaneous gas and water invasion simulation; 20 centimeters 100 nD core. Injection pressure 4,500 psi, reservoir pressure 3,000 psi. The shown values were pick at a simulated time of 5, 10, 30, 60 and 120 minutes. 63

Figure 43: Gas saturation and pressure profiles. One-centimeter zooms over gas phase on simultaneous gas and water invasion simulation; 20 centimeters 100 nD core. Injection pressure 4,500 psi, reservoir pressure 3,000 psi. The shown values were pick at a simulated time of 5, 10, 30, 60 and 120 minutes. 64

Figure 44: Cumulative volumes. Water cumulative volume comparison between single invasion and combined invasion. Simultaneous gas and water invasion (combined) simulation on 100nd core. Injection pressure 4,500 psi, reservoir pressure 3,000 psi. Volume at reservoir conditions. 65

Figure 45: Cumulative volumes. Gas cumulative volume comparison between single invasion and combined invasion. Simultaneous gas and water invasion (combined) simulation on 100nd core. Injection pressure 4,500 psi, reservoir pressure 3,000 psi. Volume at reservoir conditions. 65

Figure 46: Cumulative volumes versus time plots. Single water invasion (top left), single gas invasion (top right), and simultaneous water and gas invasion (bottom row) were simulated in semi-infinite 10md to 100nd cores with initial pressure of 3,000 psi. The fluids were injected at constant pressure of 4,500 psi along the simulated invasion. The total simulated time was 120 minutes. Volumes at reservoir condition. 69

Figure 47: Invasion length versus time plots. Single water invasion (top left), single gas invasion (top right), and simultaneous water and gas invasion (bottom row) were simulated in semi-infinite 10md to 100nd cores with initial pressure of 3,000 psi. The fluids were injected at constant pressure of 4,500 psi along the simulated invasion. The total simulated time was 120 minutes. 70

Figure 48: Invasion length vs sqrt of time plot. Single water invasion (top left), single gas invasion (top right), and simultaneous water and gas invasion (bottom row) were simulated in semi-infinite 10md to 100nd cores with initial pressure of 3,000 psi. The fluids were injected at constant pressure of 4,500 psi along the simulated invasion. The total simulated time was 120 minutes. 71

Figure 49: Invasion length versus Permeability plot. Single gas invasion, water invasion, and simultaneous water and gas invasion were simulated in a semi-infinite 10md to 100nd cores with initial pressure of 3,000 psi. The fluids were injected at constant pressure of 4,500 psi along the simulated invasion. The show values were pick at a simulated time of 60 minutes. 72

Figure 50: Cumulative volumes versus time plots. Single water invasion (top left), single gas invasion (top right), and simultaneous water and gas invasion (bottom row) were simulated in semi-infinite 100nd core with an initial pressure of 3,000 psi. The fluids were injected at constant pressure varying from 3,250 psi to 5,500 psi along the simulated invasions. The total simulated time was 120 minutes. Volumes at reservoir condition. 75

Figure 51: Invasion length versus time plots. Single water invasion (top left), single gas invasion (top right), and simultaneous water and gas invasion (bottom row) were simulated in semi-infinite 100nd core with an initial pressure of 3,000 psi. The fluids were injected at constant pressure varying from 3,250 psi to 5,500 psi along the simulated invasions. The total simulated time was 120 minutes. 76

Figure 52: Invasion length versus square root of time plots. Single gas invasion, water invasion, and simultaneous water and gas invasion were simulated in a semi-infinite 100nd core with an initial pressure of 3,000 psi. The fluids were injected at constant pressure varying from 3,250 psi to 4,500 psi along the simulated invasion. The show values were pick at a simulated time of 60 minutes. 77

Figure 53: Invasion length versus delta pressure. Oil invasion, Single gas invasion, single water invasion, and simultaneous water and gas invasion were simulated in a semi-infinite 100nd core with 3,000 psi of initial pressure. The fluids were injected at constant delta pressure varying from 3,250 psi to 4,500 psi along the simulated invasion. The show values were pick at a simulated time of 60 minutes. 78

Figure 54: Invasion length versus pressure plot for gas viscosity sensitivity. Gas invasion was simulated in a semi-infinite 100nd core with 3,000 psi of initial pressure, varying gas viscosity form 0.0002 cp to 0.2 cp. The fluid was injected at constant pressure of 3250 psi to 4,500 psi along the simulated invasions. The show values were pick at a simulated time of 60 minutes. 79

Figure 55: Invasion length versus gas viscosity plot. Gas invasion was simulated in a 100nd reservoir with 3,000 psi of initial pressure varying gas viscosity form 0.0002 cp to 0.5 cp. The fluid was injected at constant pressure of 4,500 psi along the simulated invasion. The shown values were pick at a simulated time of 30, 60, 90 and 120 minutes. 82

Figure 56: Invasion length versus Oil Compressibility plot. Oil invasion, Single gas invasion and water invasion were simulated in a semi-infinite 100nd core with 3,000 psi of initial pressure. The fluids were injected at constant pressure of 4,500 psi along the simulated invasion. The shown values were pick at a simulated time of 60 minutes. 84

Figure 57: Invasion length versus time plot. Single simulated and calculated (using $k0.5$ dependency) water invasion profiles for 1md, 10μd, and 100nd (baseline case) cores with 3,000 psi of initial pressure. The fluids were injected at constant pressure of 4,500 psi along the simulated invasion. The total simulated versus calculated time was 120 minutes. 87

Figure 58: Invasion length versus time plot. Single simulated and calculated (using $p0.75$ dependency) water invasion profiles for 100nd cores with 3,000 psi of initial pressure. The fluids were injected at constant pressures of 3500 psi, 4,500 psi (baseline case), and 5500 psi, along the simulated invasion. The total simulated versus calculated time was 120 minutes.........88

Figure 59: Invasion length versus time plot. Single simulated and calculated (using $Co0.2$ dependency) water invasion profiles for 100nd cores with 3,000 psi of initial pressure. The fluids were injected at a constant pressures 4,500 psi, for 0.00002, 0.00003 (baseline), and 0.00005 $psi-1$ along the simulated invasion. The total simulated versus calculated time was 120 minutes...89

Figure 60: Invasion length versus time plot. Single simulated and calculated (using $k0.5$ dependency) gas invasion profiles for 1md, 10µd, and 100nd (baseline case) cores with 3,000 psi of initial pressure. The fluids were injected at constant pressure of 4,500 psi along the simulated invasion. The total simulated versus calculated time was 120 minutes. 90

Figure 61: Invasion length versus time plot. Single simulated and calculated (using $p0.94$ dependency) gas invasion profiles for 100nd cores with 3,000 psi of initial pressure. The fluids were injected at constant pressures of 3500 psi, 4,500 psi (baseline case), and 5500 psi, along the simulated invasion. The total simulated versus calculated time was 120 minutes........91

Figure 62: Invasion length versus time plot. Single simulated and calculated (using $\mu g0.13$ dependency) gas invasion profiles for 100nd cores with 3,000 psi of initial pressure. The fluids were injected at a constant pressures 4,500 psi, for 0.002, 0.02 (baseline), and 0.2 centipoises along the simulated invasion. The total simulated versus calculated time was 120 minutes...92

Figure 63: Invasion length versus time plot. Single simulated and calculated (using $Co0.2$ dependency) gas invasion profiles for 100nd cores with 3,000 psi of initial pressure. The fluids were injected at a constant pressures 4,500 psi, for 0.00002, 0.00003 (baseline), and 0.00005 $psi - 1$ along the simulated invasion. The total simulated versus calculated time was 120 minutes...93

Chapter 1: Introduction

1.1. PROBLEM STATEMENT

Unconventional reservoirs have become relevant as a new source of hydrocarbon reserves over the last years because off the need generated by the growing energy demand. IEA (2020) forecasts an average of one million barrels per year consumption growing to year 2025. Because the world´s declining oil rate, it is necessary the average addition of 20 million barrels of incremental oil production year to year to fulfill world requirements. The big declines of conventional reservoirs posted by countries like Venezuela, Colombia, the UK, Russia, Egypt, Nigeria, and Angola show the need to develop unconventional reservoirs even with the demanding challenge they represent.

Ilk (2011) said the term unconventional is related to the complexity to characterize, describe, and produce oil, due to permeability principally ranges from low to ultra-low values on those reservoir systems. Therefore, the application of well stimulation operations like hydraulic fracturing is needed to grant hydrocarbon production. The fluid used to generate the fracture also results in fluid invasion (leak-off) into the rock matrix affecting potentially fracture geometry, and hydrocarbon permeability (Luo, 2020). Consequently, the understanding of fluid leak-off behavior at laboratory, and field scale is a key factor to choose the stimulation fluid that improves oil production.

Numerical simulation is the most feasible approach, considering the complexity of an analytical solution that will include the key aspects affecting fluid invasion in unconventional reservoirs, and because of the current laboratory limitations recreate real reservoir conditions also. Earlier work developed by Luo (2020) supports the first step on reservoir simulation simplest model and opens the door for a broader study of reservoir scale phenomenon.

1.2. RESEARCH OBJECTIVES

- Replicating laboratory core displacement test by numerical simulation to extrapolate the process on ultra-low permeabilities.
- Defining field case parameters to simulate numerically fluid invasion phenomena at reservoir conditions.
- Validating classical model leak-off coefficient dependencies at low and ultra-low permeability reservoir conditions using numerical simulation.

1.3. THESIS DEVELOPMENT

This work is organized in seven chapters. Chapters 3-4 are fully focused to finite core invasion displacement simulation and permeability proportionality analyses. Chapter 5-6 focus on reservoir like behavior, and how leak off volumes depend on permeability, delta pressure, gas viscosity, and oil compressibility dependencies. Finally, Chapter 7 review this work, highlights the main conclusions, and opens the door to further research approaches.

In Chapter 3, I attempt to model the results obtained in the laboratory test using a numerical simulator as a starting point to extrapolate this process at reservoir conditions. The numerical simulator is a powerful tool to manage time related issues; low to ultra-low permeability core laboratory displacement tests require huge amount of time (sometimes months), and also size problems related with the cores dimensions, and the devices used to run the tests (maximum allowed core length 2-4 feet).

In Chapter 4, simulation was used to extrapolate the results from the laboratory 10 millidarcy permeability rock to the ultra-low permeability rocks of the field of 100 nanodarcy. This process was performed in 3 new numerical cores of: 1 millidarcy, 10 microdarcy, and 100 nanodarcy. Those magnitudes were chosen, assuming the square root of permeability dependency stated in the general leak-off model drives the fluid invasion permeability correlation. The permeability approach was executed for the three fluid invasion cases: water invasion, gas invasion, and foam invasion (combination), keeping constant fluid properties, boundary conditions and other reservoir parameters listed earlier. The simulation shows the behavior of fluid leak-off in ultra-low permeabilities avoiding long time laboratory fluid invasion tests.

In Chapter 5, I attempt to simulate the behavior of fluid leak-off during fracturing operations. The preset boundary conditions will chance to perform an accurate simulation over fluid invasion phenomena in the field. Rock properties and rock fluid interaction remain constant to extrapolate the numerical core properties on a field scale case. Once again low to ultra-low permeabilities vary form 10 md to 100 nD, which are representative magnitudes for unconventional reservoirs. Therefore, the main goal of this chapter is to generate a numerical simulation at reservoir conditions, which corroborate the dependencies assumed in the general leak model under similar assumptions and parameters addressing the 100nD reservoir case.

In Chapter 6, I use the numerical model to understand how permeability, delta pressure, gas viscosity, and oil compressibility affect the leak-off rate in semi-infinite rectilinear flow. Some of those parameters were studied in previous chapters but here I focus my effort to validate the listed dependencies under the reservoir boundary conditions embodied in the semi-infinite core simulations. The goal of this chapter is to find the proper dependencies that describe fluid leak-off behavior at reservoir conditions devising new paths that aim future research on this topic.

Chapter 2: Literature Review

FLUID LEAK-OFF

When fracturing fluid is injected into the subsurface, besides creating fractures, some of the fluid is lost into the formation. The forces driving the fracturing fluid movement into the formation is the over pressure of the fluid and the capillary forces that attract the wetting fluid into the formation. Washburn (1921) studied the dynamics of capillary flow, and stated one of the first approaches on the invasion of fluids in porous media postulating the following equation [2.1] (being η; viscosity, and k; a variable independent of the nature of the liquid), in which he determined the volume that penetrates an array of capillary tubes with constant pressure drive behind the fluid penetration. He associated this dependency to a concept called *Penetration Coefficient*. Even when this relationship was valid for his laboratory test arrangement, it presented an early interpretation of the invasion fluid phenomenon in porous media, treated more in detail in the developing of the conventional leak-off model.

$$V = k\left(\frac{t}{\eta}\right)^{\frac{1}{2}} \qquad [2.1]$$

The formal study of fluid invasion in the reservoir was initially conducted and bounded by Howard & Fast (1957). They performed the primary studies of leak-off, and leak-off coefficient, which is a phenomenon occurring in drilling and/or fracturing operations when the fluid used, is lost into the formation or into the porous media. They developed the first filtrate equation, which is validated for three separate leak-off processes: *Displacement and compressibility of reservoir fluid*, *Invasion of the formation by filtrate or fracturing fluid*, *Buildup of an external filter cake.*

$$V_{inv} = AC\sqrt{t} \qquad [2.2]$$

A is the cross-sectional area, and C, known as fracturing fluid coefficient, will be known later as leak-off coefficient. As it can be seen, the fluid invasion equation [2.2] showed a proportional relationship to the square root of time. Furthermore, this condition applies to the three leak-off processes mentioned priorly.

In addition to Howard and Fast, Hall & Dollarhide (1964) designed a test to demonstrate that the fracturing fluid loss in dynamic conditions behaved proportional to time, differing from the accepted assumption of the square root of time dependency. Using several kerosene based fracturing fluids concluded the fluid-loss was proportional to shear rate and showed the first ideas on permeability and pressure dependencies. A broader work on fluids loss behavior was presented later when they applied the dynamic test to oil and water based fracturing fluids, concluding the relevance in the designing, and the selection of fluid loss control agents that favor fracture geometry, and optimize operational cost (Hall & Dollarhide, 1968).

On the other hand, Williams (1970) rather than considering leak-off as three different process, introduced the idea of treating fluid invasion in three periods of time. The first period is related to the time before cake is formed, in this period the invasion is governed by the formation flow resistance to the fracturing fluid. In the second period, the cake is generated due to the deposition effect. Finally, in the third period, no more fracturing fluid is deposited due to the high-velocity fluid in the fracture. Williams called this period: *dynamic leak-off*, grouping the earlier two stages on a quantity named *spurt volume.* Figure 1 resumes the work proposed by Williams.

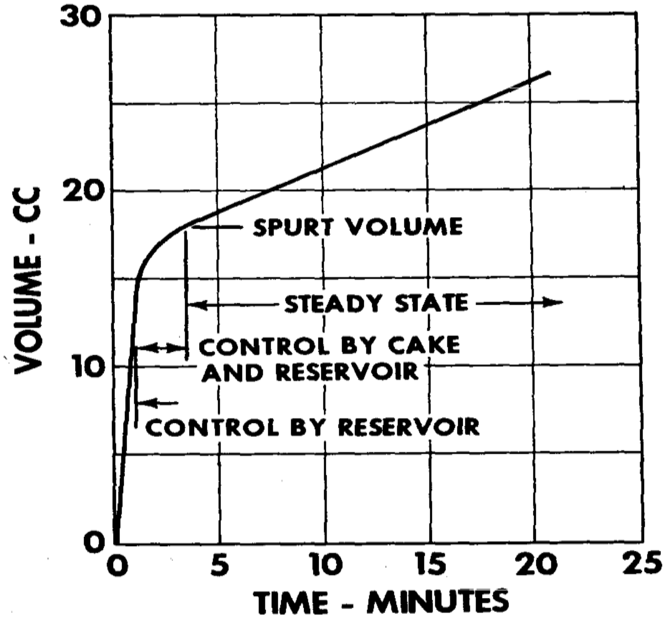

Figure 1: Experimental fluid los control curve for dynamic fluid-loss experiment (Williams, 1970).

Later, Gulbis (1984) performed a comparative study between dynamic, and static fluid-lost test with water-based fracturing fluid on low permeability cores. Using a similar arrangement as Williams, determined both test (static, and dynamic) tended to behave similar after 2 hours of run. Prior assumption applied only on low permeability cores where fluid-loss velocity remained constant. On the other hand, in the case of high permeability cores, Gulbis observed that the velocity decreased with time, making test homologation not possible for this permeability scenario. The effect of pressure drop was analyzed shallowly for both permeability cases, showing a fuzzy proportionality. Even when similar behaviors where expected for different permeability scales of magnitude, the experiment demonstrated a discontinuity on small scale cases.

Simultaneously, Settari (1984), proposed one of the deepest and broadest analyses on leak-off concepts, and classical leak-off modelling review developing a strong base framework on this topic. On this work showed a clear way to simulate the effect of hydraulic fracturing on three dimensions, considering the three mechanisms that take place on hydraulic fracturing fluid leak-off, occurring externally on high permeability rocks, or internally in low permeability ones. Finally, they summarize earlier works, and proposed a widely accepted new interpretation on fluid leak-off phenomenon theory and applications.

2.1. Reservoir Zone Leak-off Approach

Reservoir region lacks fracturing fluid content but require the influence of pressure to displace the fluids that saturate the reservoir away from fracture face. Economides & Nolte (2000) argued the following conditions to formulate a model that fit the physics over this phenomenon:

- Constant pressure drops Δp_c between the reservoir interface and the far-field reservoir.
- Compressible flow with constant total compressibility C_t.
- Slow movement of the front of the invading fluid.
- An infinite reservoir.

The analytical solution for this case is taken from (Collins, 1961), where the relationship in equation [2.3] has been developed:

$$u_L = \frac{C_c}{\sqrt{t}} \qquad [2.3]$$

Compressibility control leak-off coefficient in equation [2.4] has the following functional form with: k_r; reservoir permeability, μ_r; Reservoir fluid viscosity, and C_t; total compressibility:

$$C_c = \sqrt{\frac{k_r C_t \phi}{\pi \mu_r}} \Delta p_c \qquad [2.4]$$

2.2. Leak-off Combined Mechanisms

In addition to the reservoir zone leak-off, cake and filter cake leak-off mechanisms affect field operations. The three leak-off mechanisms occur simultaneously and can be modelled introducing: C_t; Total leak-off coefficient, which is defined considering the leak-off velocities must be equal for every case providing the equality in equation [2.5](Economides & Nolte, 2000):

$$\frac{C_t}{\sqrt{t}} = \sqrt{\frac{k_{cake} \alpha \Delta p_{cake}}{2\mu_{fil}(t - t_{sp})}} = \sqrt{\frac{k_{fil} \phi \Delta p_v}{2\mu_{fil} t}} = \sqrt{\frac{k_r C_t \phi}{\pi \mu_r t}} \Delta p_c \qquad [2.5]$$

Total Pressure drop Δp_{total} is the result of each pressure perturbation along the three different flow regions, which is also the pressure difference between fracturing pressure, and far reservoir pressure as follows in equation [2.6]:

$$\Delta p_{cake} + \Delta p_v + \Delta p_c = \Delta p_{total} \qquad [2.6]$$

As a further matter, Williams et al. (1979) neglected spurt volume and time, presenting C_t; total leak-off coefficient as combination of the three-control leak-off coefficient parameters, considering the cake independent of pressure as shown in equation [2.7].

$$C_t = C_{wcv} = \frac{2C_cC_vC_w}{C_vC_w+\sqrt{C_w^2C_v^2+4C_c^2(C_v^2+C_w^2)}} \qquad [2.7].$$

When the cake is highly pressure sensitive, this equation must be altered, and takes the following functional form presented in equation [2.8] (Economides & Nolte, 2000):

$$C_t = C_{cv} = \frac{2C_cC_v}{C_v+\sqrt{C_v^2+4C_c^2}} \qquad [2.8]$$

2.3. General Leak-off Model

In order to develop a general functional form to deal with the complexity of fluid leak-off phenomena like: the compressibility of the invading fluids, pressure dependency, and the volume previously leaked-off into the reservoir, Settari (1985) proposed equation [2.9] for filter cake region, which describes a new leak-off coefficient parameter avoiding reservoir zone leak-off effect.

$$\overline{C_v} = \frac{2C_v^2\sqrt{t}}{V_L} \qquad [2.9]$$

The equation proposed for cake region is the following:

$$\overline{C_w} = \frac{2C_w^2\sqrt{t}}{V_L} \qquad (2.18)$$

2.4. Newer Considerations

Ultimately, the study of the neglected reservoir zone leak-off effect is brought back to research scene by Luo (2020), who demonstrated in the laboratory that the behavior of fluid leak-off in reservoir region deviated from general assumptions made in the classic leak-off model. Actually when the classical model is independent of the nature of the fluids (liquid, gas or both), laboratory results taken from the low permeability core confirmed fluid leak-of is not well described using square root of time dependency in the case of gas invasion. This contradiction to the classical leak-model open the door for a broader research in unconventional reservoirs fluid leak-off, and the behavior at reservoir conditions, which is not able to reproduce at laboratory at this moment. The analysis of fluid invasion phenomena in unconventional reservoirs (low to ultralow permeability), extending the base concepts explored by Luo using simulation is the main scope of this document, and will be treated in the following chapters.

Chapter 3: Finite Core Invasion Test Simulation Matching

Unconventional reservoirs require the application of rock stimulation techniques like fracturing, to produce hydrocarbons. The lack of permeability is a challenge to develop this kind of reservoirs, but fracturing has proven its effectivity. This technique can use several different fracturing fluids like water, gas, or foam (water/gas combination). Determining how much of the fracturing fluid invades the porous media is a key factor to understand the impact in the well productivity and reservoir development. I first show Luo's experiments on fracturing fluid invasion, and then discuss how the results can be understood using numerical simulation.

3.1. LABORATORY TEST DESCRIPTION

Luo (2020) designed a test to determine the physics behind fluid invasion in unconventional reservoirs. The test consists of one core of 28 centimeters of length (11 inches) per 3.81 centimeters (15 inches), which is initially fully saturated by oil (n-heptane). Using control pressure systems on both sides was possible to keep constant the desired boundary conditions: Injection pressure at 620 psi for single phase invasion (gas, or water), and 650 psi in the case of combined invasion (gas and water simultaneously). On the other hand, for both cases the core initial pressure is set to be 600 psi. The test was run for two hours, where a single injector-producer well system in a reservoir was mimic to achieve the expected behavior of the fluid invading the porous media during hydraulic fracturing operations. With the aid of the CT scan, and keeping pressure boundary conditions, saturation profiles were determined at certain times during the test.

The goal of this test was to mimic the fluid invasion on a generated fracture during operations, not to mimic the fracture generation, geometry, or any other aspect of the rock mechanics. The rock used by Luo had an estimated absolute permeability of 10 md, and a porosity of 22%, those rock properties will be deeply discussed later this chapter. Figure 2 shows a schematic representation of the array used by Luo.

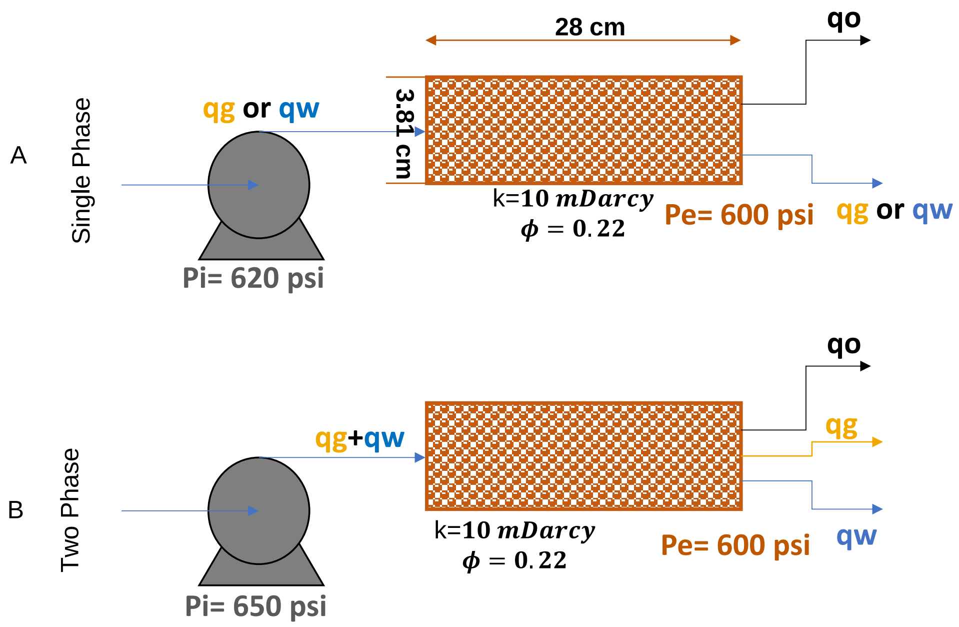
A
Single Phase
qg or qw
3.81 cm
28 cm
qo
k=10 mDarcy
ϕ = 0.22
Pe= 600 psi
qg or qw
Pi= 620 psi
B
Two Phase
qg+qw
qo
qg
qw
k=10 mDarcy
ϕ = 0.22
Pe= 600 psi
Pi= 650 psi

Figure 2: Laboratory test Scheme: A) Single phase Invasion, B) Two phase Invasion (Luo, 2020).

Luo (2020) made a first approach in the laboratory designing a test to evaluate the magnitude of fluid invasion for different fracturing fluids including water frac, a gas frac, and foam (combination) in a low permeability core. With the use of CT Scan, it was possible to measure the saturation profile into the rock, and the effect of the pressure due to the injection of different fluids in the porous medium. The results of this experiment can be seen in Figure 3 for water frac, in Figure 4 for gas frac, and in Figure 5 for foam frac (combination).

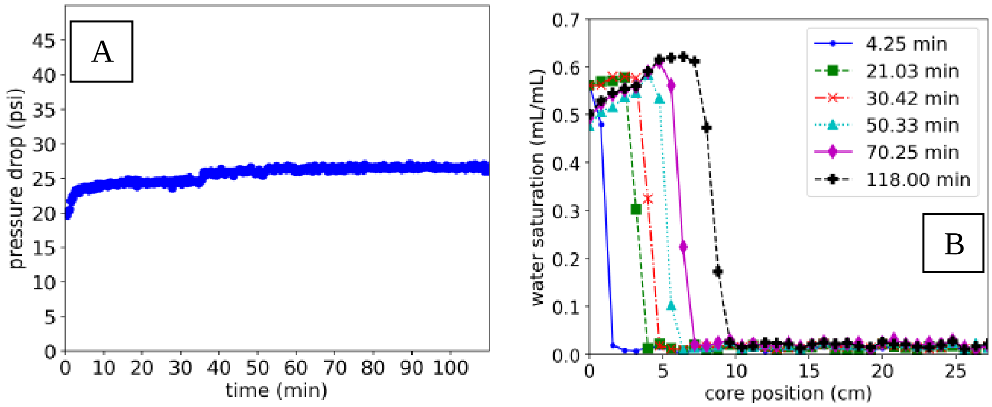

Figure 3: Water Invasion into an oil-saturated core, the test was performed injecting water with a pressure of 620 psi in the pressurized core at 600 psi. The CT scan was used to measure fluid saturation at 4.25, 21.03, 30.42, 50.33, 70.25, and 118 minutes after the test started. The experimental results: A) Shows a pressure drop averaging 20 psi along the test validating the constant pressure displacement, B) Shows saturation profile measured with the CT scan to determine the fluid invasion length along the test (Luo, 2020).

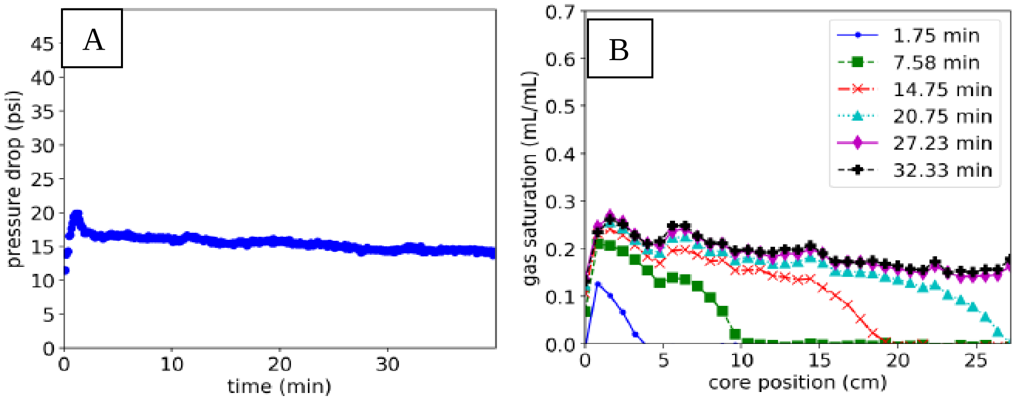

Figure 4: Gas Invasion into an oil-saturated core, the test was performed injecting gas with a pressure of 620 psi in the pressurized core at 600 psi. The CT scan was used to measure fluid saturation at 1.75, 7.58, 14.75, 20.75, 27.23, and 32.33 minutes after the test started. The experimental results: A) Shows a pressure drop averaging 20 psi along the test validating the constant pressure displacement, B) Shows saturation profile measured with the CT scan to determine the fluid invasion length along the test (Luo, 2020).

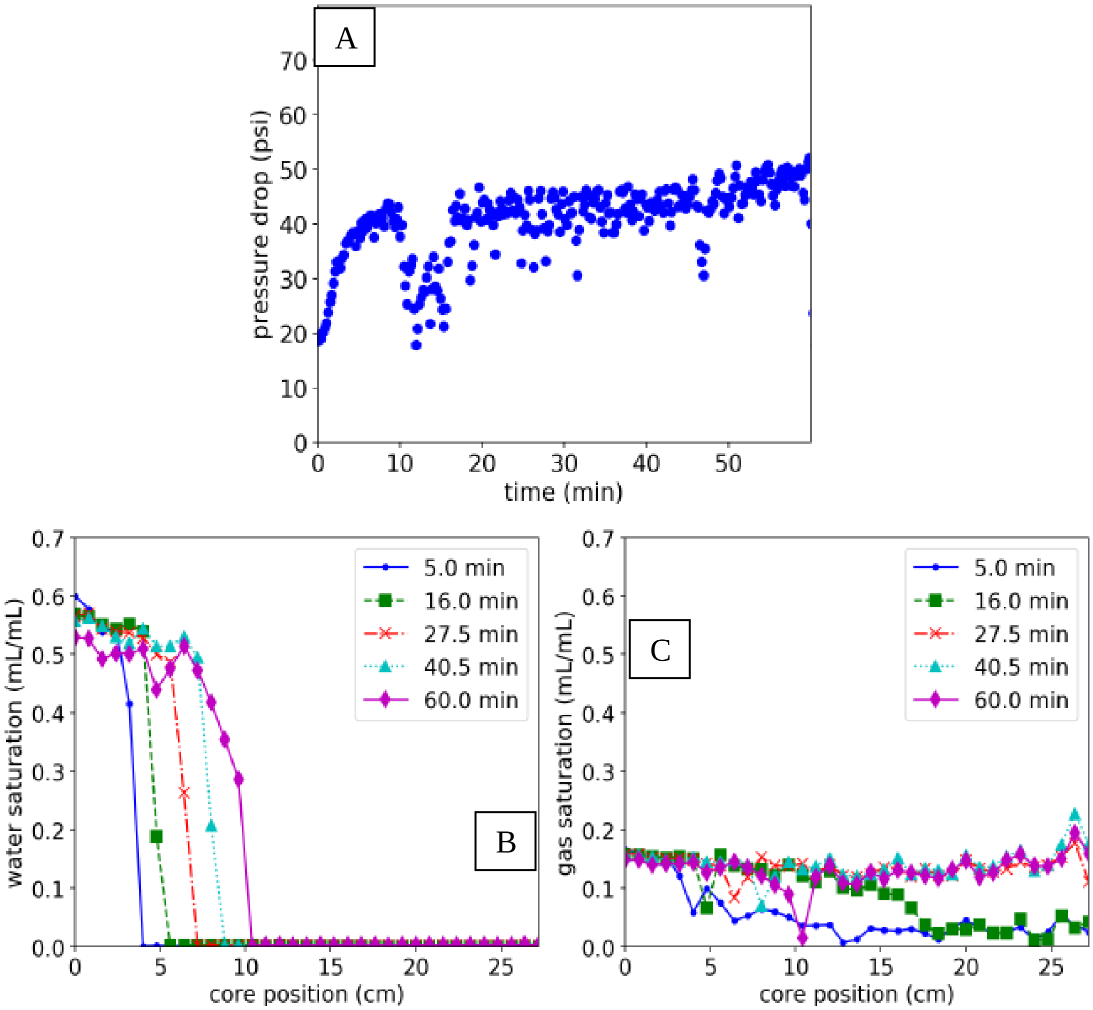

Figure 5: Foam Invasion into an oil-saturated core, the test was performed injecting foam (gas and water combination) with a pressure of 650 psi in the pressurized core at 600 psi. The CT scan was used to measure fluid saturations at 5, 16, 27.5, 40, and 60 minutes after the test started. The experimental results: A) Shows a pressure drop averaging 50 psi along the test validating the constant pressure displacement, B) Shows saturation water profile measured with the CT scan to determine the fluid invasion length along the test, C) Shows gas saturation profile measured with the CT scan to determine the fluid invasion length along the test (Luo, 2020).

Laboratory limitations just allow the analyses in a core scale size; therefore, a field magnitude study must be done with simulation initially. Simulation opens the door for a broader scope using as starting point the results obtained in the lab with a real rock, and then extrapolating this data to a bigger scale. Using several sensitivities is possible to find the effect of fluids in the rock, and the dynamics in the porous media in a field scale.

The simulation matching depends on several factors like kind of fluids (oil, water, Gas), PVT properties, rock properties, time scale, test conditions (pressure and temperature), and reservoir simulation models, which will be discussed on this chapter. In order to run the simulations the reservoir simulation software chosen is CMG IMEX (Computer Moldeling Group Limited, 2017), which is a robust and versatile simulator proven in several unconventional reservoir simulations, with complement modules for: PVT properties determination, three phase flow in porous media, fracturing, and compositional simulations (Al-Qassim & AlDaesari, 2017). Independently, the procedure used in this research should be replicable in other numerical simulation software.

3.2. SIMULATION PROCESS

Here I attempt to model the results obtained in the laboratory test using a numerical simulator as a starting point to extrapolate this process at reservoir conditions. The numerical simulator is a powerful tool to manage time related issues; low to ultra-low permeability core laboratory displacement tests require huge amount of time (sometimes months), and also size problems related with the cores dimensions, and the devices used to run the tests (maximum allowed core length 2-4 feet).

In order to begin the simulation, some input parameters must be loaded to start the process. The input parameters were divided in 4 categories: Numerical parameters, Reservoir Parameters, Fluid Parameters, and Rock-Fluid parameters. Each kind of parameter must be matched with the laboratory test conditions, granting the obtained simulation data suit the same physical conditions, this allows the simulation of several analyses scenarios, that might consume huge time, or would not be physically run at laboratory.

3.2.1. Numerical Parameters

Laboratory test is simulated in one-dimension model using Cartesian coordinates; the length corresponds to the core dimension of 27.94 cms in x-axis, and 3.81 cms in both y-axis and z-axis. The core was sliced in 35 blocks to determine the saturation and pressure profile in the same number points the CT scan saturation data was processed. Those dimensions will remain constant for finite core simulations and sensitivities. Because the fluids in a hydraulic fracturing operation are subjected to an average 120-minute exposure time with the reservoir, the time is set to two hours for every simulation. This time corresponds to 120 minute-steps. Figure 6 shows the representation of the core dimensional model.

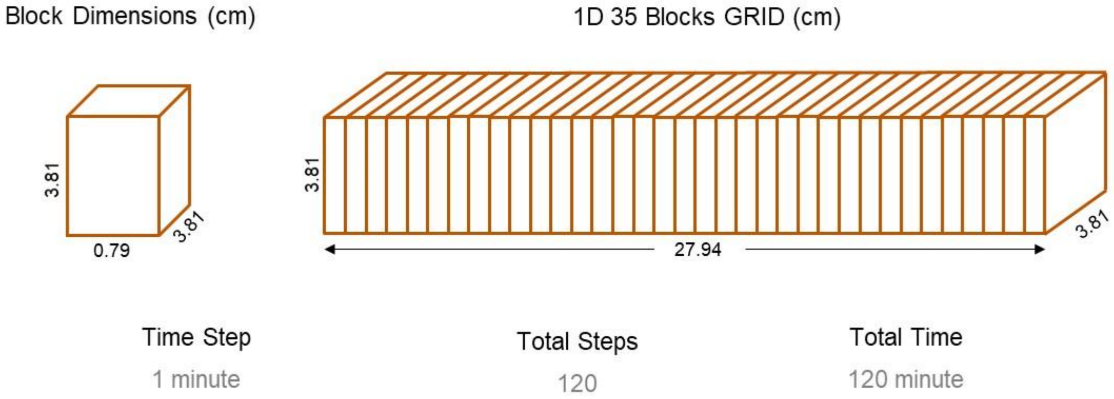
Block Dimensions (cm)
1D 35 Blocks GRID (cm)
3.81
0.79
3.81
3.81
27.94
3.81
Time Step
1 minute
Total Steps
120
Total Time
120 minute

Figure 6: Dimensional model. Finite core test simulation.

3.2.2. Reservoir Parameters

The core displacement test will be simulated as a single one-dimension reservoir with two wells; An injector well for the invading fluid (gas, water, both), and a producer to maintain reservoir boundary condition on the opposing side. The following are the detailed parameters of the reservoir configuration:

3.2.2.1. Wells

Laboratory test will be simulated using two wells (one injector, one producer) for single invasion experiment, and three wells (two injectors, one producer) in foam invasion case. The producer well is set to be producing at a bottom-hole pressure of 600 psi, and the injectors will be configurated to be injecting at bottom-hole pressure of 620 psi (single invasion), and 650 psi (foam invasion); In this case two injectors wells will be created at the same coordinate (same block) injecting two different fluids (Gas, Water).

CMG IMEX limits the size of the well radius considering the smaller dimension size in the well cross-sectional area. In order to have a control parameter to grant both pressure boundary conditions, well orientations will be in x-axis; this setting will allow changes in well radii independently of the corresponding Δx (number of slices). In the most of cases, the simulations run with wells oriented in z-axis did not converge.

3.2.2.2. Pressure and Temperature

The simulation model will be run with constant temperature of 80°F and two boundary pressure conditions controlled by the injector well (or wells): 620 psi for single invasion; 650 psi for foam invasion, and the producer will be set in both cases to produce at a bottom-hole pressure of 600 psi. This configuration represents the simpler form of reservoir model, but the complexity remains in the three-phase flow behavior and interactions.

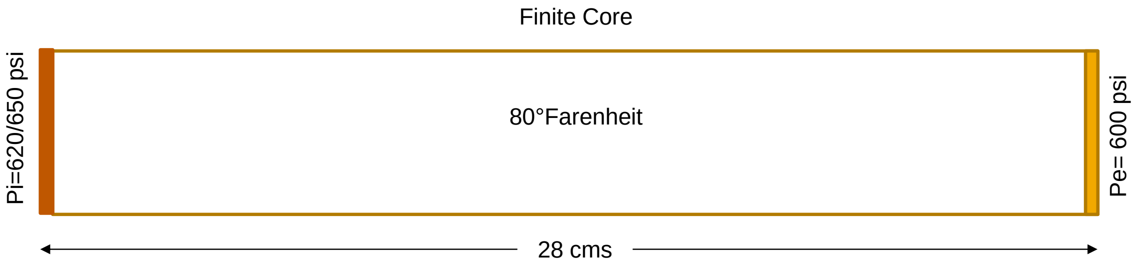

Figure 7: Finite core Pressure-Temperature boundary conditions. Injection pressure: 620 psi (single water or gas invasion), 650 psi (simultaneous water and gas invasion). Constant 80°F temperature along the 10 md 28 centimeters core.

3.2.2.3. Fluid Properties

The invasion test involved the use of three different fluids to replicate the fluid behavior in the reservoir, an oleic fluid: which will be n-heptane, water, and gas: in this case Nitrogen. With the use of the CMG module Win Prop, the fluid properties will be determined at P-T conditions loaded early. Table 1 Shows the PVT parameters for n-heptane and nitrogen, Table 2 shows water properties. The parameters were calculated using Win Prop.

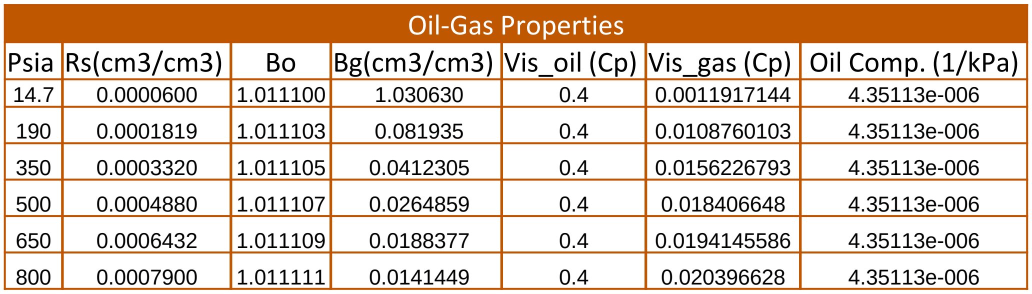

Oil-Gas Properties						
Psia	Rs(cm3/cm3)	Bo	Bg(cm3/cm3)	Vis_oil (Cp)	Vis_gas (Cp)	Oil Comp. (1/kPa)
14.7	0.0000600	1.011100	1.030630	0.4	0.0011917144	4.35113e-006
190	0.0001819	1.011103	0.081935	0.4	0.0108760103	4.35113e-006
350	0.0003320	1.011105	0.0412305	0.4	0.0156226793	4.35113e-006
500	0.0004880	1.011107	0.0264859	0.4	0.018406648	4.35113e-006
650	0.0006432	1.011109	0.0188377	0.4	0.0194145586	4.35113e-006
800	0.0007900	1.011111	0.0141449	0.4	0.020396628	4.35113e-006

Table 1: Oil-Gas PVT properties.

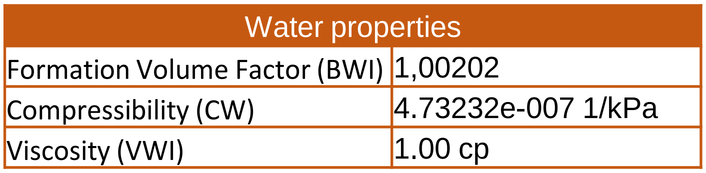

Water properties	
Formation Volume Factor (BWI)	1,00202
Compressibility (CW)	4.73232e-007 1/kPa
Viscosity (VWI)	1.00 cp

Table 2: Water PVT properties.

3.2.2.4. Porosity and Permeability

Simulations were done with constant porosity of 22% all along the cores matching the laboratory test and will remain constant for field simulation as well. Permeability will vary from 10 millidarcy to 100 nanodarcy. Higher permeabilities were used to model laboratory invasion test, and the lower permeabilities are used to model the fluid behavior in the field. Permeability and porosity will be loaded in CMG IMEX as a constant array for each one of the cases.

3.2.2.5. Rock-Fluid Interactions

The main parameter that must be suited to match the simulations is the rock-fluid interaction. Because the process occurring in the test could involve two or three fluid interactions, the proper relative permeability model must be chosen. In the case of single invasion, core-type relative permeability model was used to generate relative permeability curves for water and nitrogen. Figure 8 shows water-oil relative permeability, and Figure 9 shows gas-oil relative permeability. Due to the water-wet nature of the laboratory rock used in the test, Stone 1 is the most suitable model to replicate the three-phase relative permeability (Stone, 1970). This model will be used in the further field simulations also. Figure 10 shows three phase saturation ternary diagram.

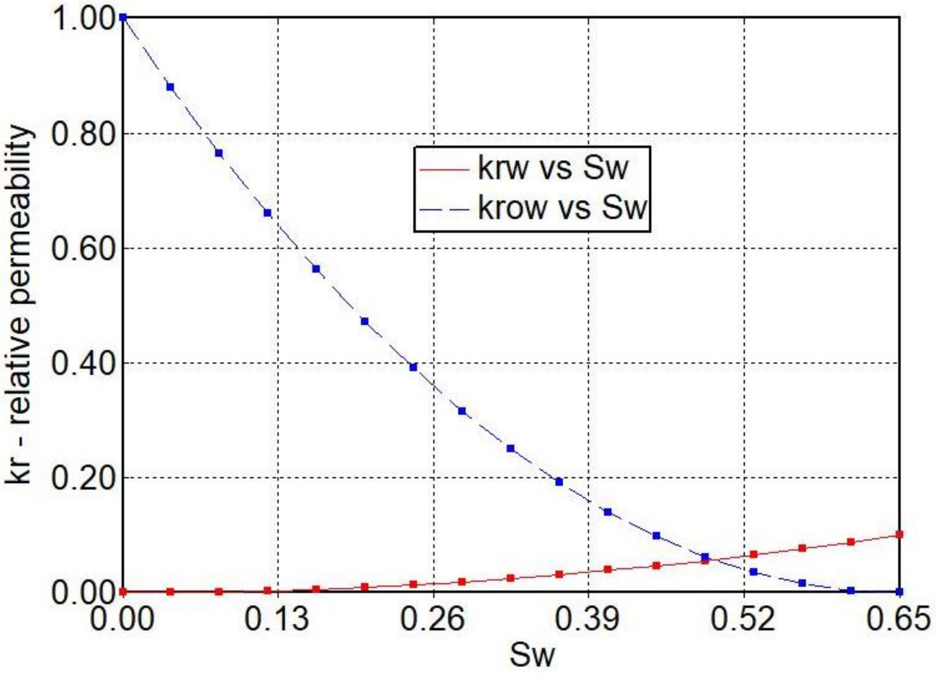

Figure 8: Simulated oil-water relative permeability curve.

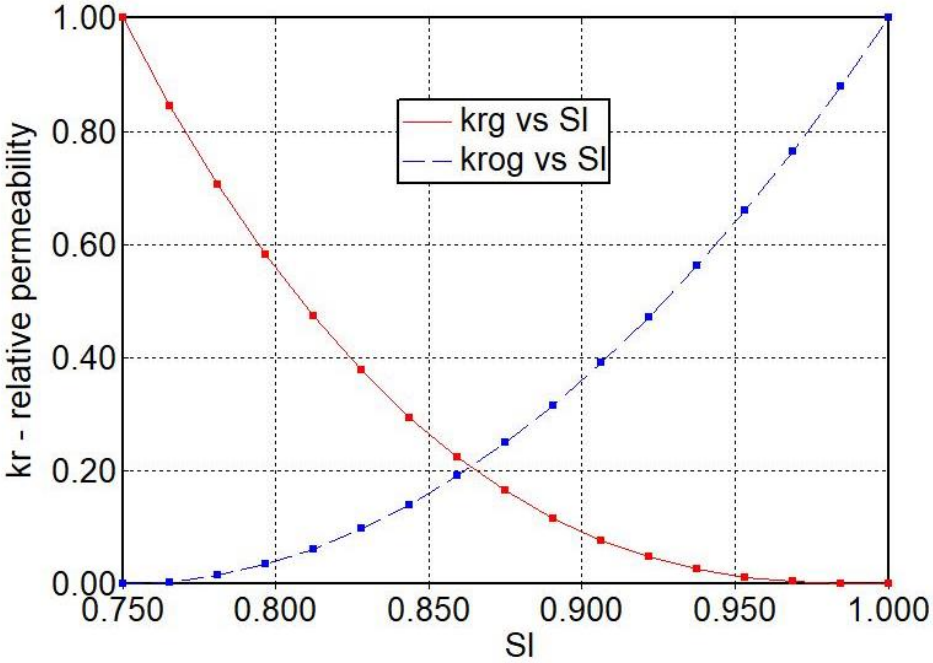

Figure 9: Simulated gas-oil relative permeability curve.

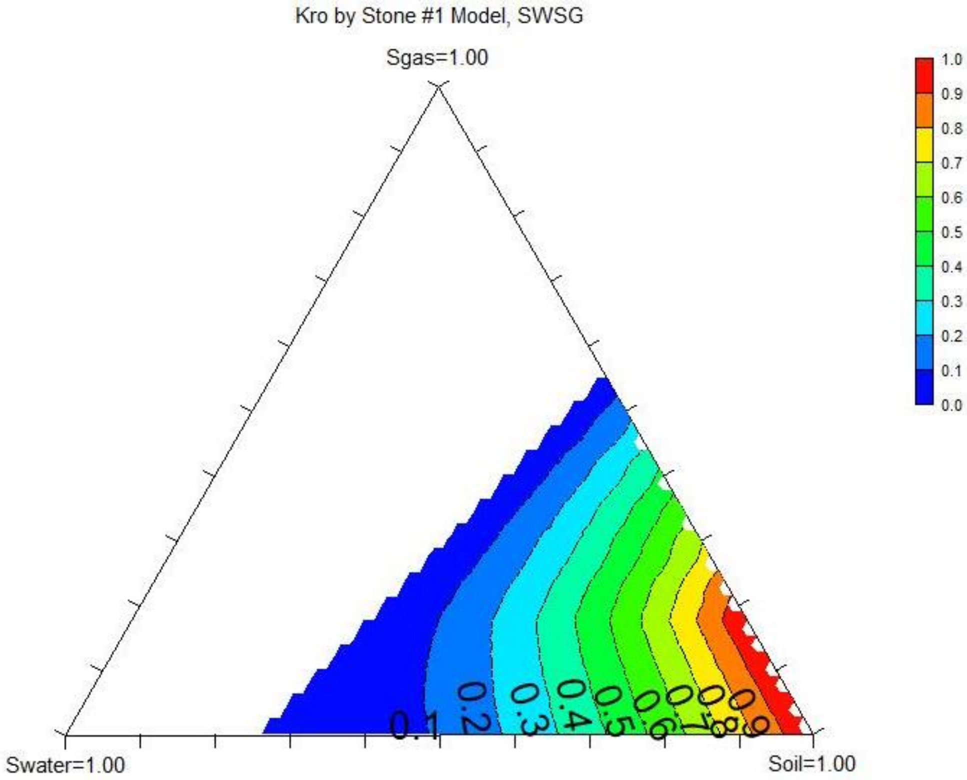

Figure 10: Three-phase isoperms used in the foam (combination) simulation.

3.3. WATER INVASION TEST SIMULATION

I first simulated the water invasion laboratory test using the parameters listed in section 3.2. The water saturation profiles measured in the CT scan by Luo were matched using the oil-water relative permeability curves to obtain comparable water invasion lengths at the same picked times. This process was repeated for gas and foam (combination) invasion test to match invasion profiles in the core.

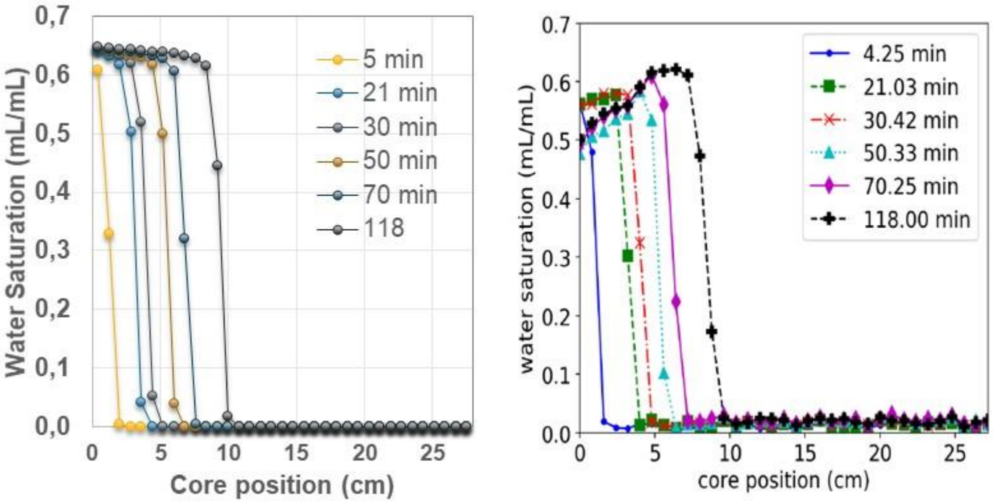

Figure 11: Laboratory water saturation profile. Simulated water Profile (left), Measured water-profile (right) (Luo, 2020). Single water invasion simulated test.

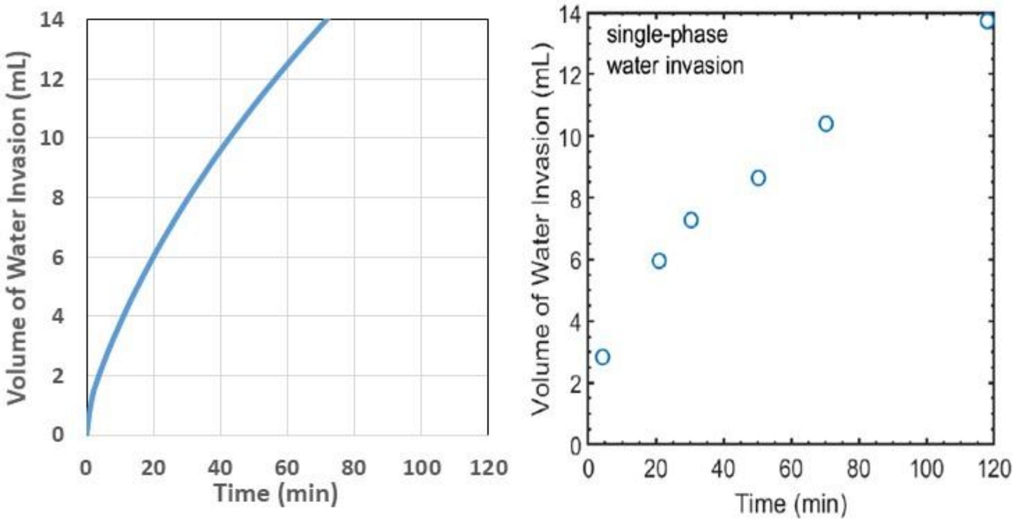

Figure 12: Cumulative water Invasion vs Time. Simulated Cumulative water (left), Measured Cum Water (right) (Luo, 2020). Single water invasion simulated test.

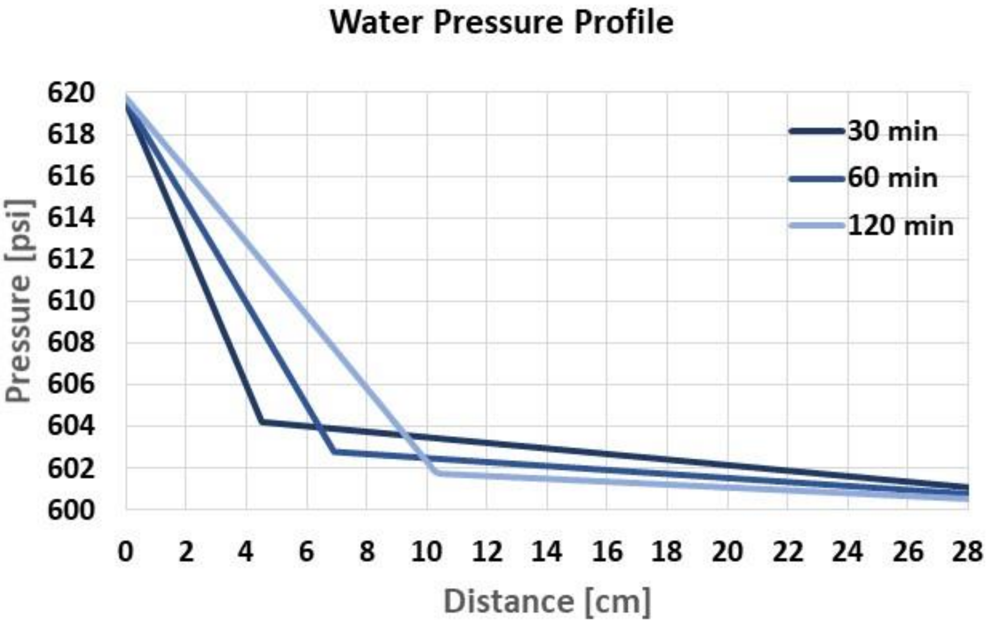

Figure 13: Water pressure profile. Single water invasion simulated on 10md; initial pressure of 600 psi. The water was injected at constant pressure of 620 psi along the simulated invasion. The shown values were picked at a simulated time of 30, 60 and 120 minutes.

Figure 11 shows the match between the simulated and the measured profile. It is possible to see the corresponding close average residual oil saturation on both plots, and the same distance traveled by the waterfront. The simulated water profile shows the water saturations similitude at the same invasion times, proving a model that fits with the realistic behavior of the fluid invasion in the laboratory core.

Figure 12 presents cumulative water invasion volume vs time at reservoir conditions, it can be seen the volumes do not fit accurately, despite they have the same square root of time behavior. The result showed, is expected because the cross-sectional area between simulation and laboratory cores is not the same. The difference is approximately 1.27 times, which is the ratio of the cross-sectional areas between simulated and laboratory core. When cumulative volume is normalized to cross-sectional area, invaded cumulative volume show an accurate fitting.

Finally, the simulated pressure profile in Figure 13 shows the pressure distribution along the core at various times. It validates the set boundary conditions on both sides and can be seen most of the injection pressure drop is taken up behind the waterfront. For this invasion case, the 80% of injection pressure drop took place at the first 4 centimeters after 30 minutes, and 90% of the pressure dropped in the first 10 centimeters when the simulated test was finished after 120 minutes. These positions are seen to correspond to the waterfront positions in Figure 12, and no water breakthrough occurred neither.

3.4. GAS INVASION TEST SIMULATION

Now that water invasion test has been matched, I focus the numerical simulation to reproduce gas invasion behavior in the core. In this simulation water was replaced by nitrogen, which involves new parameters of interest like fluid compressibility and lower viscosity. The saturation profile matching was performed using the gas-oil relative permeability curves in the same way water profile was tuned. Unlike water simulation, gas (nitrogen) invasion simulation presents complex challenge considering the pressure dependent properties that compressible fluids have. In this case CMG Win Prop module was useful to replicate PVT nitrogen properties correctly.

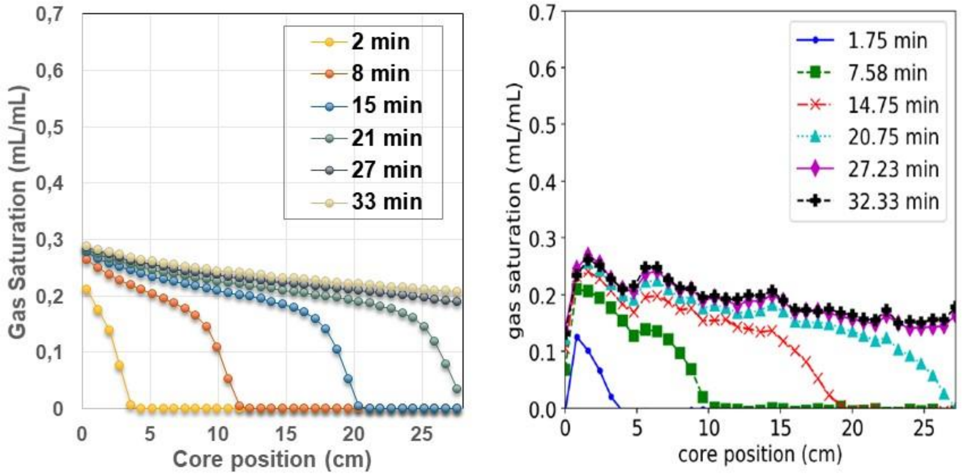

Figure 14: Laboratory gas saturation profile. Simulated gas profile (left), Measured gas profile (right) (Luo, 2020).

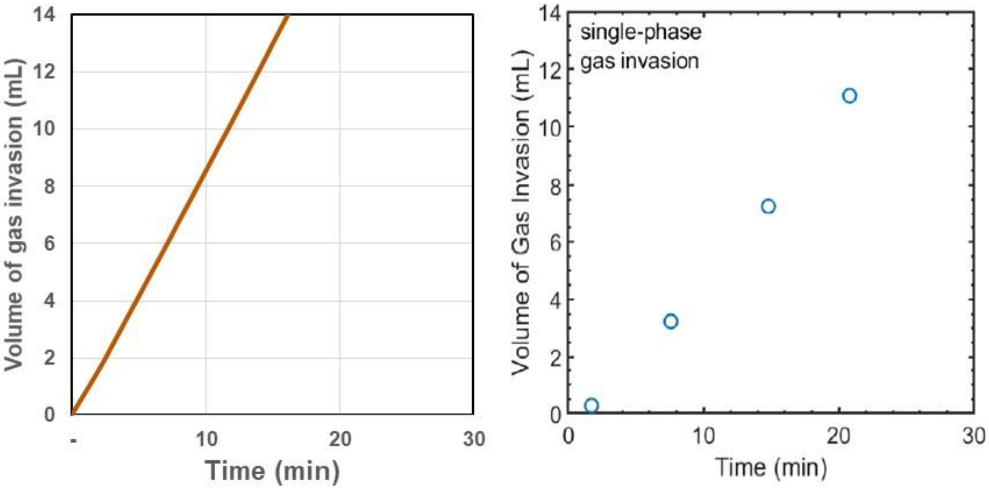

Figure 15: Laboratory gas invaded volume vs time. Simulated gas invaded volume (left), Measured gas invaded volume (right) (Luo, 2020).

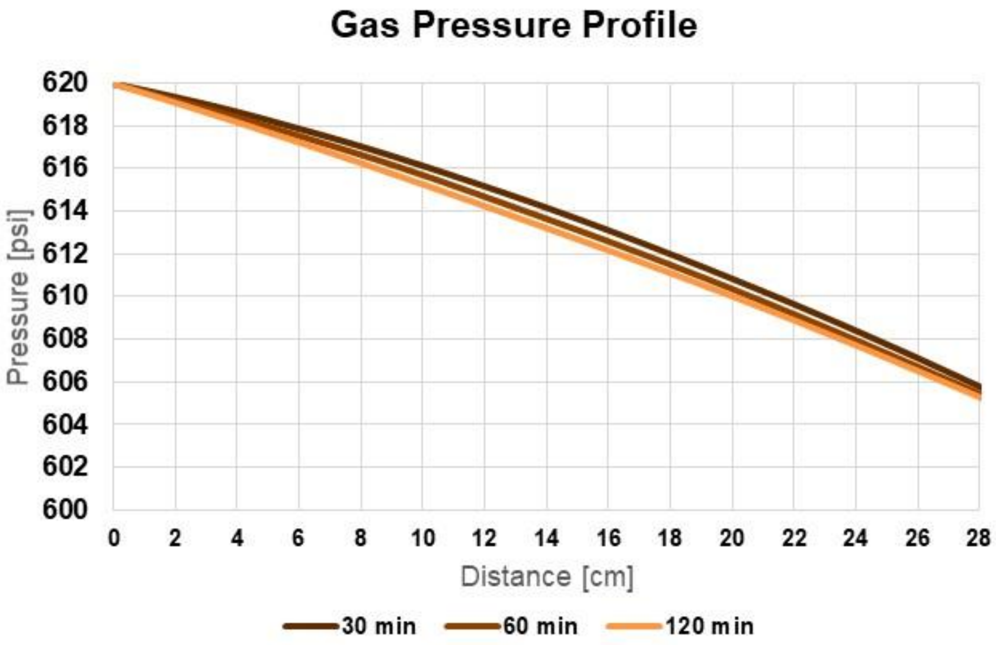

Figure 16: Gas pressure profile. Single gas invasion simulated on 10md; initial pressure of 600 psi. The gas was injected at constant pressure of 620 psi along the simulated invasion. The shown values were picked at a simulated time of 30, 60, and 120 minutes.

Figure 14 compares simulated saturation profile versus gas saturation measured at laboratory test. The residual oil saturation correlation matched accurately, and the front position along the core correspond to the gas advance in the test. The fitting also shows gas breakthrough occurring at 22 minutes approximately, which was observed at the same time in the laboratory saturation CT Scan measurement also.

In addition to saturation profile fitting, Figure 15 shows the correlation between simulated and measured cumulative volumes. The correct volume fitting is possible by normalizing invaded volume with the determined cross-sectional area ratio of 1.27 times like it was performed in the water invasion simulation. Furthermore, it is possible to see both cumulative behaviors are not proportional to square root of time like would be assumed considering the general leak-off model statements, instead linear behavior before gas breakthrough was seen. Using the laboratory test results, Luo (2020) explored this contradictory behavior in his dissertation and confirmed the relevance of research approach on reservoir leak-off phenomena general model validation.

Finally, Figure 16 presents the gas invasion pressure behavior, that is not comparable with water pressure profiles, where the most percentage of injection pressure drop took place behind waterfront. In the gas case, injection pressure drop takes place along the gas invasion profile exposing the effect of fluid compressibility. Moreover, when gas breakthrough occurred, the pressure distribution tended to be constant along the core as can be seen in the profiles at 27 and 33 minutes. Similarly, invaded volume tends to be constant after breakthrough exhibiting two different invasion behaviors at this boundary conditions.

3.5. FOAM INVASION TEST SIMULATION (WATER AND GAS COMBINATION)

Fracturing and drilling operations also experience the invasion of combined fluids like foam to generate fractures, or nitrogenated muds in drilling to perform underbalance operations (Guo & Ghalambor, 2004). Using the laboratory simulation matches for water and gas invasion, in this section I attempted to simulate foam invasion, a combination of previous simulated invasion processes. The three-phase relative permeability tuning is the key factor to fulfill the simulation matching, considering the other simulation parameters remained constant. The results are presented in Figures 17, 18, 19, 20 and 21.

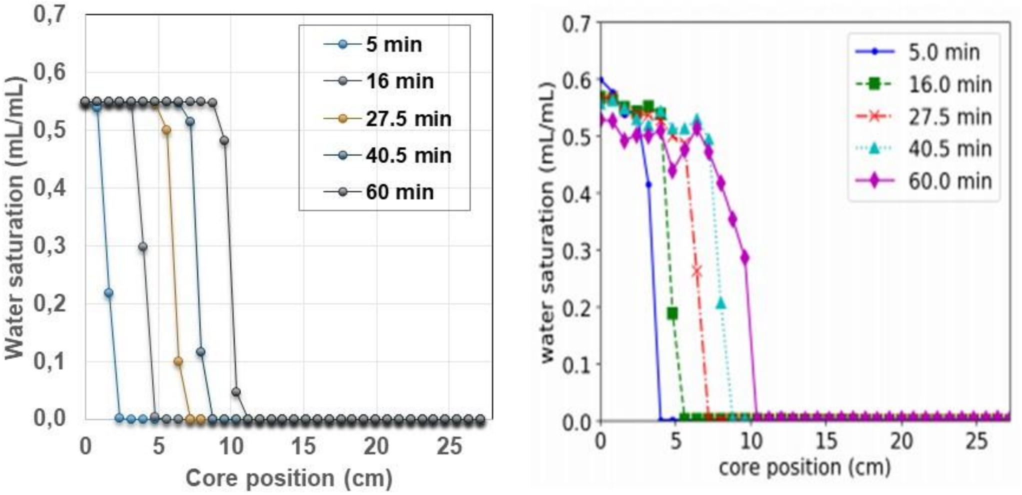

Figure 17: Laboratory water saturation profile. A) Simulated water combined profile, B) Measured water combined profile (Luo, 2020).

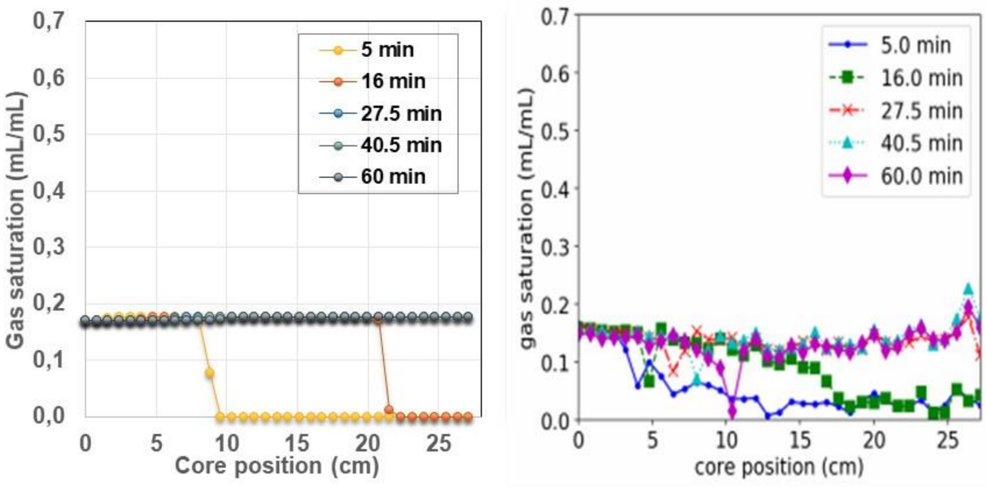

Figure 18: Laboratory gas saturation profile. A) Simulated gas combined profile, B) Measured gas combined profile (Luo, 2020).

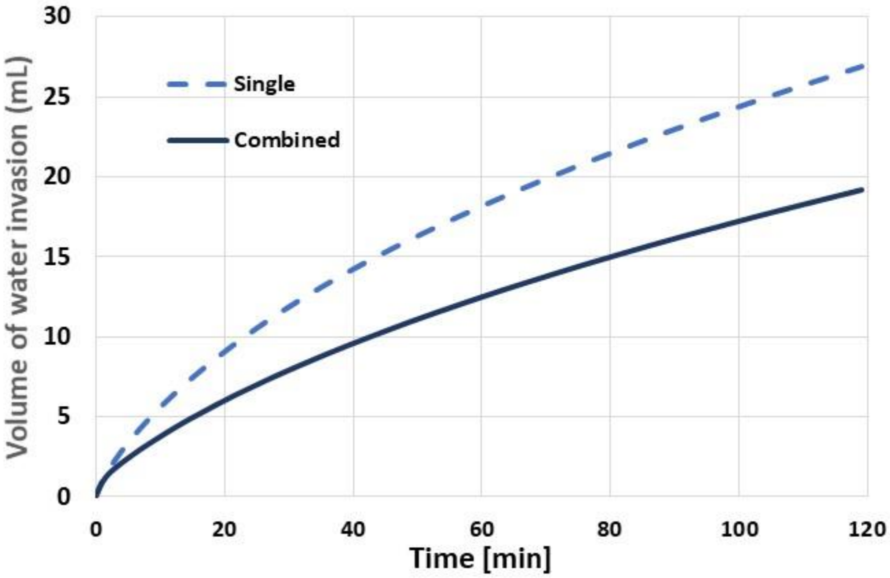

Figure 19: Cumulative volumes. Water cumulative volume comparison between single invasion and foam invasion. Simultaneous gas and water invasion (foam) simulation on 10 md core. Injection pressure 650 psi, reservoir pressure 600 psi. Volume at reservoir conditions.

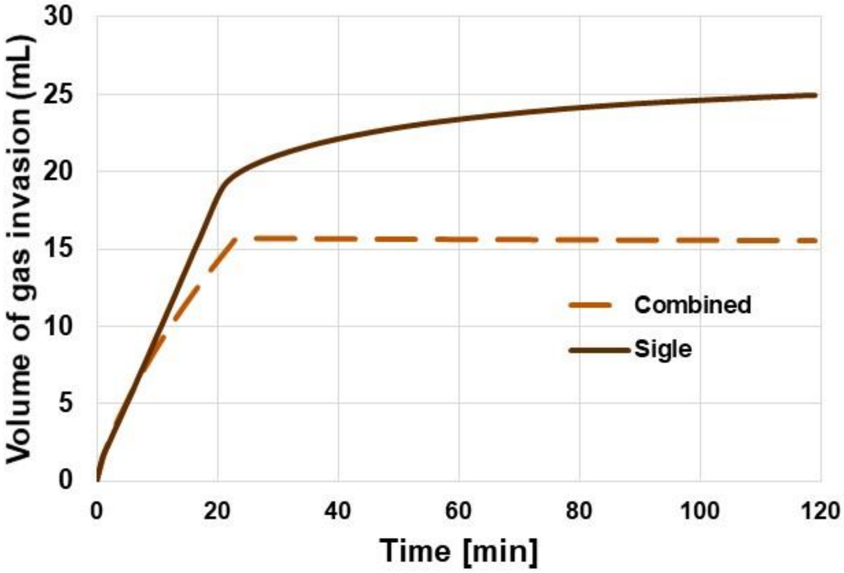

Figure 20: Cumulative volumes. Gas cumulative volume comparison between single invasion and foam invasion. Simultaneous gas and water invasion (foam) simulation on 10md core. Injection pressure 650 psi, reservoir pressure 600 psi. Volume at reservoir conditions.

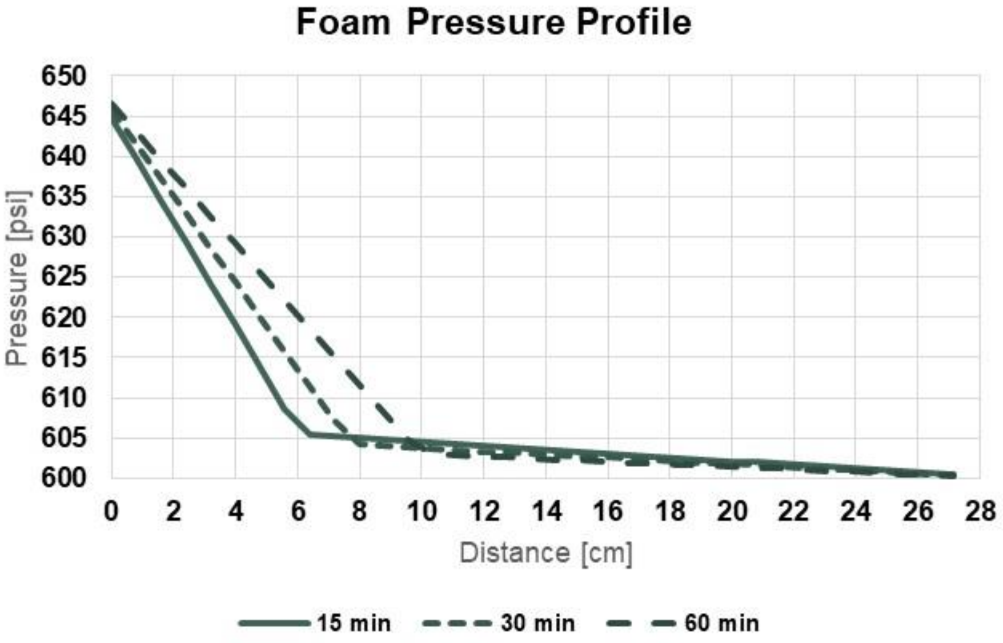

Figure 21: Foam pressure profiles. Simultaneous gas and water invasion (foam) simulated on 10md core; initial pressure of 600 psi. The gas and water were injected at constant pressure of 650 psi along the simulated invasion. The shown values were pick at a simulated time of 15, 30, and 60 minutes.

Figure 17 shows the effect of foam invasion, that reduces the water average front saturation from 60% to 55%, like was seen in the plot, this behavior is due to the action of water and gas invasion competition inside the core. The water invasion length is highly affected because in the single invasion water travels 10 cms after 120 minutes, and the same distance is reach after 60 minutes in the foam case, which inferred that the water moves two times faster than in single displacement.

On the other hand, Figure 18 shows a significant reduction in the average gas saturation between single invasion and foam invasion; the combined effect reduced the saturation percentage from 25% to 18% approximately, which is a 30% reduction.

Furthermore, comparing the traveled distance after 15 minutes in both single and foam invasion, the invaded length is the same, approximately 22 cms. Even when the fluid invasion velocity has not been affected, the volume invaded should decline responding to the gas saturation reduction.

Figure 19 complements water saturation profiles presenting the cumulative invade volume related to the foam invasion. The plotted water cumulative volumes show the same square root of time depending behavior, and according to the saturation reduction, cumulative volume in combined case also decrease. This data reflects the relevant effect of combined invasion with the aim of controlling water leak off inside the core, and the reservoir, respectively.

Figure 20 corroborated the before breakthrough linear volume invasion behavior seen in the single gas invasion. Therefore, the assumptions stated in the general leak-off model did not corresponded to the foam experiment results, even considering the current boundary conditions. The control of gas invasion could contribute positively under controlled conditions to minimize the permeability damage caused by gas trapping damage mechanism (Luo, 2020).

Finally, figure 21 shows the foam pressure profiles is consistent with the expected behavior of the three immiscible fluids. The plot shows the composite effect of the foam front inside the core, where there is a pick after 60 minutes (at 10 centimeters) corresponding to the waterfront displacement, in this point the injection pressure has dropped 90%. A complementary effect of compressibility is seen after 10 centimeters corresponding to the gas phase, which breakthrough occurred at 22 minutes after the test began. Foam invasion fitting fulfills the first step to extrapolate the simulation process to further permeability scenarios, those will be address in the next chapter.

3.6. SUMMARY

In this chapter were selected the parameters to fulfill Luo´s laboratory invasion tests. Using numerical simulation, it was possible to successfully reproduce the laboratory results for water invasion, gas invasion, and foam invasion. The match was performed considering saturation profiles, cumulative volumes, and pressure profile. Each invasion case presented a proper behavior corresponding to the fluid properties and interactions like was seen in the laboratory affecting pressure profile, invasion length and invaded volumes. The simulation results supported the further permeability sensitivities over the finite core displacements to estimate the proper dependency.

Chapter 4: Finite Core - Low to Ultra Low Permeability

In this chapter the simulation was run from the 10 millidarcy permeability rock to ultra-low permeability range of 100 nanodarcy. This process was performed in 3 new numerical cores of: 1 millidarcy, 10 microdarcy, and 100 nanodarcy. Those magnitudes were chosen, assuming the square root of permeability dependency stated in the general leak-off model drives the permeability correlation (Settari A. , 1985). The permeability approach was executed for the three fluid invasion cases: water invasion, gas invasion, and foam invasion (combined invasion). The fluid properties, boundary conditions, and other reservoir parameters listed earlier remained constant to successfully evaluate the effect of permeability. The sensitivity explored the behavior of fluid leak-off in ultra-low permeabilities presenting and option to deal with long time laboratory fluid invasion tests.

4.1. WATER INVASION RESULTS

In water invasion simulation, I performed four sensitivities considering 10mD, 1mD, 10µD, and 100nD cores to evaluate the effect of permeability over the laboratory test arrangement. The results are presented in Figures 22, 23, and 24 addressing saturation profiles, cumulative volumes, and pressure behavior approach.

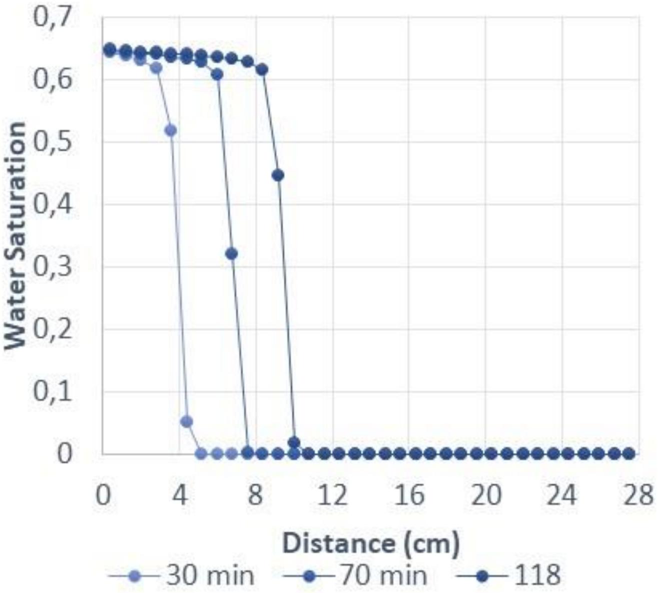

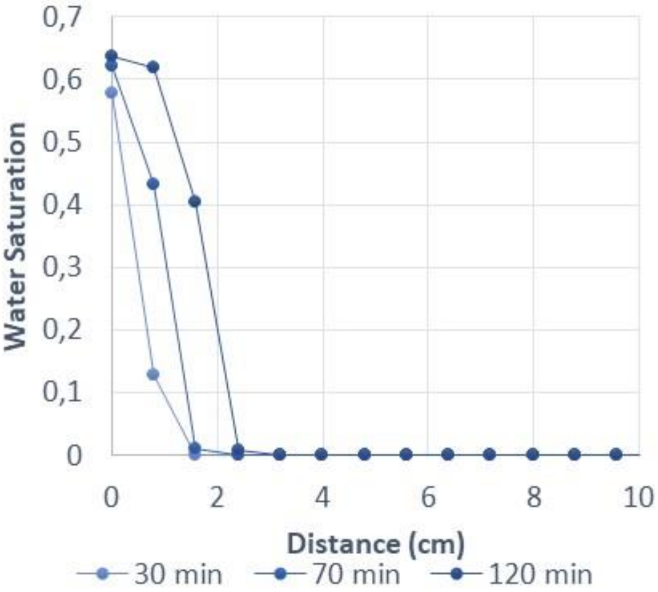

Figure 22: Water saturation profiles. Single water invasion simulated on 10md (top) and 1md (bottom) core; initial pressure of 600 psi. The water was injected at constant pressure of 620 psi along the simulated invasion. The shown values were pick at a simulated time of 30, 70 and 118 minutes.

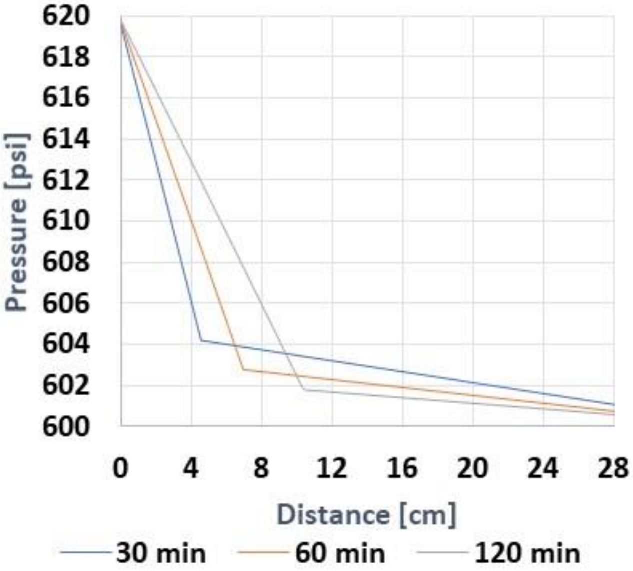

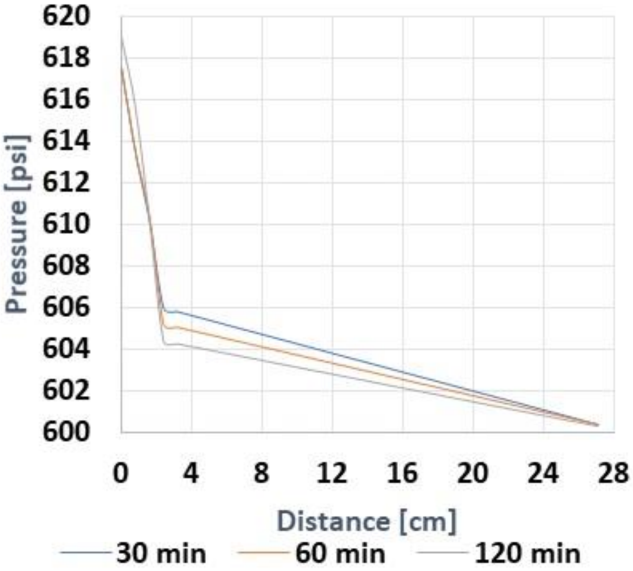

Figure 23: Water Pressure profiles. Single water invasion simulated on 10md (top) and 1md (bottom) core; initial pressure of 600 psi. The water was injected at constant pressure of 620 psi along the simulated invasion. The shown values were pick at a simulated time of 30, 60 and 120 minutes.

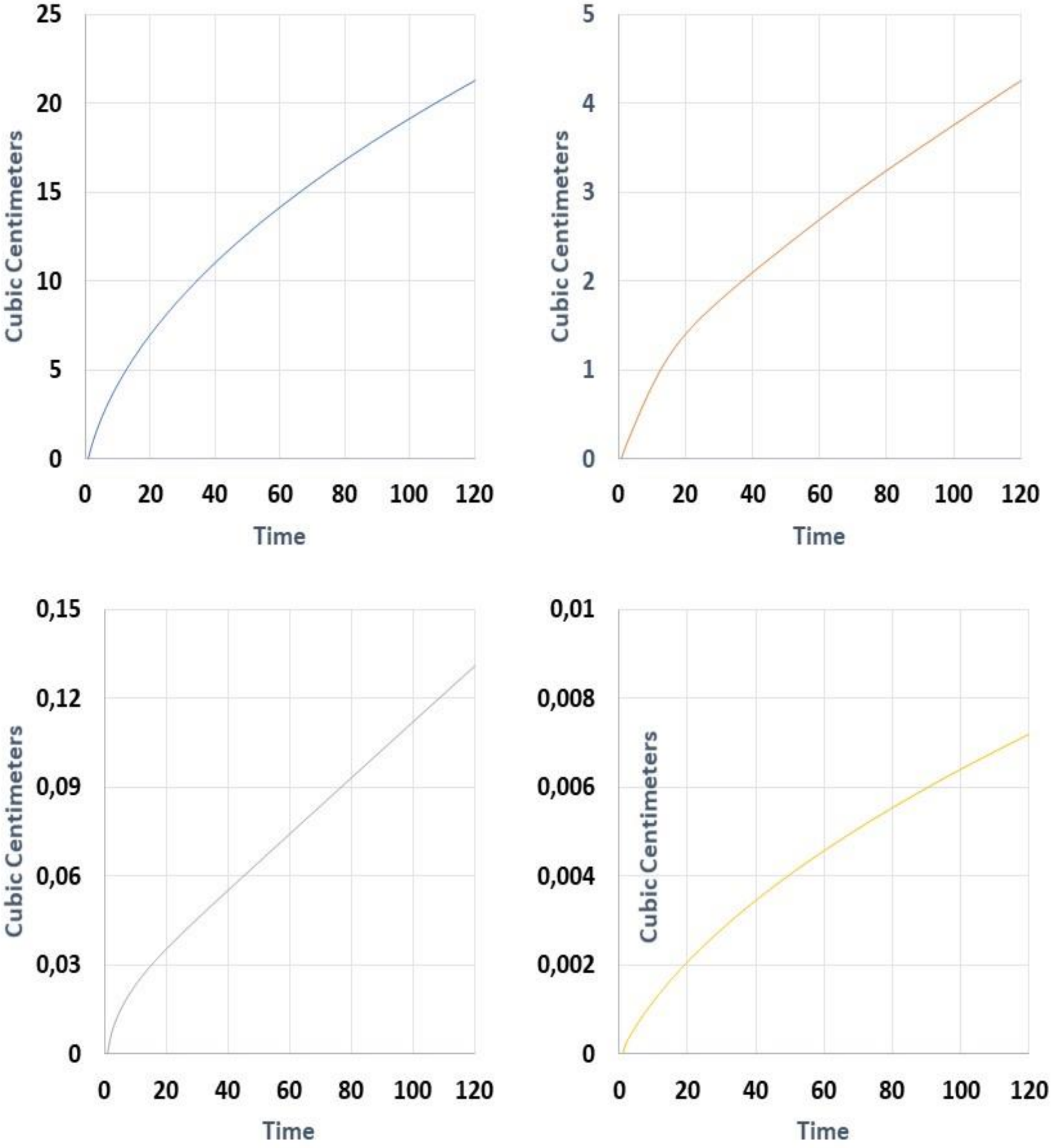

Figure 24: Cumulative volumes. Single water invasion simulated on 10md (top left), 1md (top right), 10µd (bottom left) and 100nd (bottom right) cores; initial pressure of 600 psi. The water was injected at constant pressure of 620 psi along the simulated invasion. The simulated invasion time was 120 minutes.

Figure 22 shows the water invaded the core from 10 centimeters in the 10md core (baseline), to 2 centimeters in the 1md simulation. The water saturation data corroborate, after two hours the water invasion is minimal in the lower permeability core, which implies a more extensive laboratory invasion test should be run on ultra-low permeability rocks. The invasion length reduction is expected considering the general leak-off model permeability dependency, and it corresponded with the cumulative volume profiles.

Complementing the water saturation profiles data, pressure profiles on Figure 23 correlate pressure drop with waterfront invasion length. The least the water invades the core, the injection pressure drop effect over the front cannot be seen in the profile. Therefore, for lower permeabilities the pressure drop due to the water phase is almost unseen considering the current simulated time (2 hours).

Finally, cumulative invaded volumes in Figure 24 corroborate square root of time behavior. Furthermore, the cumulative volume at the end of the test decrease drastically from 21.25 cubic centimeters in 10mD core to 0.007 cubic centimeters in 100 nD rock. Eventually, the invaded volume reduction is around 3000 times, which do not correspond to square root of permeability from 10 mD to 100 nD like was assume initially on this section. This preliminary result suggests under the test conditions, general leak-off model statements do not describe the water invasion behavior over the simulated cores.

4.2. GAS INVASION RESULTS

In this section Figures 25, 26, and 27 present saturation profiles, cumulative volumes, and pressure behavior, respectively.

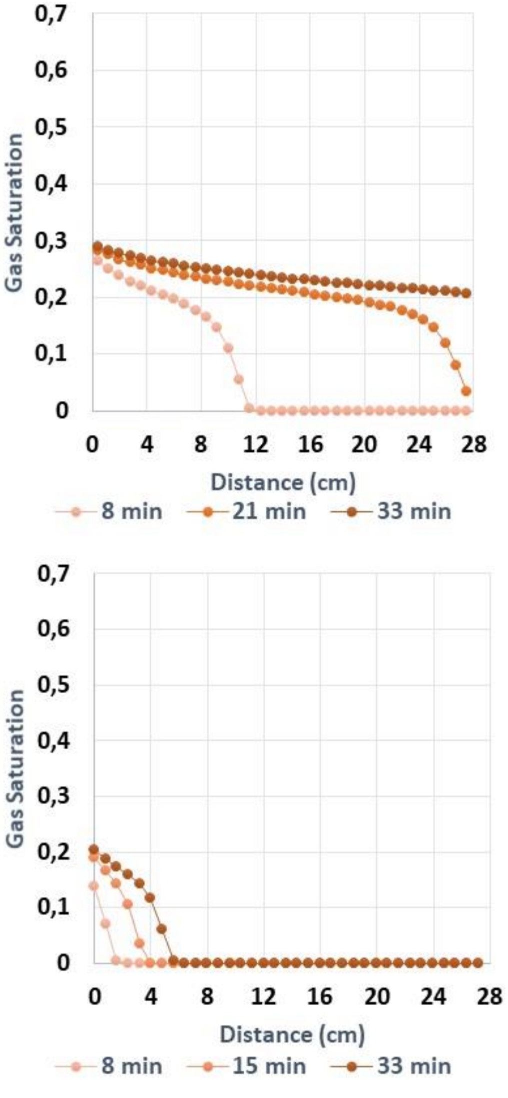

Figure 25: Gas saturation profiles. Single water invasion simulated on 10md (top) and 1md cores (bottom); initial pressure 600 psi. The gas was injected at constant pressure of 620 psi along the simulated invasion. The shown values were pick at a simulated time of 8, 21 and 33 minutes.

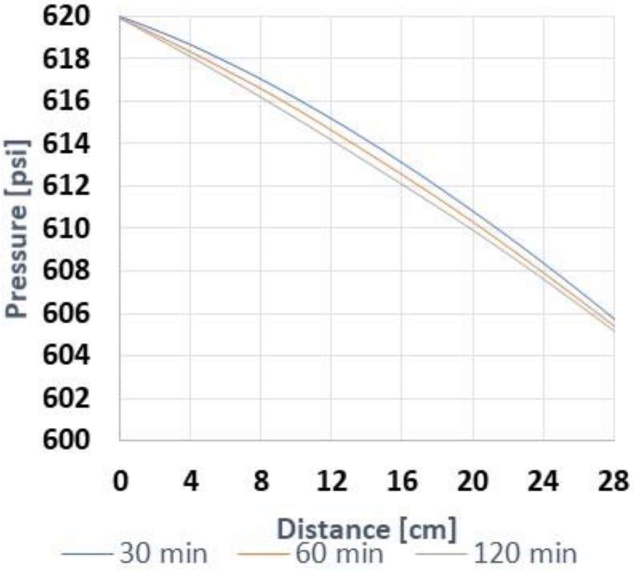

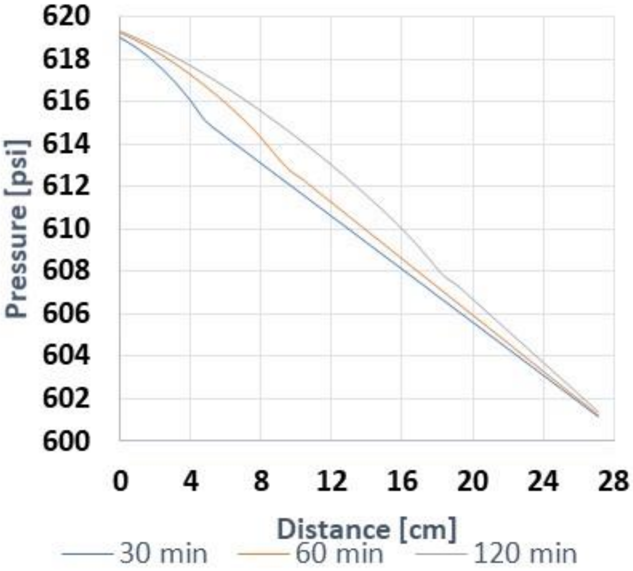

Figure 26: Gas pressure profiles. Single gas invasion simulated on 10md (top) and 1md core (bottom); initial pressure of 600 psi. The gas was injected at constant pressure of 620 psi along the simulated invasion. The shown values were pick at a simulated time of 30, 60 and 120 minutes.

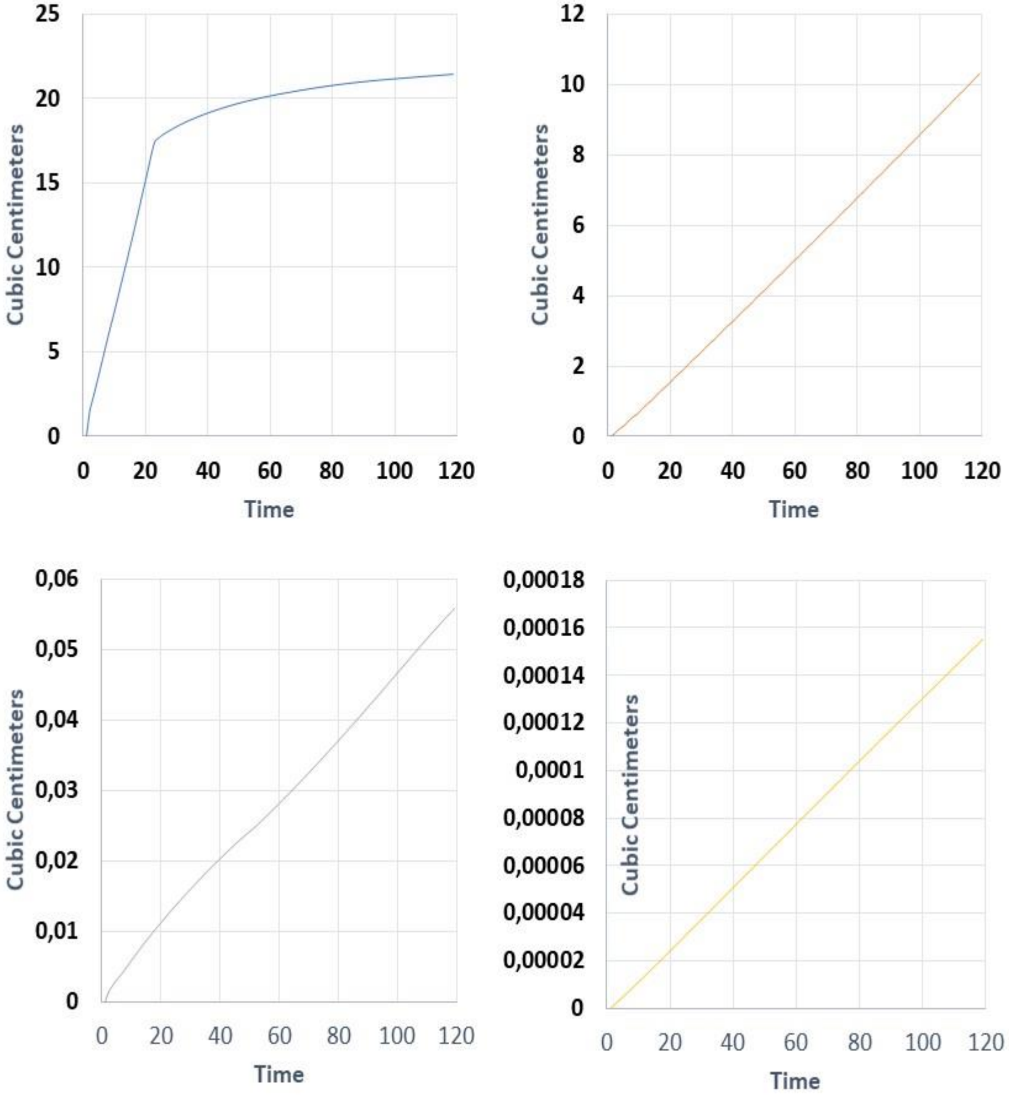

Figure 27: Cumulative gas volumes. Single gas invasion simulated on 10md, 1md, 10µd and 100nd cores; initial pressure of 600 psi. The gas was injected at constant pressure of 620 psi along the simulated invasion. The total simulated invasion time was 120 minutes.

Figure 25 reported the gas saturation profiles behavior in the 10md and 1md core, confirming the invasion length is reduced proportionally to the permeability decrease. The gas breakthrough occurred only in the 10md core at 22 minutes of the simulated time, and is only seen in the 10 millidarcy core, where permeability allows the fluid to travel from one side to the other. The 1md core served as a control point to compare waterfront advance from previous section, with the gas invasion showing the nitrogen moved 10 times faster than the water.

In addition to the gas saturation data, Figure 26 presented the pressure profile simulated for the 10md, and 1 md cores, where the gas exhibited a behavior corresponding to the gas advance into the core. The gas effect in the injection pressure profile was reduced as the permeability decreased affecting gas invasion length. Even when the same behavior was reported with the water invasion simulation, the key factor about gas invasion is the confirmed discrepancy between the expected square root of time volume dependency, and the linear behavior shown in Chapter 3.

Figure 27 shows the invaded volume behaved linearly in the 4 different permeability simulations. The correspondent case for 10 millidarcy core presents two different volume invasion regimes, this combined behavior is related to the gas breakthrough occurred, and the volume tends to be constant because of the production boundary. The linear volume invasion behavior is also seen in the lower permeability rocks because the pressure wave has not affected the farther side of the core. This behavior will be analyzed in the foam invasion test, to validate the discrepancies with the proposed dependency in the general leak-off model.

4.3. FOAM INVASION RESULTS

In this section Figure 28, and 29 present water invaded volumes, and gas invaded volumes respectively

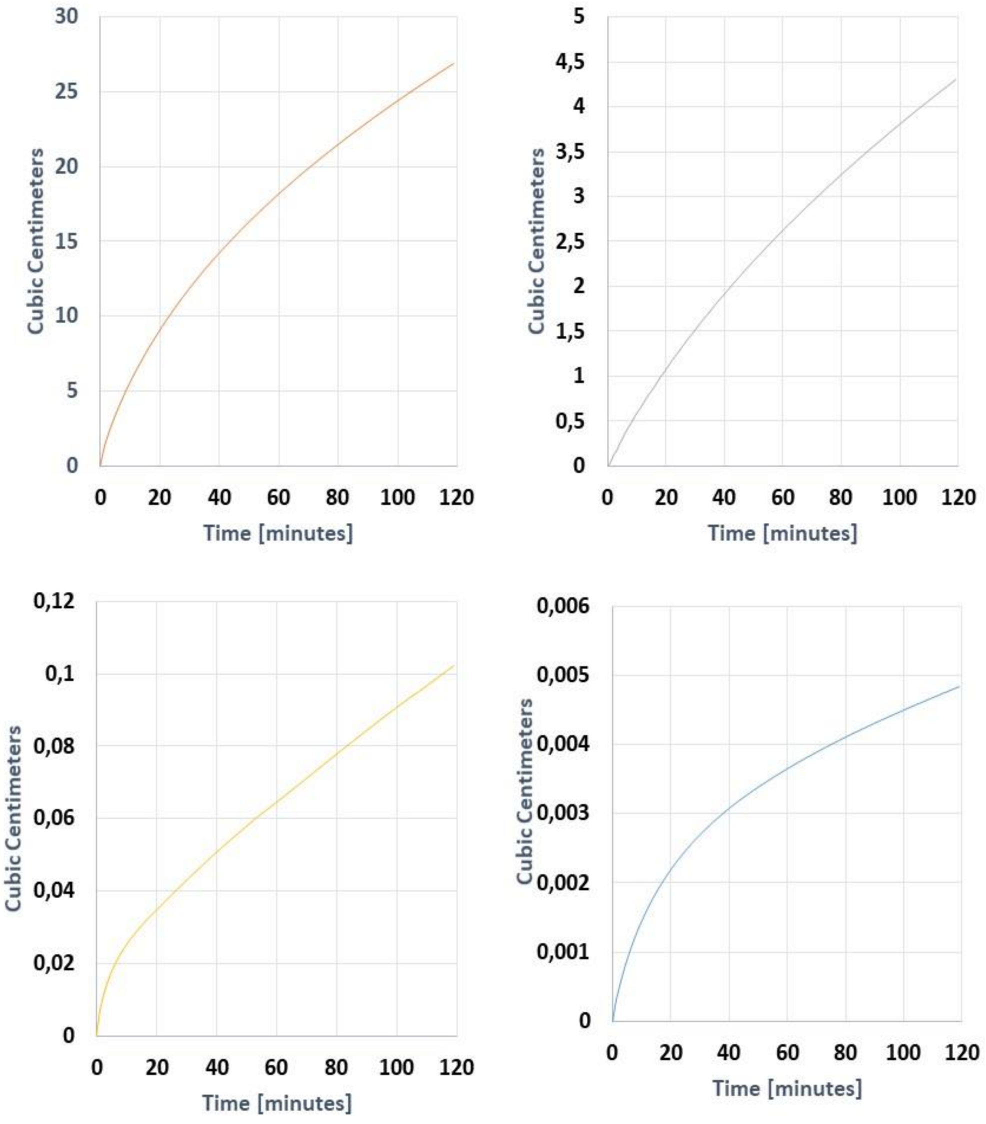

Figure 28: Cumulative water volumes. Simultaneous water and gas invasion simulated on 10md, 1md, 10µd and 100nd cores; initial pressure of 600 psi. The water fluids were injected at constant pressure of 650 psi along the simulated invasion. The simulated invasion time was 120 minutes.

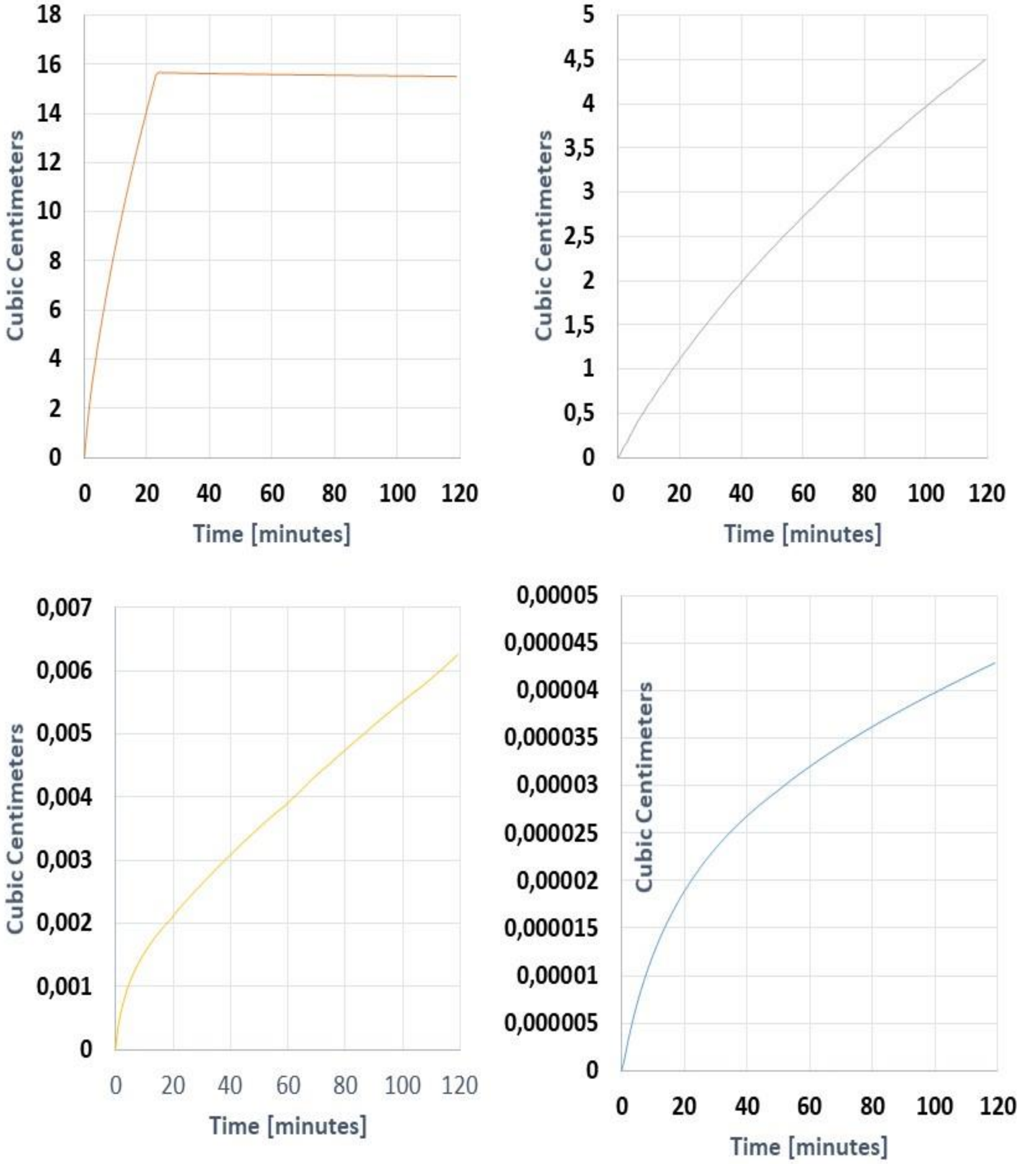

Figure 29: Cumulative water volumes. Simultaneous water and gas invasion simulated on 10md, 1md, 10µd and 100nd cores; initial pressure of 600 psi. The water fluids were injected at constant pressure of 650 psi along the simulated invasion. The simulated invasion time was 120 minutes.

The data shown in Figure 28 have the same expected square root of time behavior seen in the single water invasion. Even when the invaded volumes are smaller, those results supported the general leak model time dependency. To evaluate the correspondent permeability correlation, the invaded volumes for the three invasion cases are compared in section 4.4.

On the other hand, on Figure 29 gas combined invasion results differed from the earlier results shown for the single displacement simulation. Cumulative volumes in the plot presented a linear behavior only in the 10 mD core before breakthrough. The behavior shown in the 10 mD core is comparable with single gas invasion test but cannot be homologated to lower permeability cores were linear invasion phenomena is not clearly seen. Instead of the linear invasion behavior, the plots from 1 mD to 100 nD reveal an approximate square root of time dependency.

The results will require a deeper analysis to confirm the permeability effect in the simulated finite core invasion tests and are performed in the last section on this chapter. The further work on this section show in a clear way the permeability approach, and the future useful applications at laboratory scale, and reservoir conditions.

4.4. LEAK-OFF DEPENDENCIES

Figures 30, and 31 present the general invasion length versus permeability data performed over the three invasion scenarios at 10 minutes, and 20 minutes, respectively.

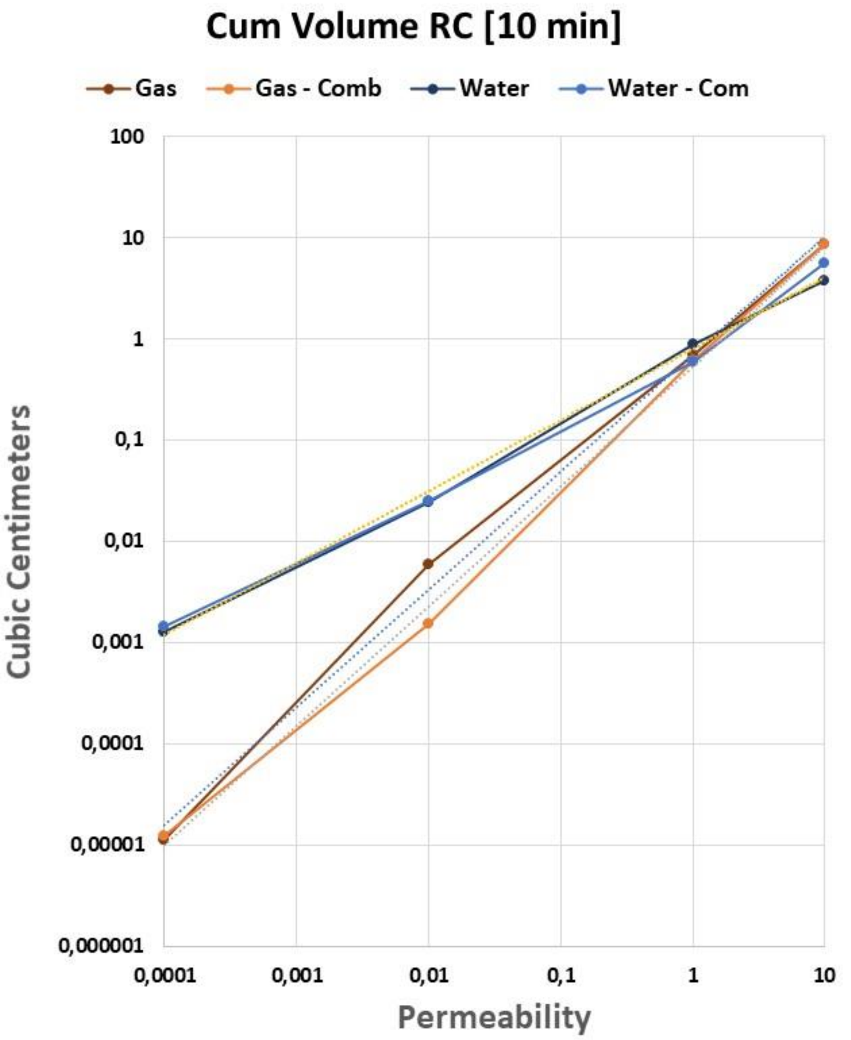

Figure 30: Invasion length versus Permeability plot. Single gas invasion, water invasion, and simultaneous water and gas invasion were simulated in a 10md to 100nd cores with initial pressure of 600 psi. The fluids were injected at constant pressure of 620 psi (single invasion), and 650 psi (combined invasion) along the simulated invasion. The show values were pick at a simulated time of 10 minutes.

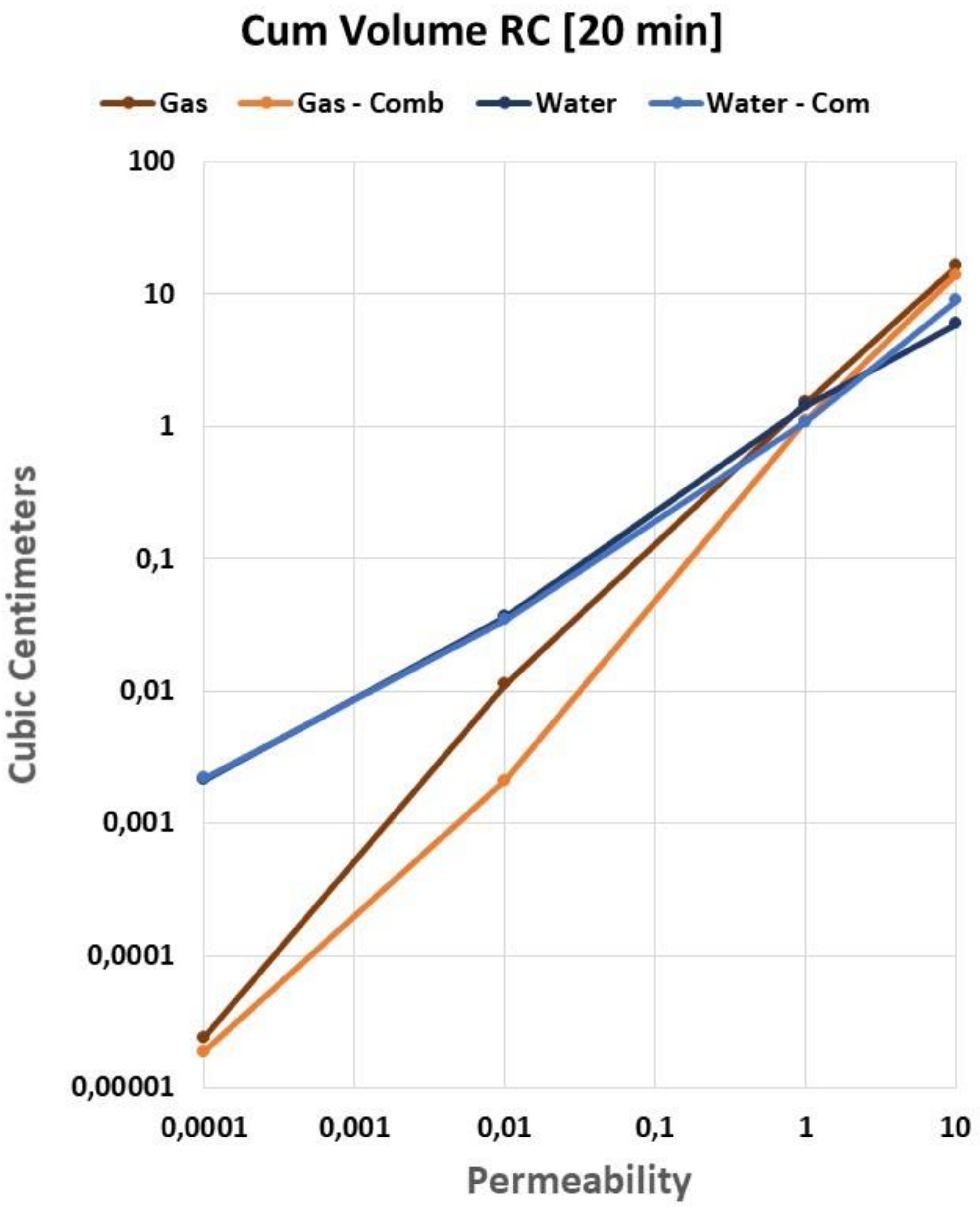

Figure 31: Invasion length versus Permeability plot. Single gas invasion, water invasion, and simultaneous water and gas invasion were simulated in a 10md to 100nd cores with an initial pressure of 600 psi. The fluids were injected at constant pressure of 620 psi (single invasion), and 650 psi (combined invasion) along the simulated invasion. The show values were pick at a simulated time of 10 minutes

Aiming the understanding of fluid leak-off on unconventional permeability cores performed in this section, all sensitives carrying permeability, fluid kind, and invasion type were evaluated at two simulation times. Trying to cut the breakthrough effect occurring in the gas invasion, the chosen times were 10 and 20 minutes recalling the gas breakthrough time was found at 22 minutes. The data shown in Figure 30 and Figure 31, present the four cores simulated volume behavior at 10 and 20 minutes, respectively. To grant satisfactory view of the overall effect, both axes are presented in logarithmic scale where two grouped tendencies clearly show the water and gas discrepant behavior.

To determine the proper relationship between fluid invasion and permeability, a potential regression was used to calculate the slopes on both cases. Blue lines represent water results for single and combined invasion, with a calculated slope for this case of 0.75 differing the square root of permeability dependency from general leak-off model (Settari A. , 1985). Otherwise orange lines for gas invasions had a slope of 1.25, offsetting the expected square root dependency. This procedure was replicated on 20 minutes data obtaining the same slope values for gas and water invasions.

In addition to the previous plots, Table 3 summaries volume dependencies simulated for finite core leak-off test at several permeabilities. Considering the results, the simulated data shows an unexpected tendency for water and gas cases, instead of square root of permeability behavior, de data could be fit using a different approach. The water invasion volume in single and combined case could be scaled using $k^{0.75}$, and gas cases can be scaled applying $k^{1.25}$. The use of simulation in combination with the accurate matching provide a feasible way to explore the limitations of the general accepted model, taking small steps in the way to produce more accurate and effective predicting tools.

	Fluid	$time$	$Permeability$
Single Invasion	Water	$t^{0.5}$	$k^{0.75}$
	Gas	t	$k^{1.25}$
Combined Invasion	Water	$t^{0.5}$	$k^{0.75}$
	Gas	t	$k^{1.25}$

Table 3: Finite core time and permeability dependencies.

4.5. SUMMARY

In this chapter I performed the permeability sensitives form 10 mD to 100 nD cores over the previous matched invasion tests. The simulations were run for three different cases: water invasion, gas invasion, and foam invasion. The results showed an unexpected permeability behavior, differing from the assumed general lek-off model square root of permeability. The dependency determined for water cases was $k^{0.75}$, and for gas cases $k^{1.25}$.

Chapter 5: Reservoir Leak-off Simulation

In this chapter, I attempt to simulate fluid leak-off behavior at reservoir conditions. The scope of the simulation is to reproduce the effect of water invasion, gas invasion, and foam invasion into a semi-infinite domain. The first driver over those simulations, was the determination of the reservoir length that suits the semi-infinite pressure wave effect on the 100nd ultra-low permeability rock. Once the reservoir pressure behavior was achieved, the invasion data was compared to validate general leak-off assumptions in the reservoir zone on each of the three invasion cases.

5.1. FIELD CONDITIONS

The pressure behavior is the main parameter to perform a valid reservoir like leak-off simulation. The key factor is to determine the simulation length that suits the semi-infinite rock behavior keeping the injection pressure constant along two hours fracturing job. The length depends directly on the rock and fluid properties, and it is affected by the interacting phases (two or three) on each case.

The simulation was performed over an imaginary reservoir with 3.000 psi of initial pressure. The expected temperature for this reservoir will be 200°F corresponding to a reservoir near 10.000 feet of depth. The pressure difference expected to perform the fracturing is 1.500 psi, which is equivalent to a constant injection pressure of 4500 psi along the 2 hours job, the maximum exposure time. Fluid properties were recalculated using Win Prop module considering the new pressure and temperature conditions enunciated above. Table 4 summarize the general simulation parameters to continue with the simulation length determination section.

RESERVOIR		
Initial Pressure	3.000 psi	
Temperature	200F	
Permeability	10mD-100 nD	
Porosity	0.22	
Model	Black-Oil	
# wells	1	**CONSTRAINS**
Injectors	1	4.500 psi BHP
Producers	0	

Table 4: Semi-infinite core simulation parameters.

5.2. CORE SCALE DETERMINATION

The reservoir condition problem studied is analogous to a semi-infinite one-dimensional core with one constant pressure boundary condition on the side. This assumption is made because the fractures are long and parallel favoring the linear fluid movement inside the reservoir. To determined proper reservoir simulation length, the analytical solution for this problem is described in Figure 32, which shows a schematic interpretation of the described time dependent problem.

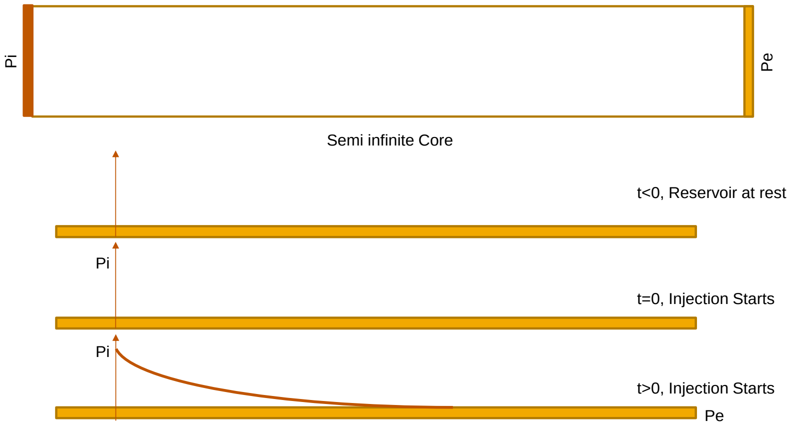

Figure 32: One dimensional semi-infinite problem. Schematic representation of the time dependent problem.

The stated problem is addressed considering the following assumptions: one-dimension, single-phase flow, homogeneous permeability, negligible gravity effects, small fluid compressibility.

$$P = P(x,t) \qquad [5.1]$$

Starting with Darcy's law statement small compressibility by Muskat (1983) among others, and mass conservation we can obtain an equation for P as a function of x and t, Deen (1998). The equation satisfies this condition is equation [5.2]:

$$\frac{\partial P}{\partial t} = \alpha \frac{\partial^2 P_x}{\partial x^2} \qquad [5.2]$$

where,

$$\alpha = \frac{k k_{rl}}{\phi c_t \mu_l} \quad \left[\frac{length^2}{time}\right] \qquad [5.3]$$

This problem obeys the following conditions

- $I.C.: At\, t \leq 0,\ P = 0,\ for\, all\, x$
- $B.C.1{:}\ At\, x = 0,\ P = P_i,\ for\, all\, t > 0$
- $B.C.2{:}\ At\, x = \infty,\ P = P_e,\ for\, all\, t > 0$

The following solution was developed by Carslaw & Jaegger (1954) in an analogous heat transfer on semi-infinite rod problem:

Dimensionless Pressure:

$$\phi = \frac{P(x,t) - P_e}{P_i - P_e}$$

$$\frac{\partial \phi}{\partial t} = \alpha \frac{\partial^2 \phi}{\partial x^2}$$

$$\phi = \phi(\eta), \quad \eta = \frac{x}{\sqrt{4\alpha t}} \text{(Dimensionles relation between varibles)}$$

$$\frac{\partial \phi}{\partial t} = \frac{\partial \phi}{\partial \eta}\frac{\partial \eta}{\partial t} = -\frac{1}{2}\frac{\eta}{t}\frac{\partial \phi}{\partial \eta}$$

$$\frac{\partial \phi}{\partial x} = \frac{\partial \phi}{\partial \eta}\frac{\partial \eta}{\partial x} = \frac{\partial \phi}{\partial \eta}\frac{1}{\sqrt{4\alpha t}}$$

$$\frac{\partial^2 \phi}{\partial x^2} = \frac{\partial^2 \phi}{\partial \eta^2}\frac{1}{4\alpha t}$$

Then,

$$\frac{\partial^2 \phi}{\partial \eta^2} + 2\eta \frac{\partial \phi}{\partial \eta} = 0$$

Now,

$$B.C.1\text{: } At\, \eta = 0, \quad \phi = 1$$

$$B.C.2\text{: } At\, \eta = \infty, \ \phi = 0$$

$$\psi = \frac{\partial \phi}{\partial \eta} = C_1 expt(-\eta^2)$$

Second Integration:

$$\phi = C_1 \int_0^n expt(-\bar{\eta}^2) + C_2$$

Applying the two Boundary Conditions:

$$\phi(\eta) = 1 - \frac{\int_0^{\eta} e^{\left(-\bar{\eta}^2\right)}}{\int_0^{\infty} e^{\left(-\bar{\eta}^2\right)}} = 1 - \frac{2}{\sqrt{\pi}} \int_0^{\eta} e^{\left(-\bar{\eta}^2\right)} = 1 - \operatorname{erf}(\eta)$$

$$\frac{P(x,t) - P_e}{P_i - P_e} = 1 - \operatorname{erf}\left(\frac{x}{\sqrt{4\alpha t}}\right) = \operatorname{erfc}\left(\frac{x}{\sqrt{4\alpha t}}\right)$$

$$\boldsymbol{P(x,t) = erf\mathbf{c}\left(\frac{x}{\sqrt{4\alpha t}}\right)(P_i - P_e) + P_e} \qquad [5.4]$$

The next parameters were used to determine diffusivity constant described in equation [5.3]: k=100 nD, $k_{rl} = 1$, ϕ=0.22, $C_t = 3 * 10^{-5} psi^{-1}$, $\mu_l = 1.04\ cp$.

$$\alpha = \frac{100}{0.22 * 3x10^{-5}\ psi^{-1} * 0.4cp}$$

$$\alpha = \frac{9.87 * 10^{-16}}{0.22 * 3x10^{-5}\ psi^{-1} * 6.44 * 10^{-8}} = 2.32 * 10^{-3} \left[\frac{cm^2}{sec}\right]$$

With the determined diffusivity constant α, we can predict the necessary core length at which the pressure falls less than 1% using the equation [5.5]:

$$4\sqrt{\alpha t} \qquad [5.5]$$

$$t = \ Frac\,Job \ = 7200\ seconds$$

$$4\sqrt{2.32 * 10^{-3} * 7200} = \mathbf{16.35\ \boldsymbol{cms}}$$

Finally, to simulate the 100nd reservoir conditions along the two hours fracturing job, it is necessary a core with minimum 17 centimeters length. Moreover, Figure 33 shows the determined core lengths to simulate proper reservoir conditions over 10mD, 1mD, 10µD, and 100nD rocks.

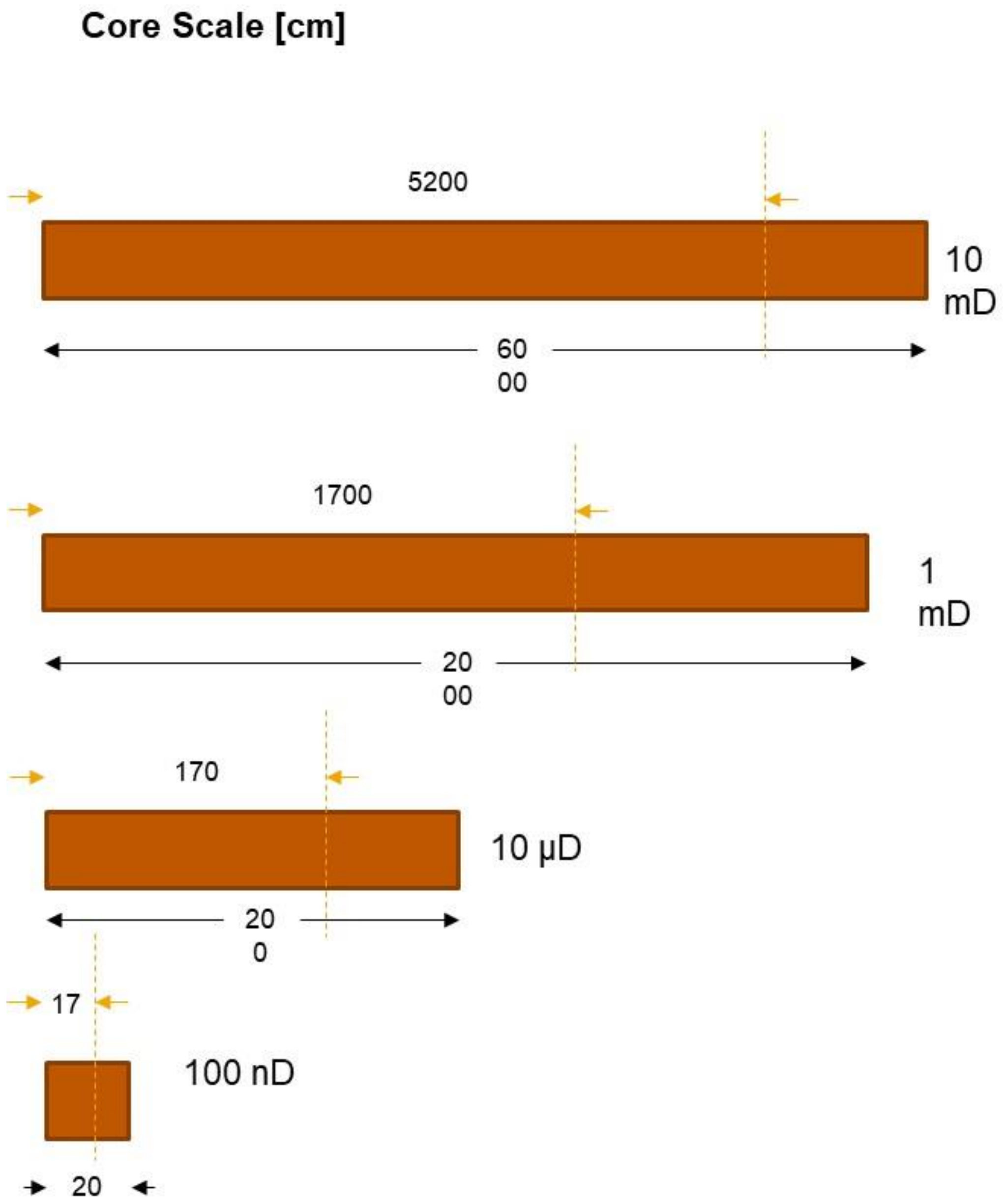
Core Scale [cm]
5200
10 mD
60 00
1700
1 mD
20 00
170
10 µD
20 0
17
100 nD
20

Figure 33: Semi-infinite behavior core lengths. Needed Core lengths for permeabilities ranging from 10md to 100nd cores were found using penetration thickness equation.

Figure 34 shows the results of the first simulation case following the stated parameters using oil as injected fluid. The most relevant detail in this case is the accurately match between the analytical solution and the numerical simulation. Now single-phase modeling fits, I feel confident to used numerical simulation to model multiphase flow that corresponds to water invasion, gas invasion, and foam invasion.

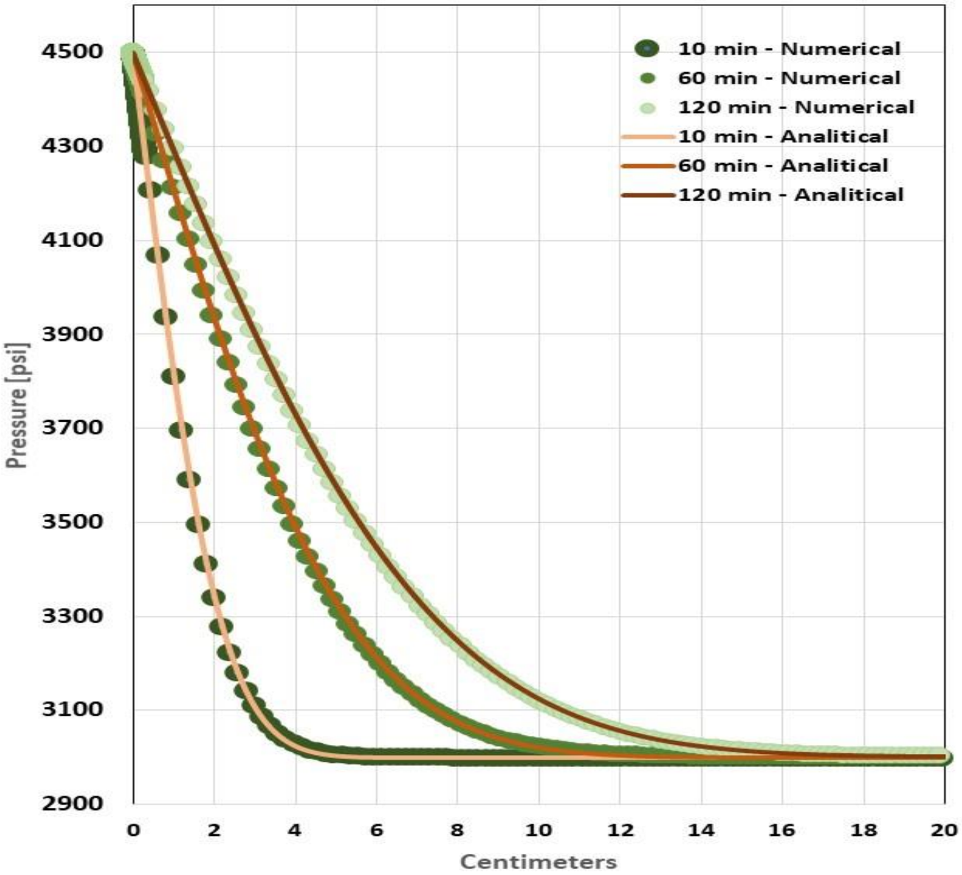

Figure 34: Analytical versus numerical solution for one phase problem. Numerical and analytical solution profiles are compared at 10, 60, and 90 minutes on a 100 nanodarcy 20 centimeters reservoir. Injection pressure: 4,500 psi, reservoir pressure 3,000 psi.

5.3. WATER INVASION

In this section I attempt to reproduce reservoir conditions to explore the behavior of water invasion in an ultra-low permeability 100 nanodarcy reservoir. The test was run to mimic the two hours exposure fracturing job in a time were the constant injection pressure constrain will introduce water into the fully oil saturated porous media.

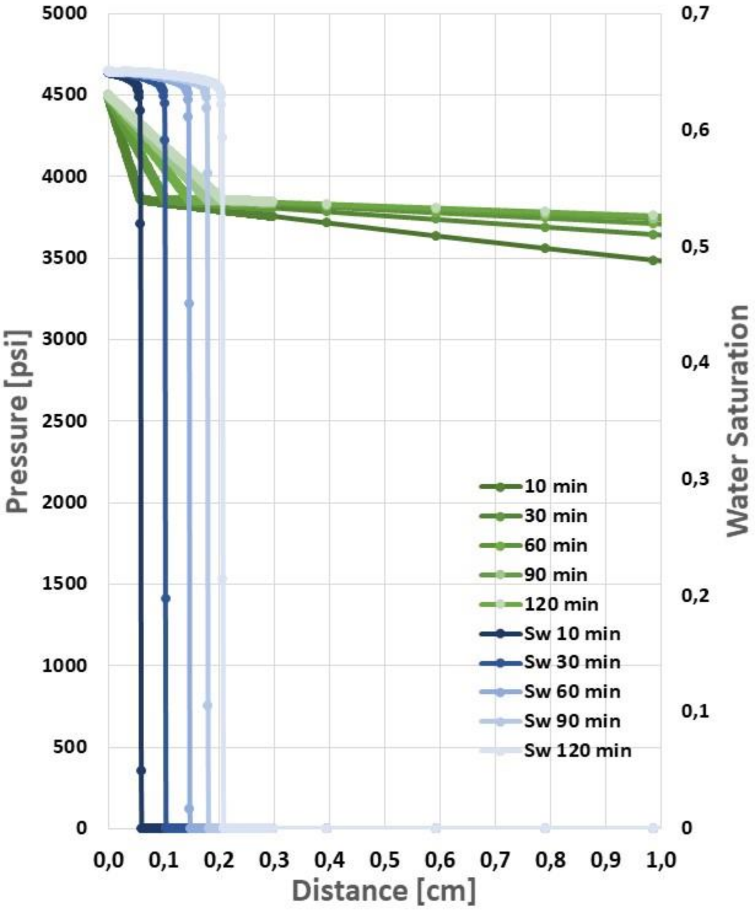

Figure 35: Water Saturation and pressure profiles. One-centimeter zooms over single water invasion simulated in a 100nd reservoir; initial pressure of 3,000 psi. The water was injected at constant pressure of 4,500 psi along the simulated invasion. The shown values were pick at a simulated time of 10, 30, 60 and 120 minutes.

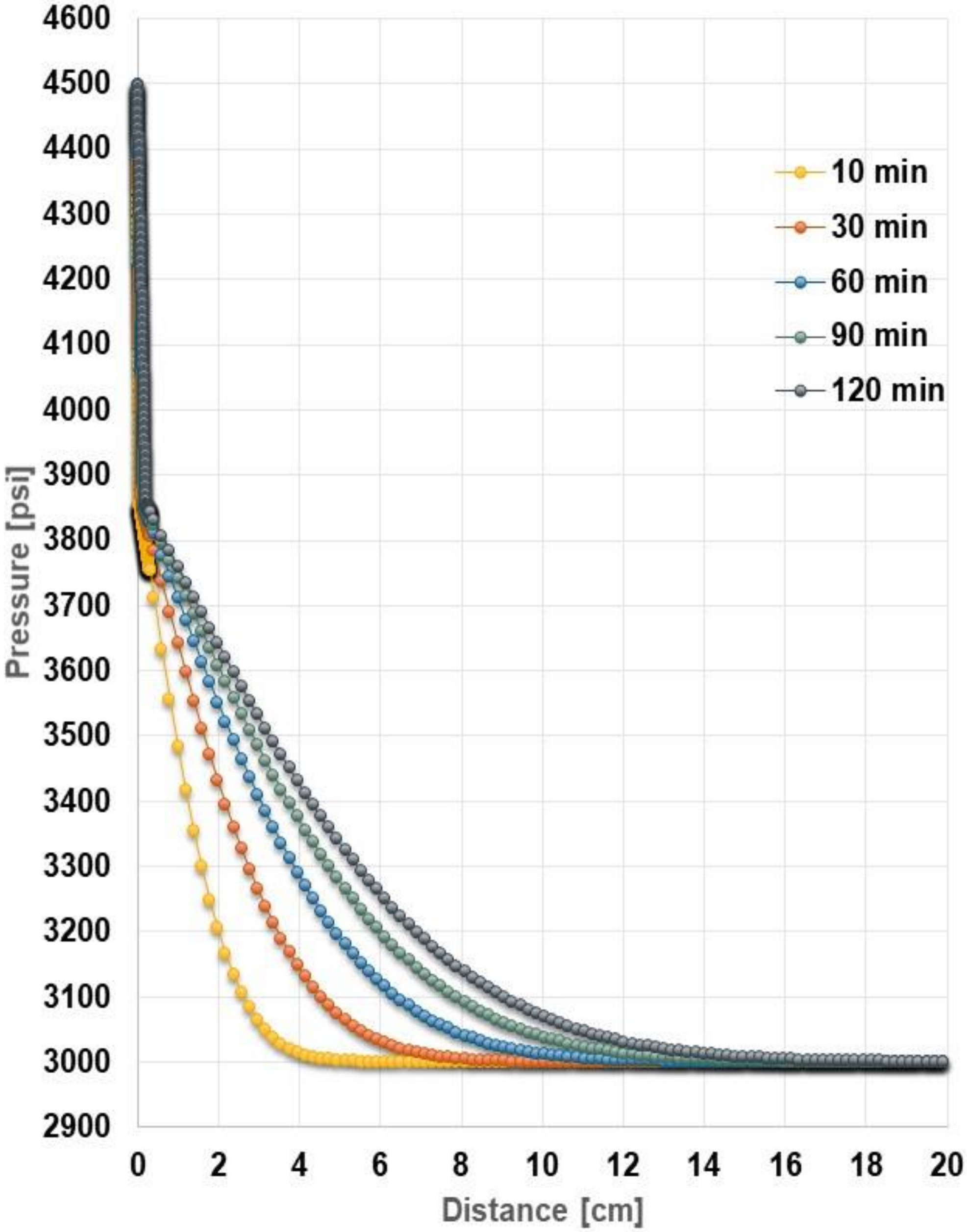

Figure 36: Pressure profile. Single water invasion simulation; 20 centimeters 100 nD reservoir. Injection pressure 4,500 psi, reservoir pressure 3,000 psi. The shown values were pick at a simulated time of 10, 30, 60 and 120 minutes.

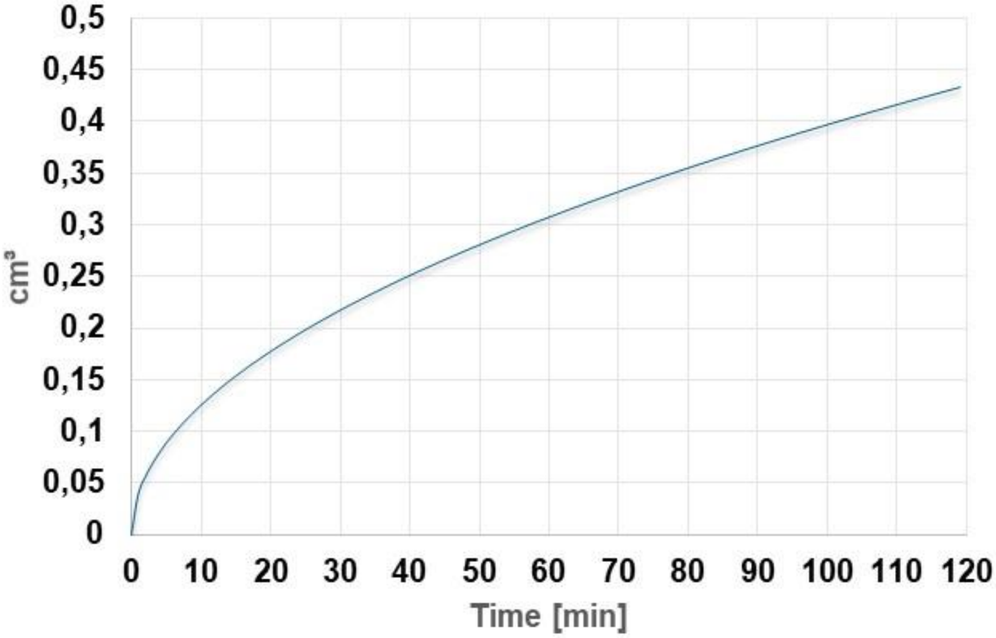

Figure 37: Water cumulative invaded volume. Single water invasion simulation on 100nd reservoir. Injection pressure 4,500 psi, reservoir pressure 3,000 psi. Volume at reservoir conditions.

Figures 35, 36, and 37 show saturation profile, pressure profile, cumulative invaded volume, respectively. The resultant saturation profile in Figure 35 shows water invasion of 0.2 centimeters at the end of the two hours exposure, therefore just 1% of the core was invaded comparing with the pressure wave propagation inside the reservoir. This can be compared to the pressure wave which propagates 17 centimeters into the reservoir.

Figure 36 presents the total pressure distribution along the reservoir, showing the boundary condition in the injector well is achieved. In the waterfront the injection pressure drops around 650 psi, which is the approximate 43% of the total pressure difference between injector well bottom-hole pressure and the initial pressure along the reservoir.

Finally, Figure 37 presents the invaded volume behavior that follows the expected square root of time dependency stated in the general leak-off model (Settari A. , 1985). The maximum water volume in the reservoir after two hours was 0.43 cubic centimeters, and the determined leak-off coefficient was 0.000233 $\frac{ft}{\sqrt{min*\mathrm{m}Darcy*psi}}$. According to the general leak-off model statements, the same leak-off value is expected in other scenarios where only permeability is changed (Settari A. , 1988).

5.4. GAS INVASION

We now analyze the single gas invasion case in 100nD permeability reservoir following the process applied in the single water invasion case. Figures 38, 39, and 40 show saturation profiles, pressure profiles, and cumulative invaded volumes, respectively.

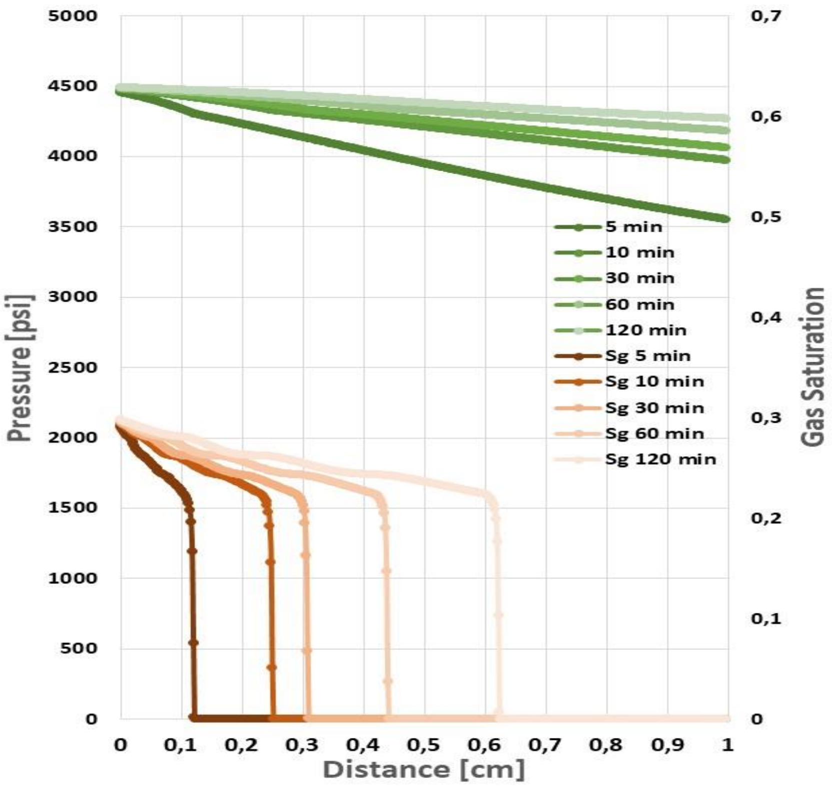

Figure 38: Gas Saturation and pressure profiles. One-centimeter zooms over single gas invasion simulated in a 100nd reservoir; initial pressure of 3,000 psi. The gas was injected at constant pressure of 4,500 psi along the simulated invasion. The shown values were pick at a simulated time of 10, 30, 60 and 120 minutes.

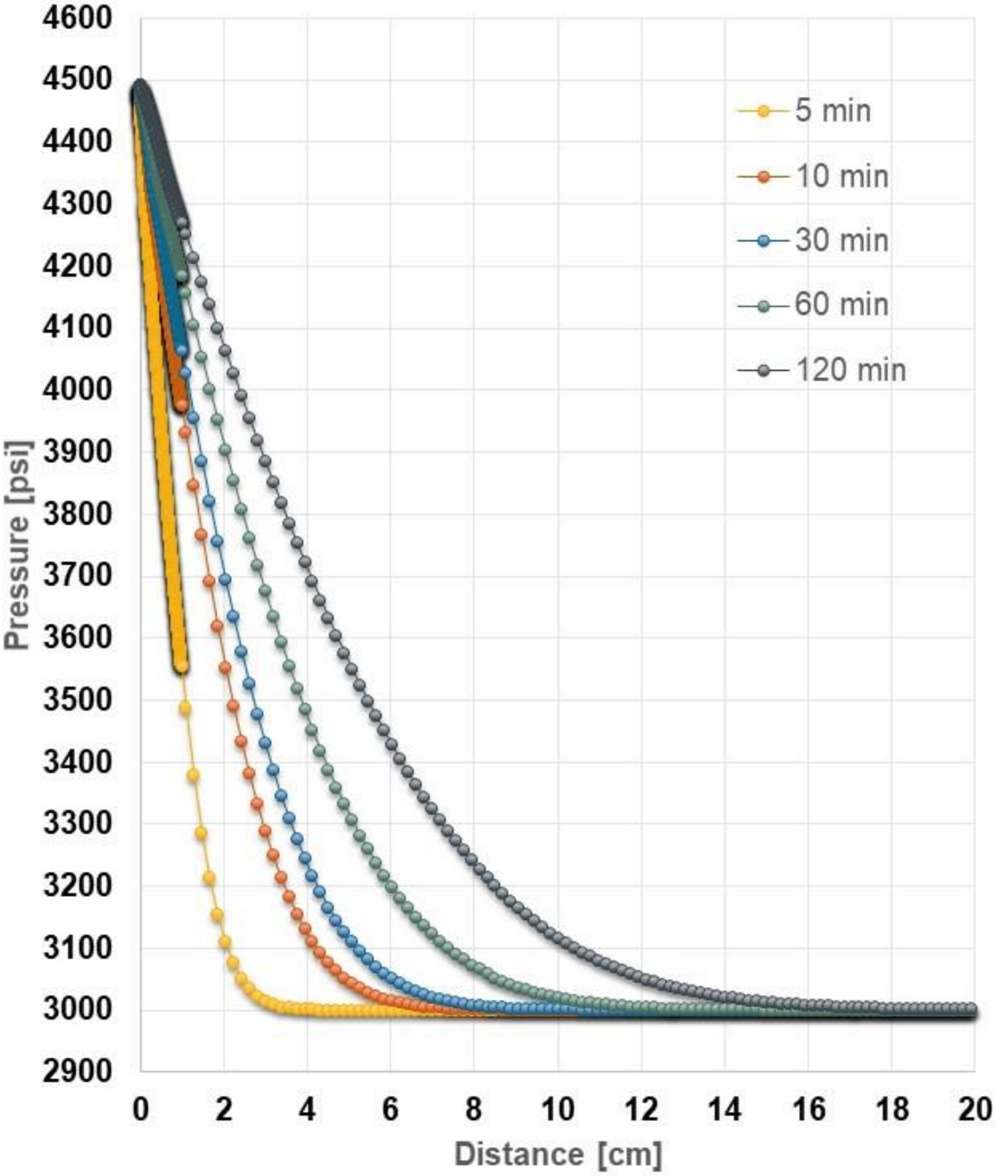

Figure 39: Gas pressure profile. Single gas invasion simulation; 20 centimeters 100 nD core. Injection pressure 4,500 psi, reservoir pressure 3,000 psi. The shown values were pick at a simulated time of 5, 10, 30, 60 and 120 minutes.

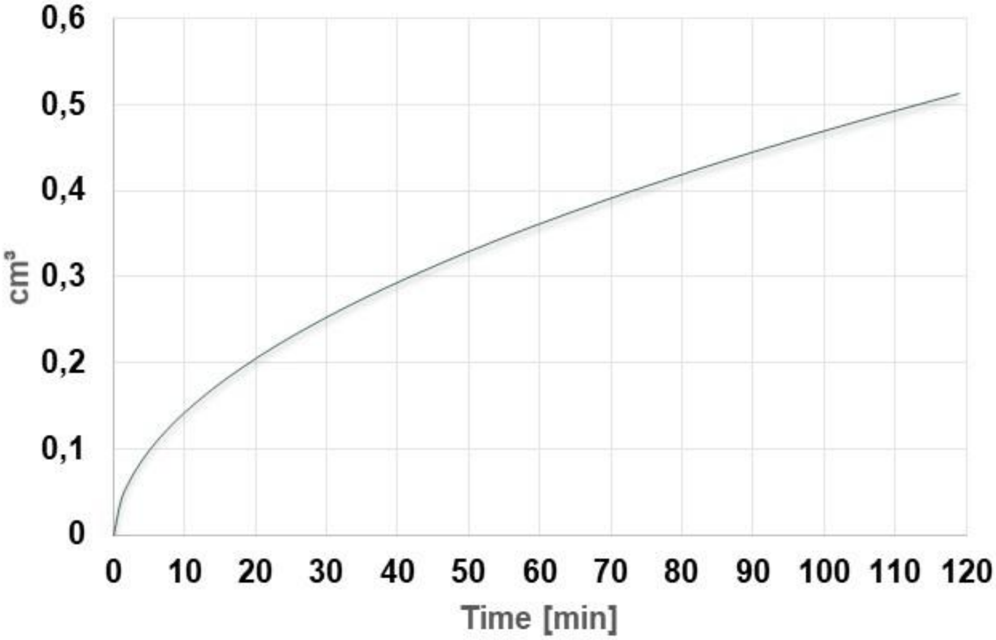

Figure 40: Gas cumulative volume. Single gas invasion simulation on 100nd core. Injection pressure 4,500 psi, reservoir pressure 3,000 psi. Volume at reservoir conditions.

Figure 38 presents saturation profiles. In this scenario the gas invades almost three times faster than water over the same time periods, this difference can be attributed to fluid mobility differences caused by the lower gas viscosity compared with the water.

In addition to saturation profiles, Figure 39 shows the ratio between fluid invasion and wave propagation is around the 3%, 3 times bigger than the single water invasion case. After 0.6 centimeters a pure compressibility pressure behavior is seen along the simulated reservoir. Moreover, the injection pressure took a minimal pressure drop perturbation in the gas front, differing from the water invasion case were 43% of the injection pressure drop took place behind the waterfront.

Finally, Figure 40 shows the gas cumulative volume profile seems to follow a square root of time volume dependency disagreeing with the observed linear behavior on finite core simulations. Moreover, this profile is congruent with general leak-off model assumptions that fit square root of time dependency (Settari A. , 1985). The estimated leak-off coefficient for this case is 0,000273 $\frac{ft}{\sqrt{min*\mathrm{m}Darcy*psi}}$, a close value to the earlier calculated water leak-off coefficient.

5.5. FOAM INVASION (COMBINATION)

We now look at the foam invasion case in 100nD permeability reservoir. Figures 41, 42 and 43, and 45 and 45 show pressure profiles, spatial invasion of both water and gas, and total volume invasion of water and gas, respectively.

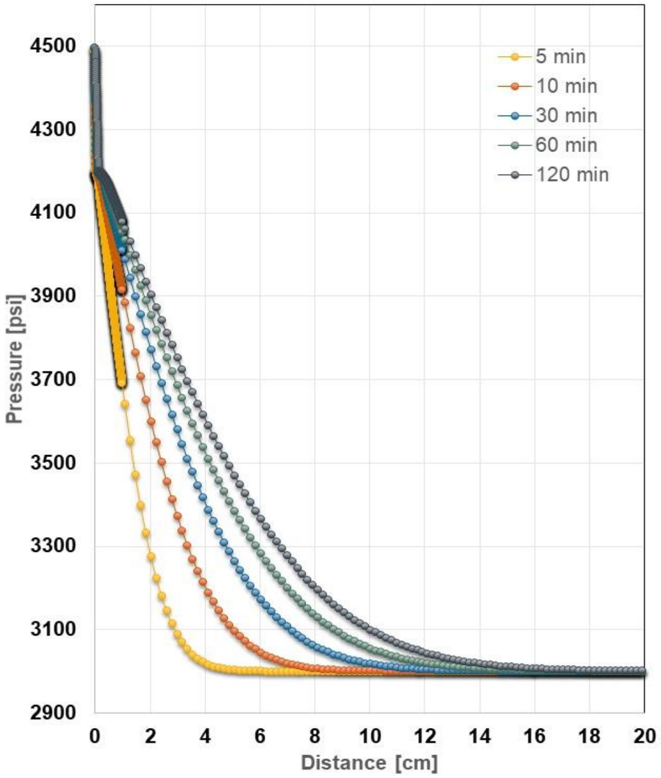

Figure 41: Pressure profile. Simultaneous gas and water invasion simulation; 20 centimeters 100 nD core. Injection pressure 4,500 psi, reservoir pressure 3,000 psi. The shown values were pick at a simulated time of 5, 10, 30, 60 and 120 minutes.

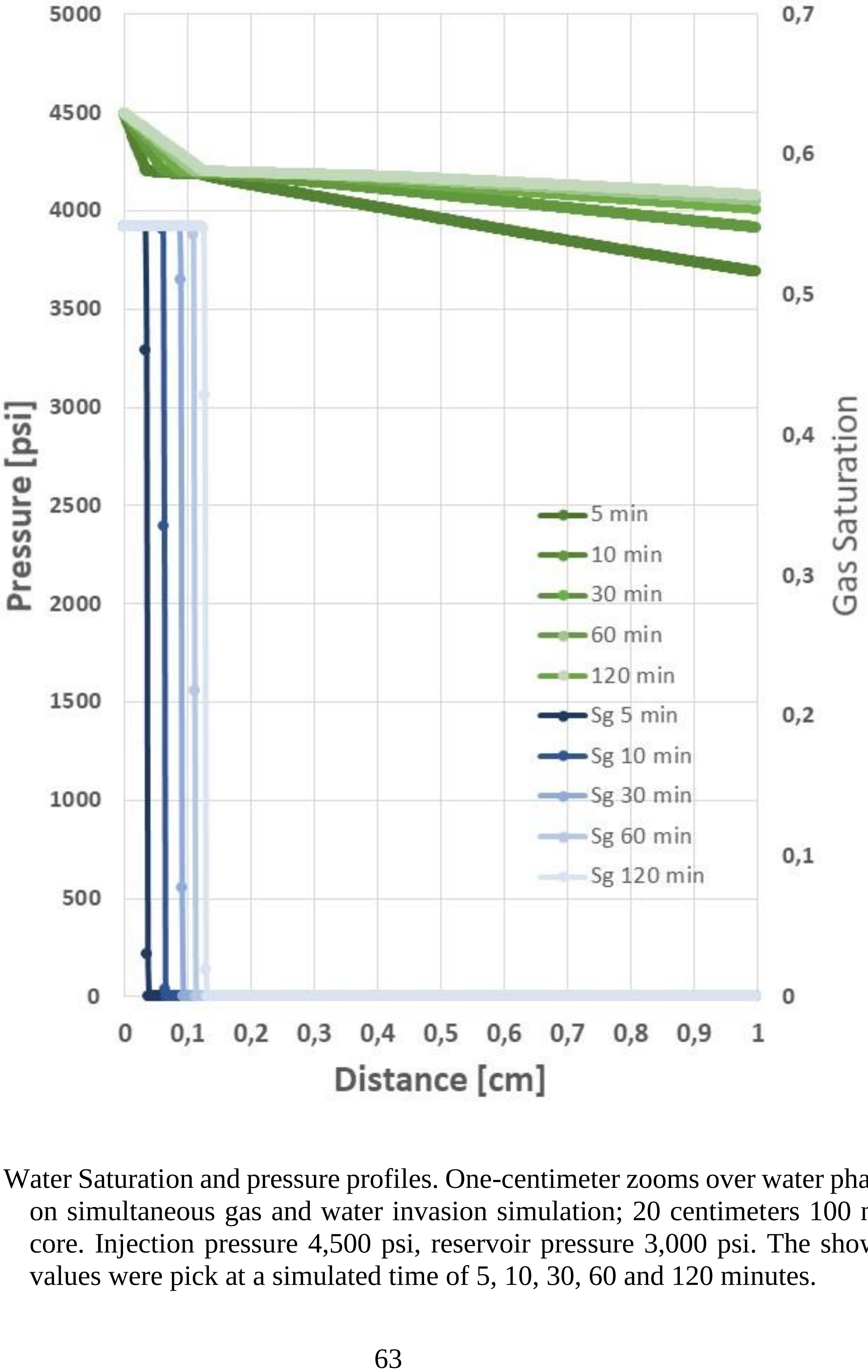

Figure 42: Water Saturation and pressure profiles. One-centimeter zooms over water phase on simultaneous gas and water invasion simulation; 20 centimeters 100 nD core. Injection pressure 4,500 psi, reservoir pressure 3,000 psi. The shown values were pick at a simulated time of 5, 10, 30, 60 and 120 minutes.

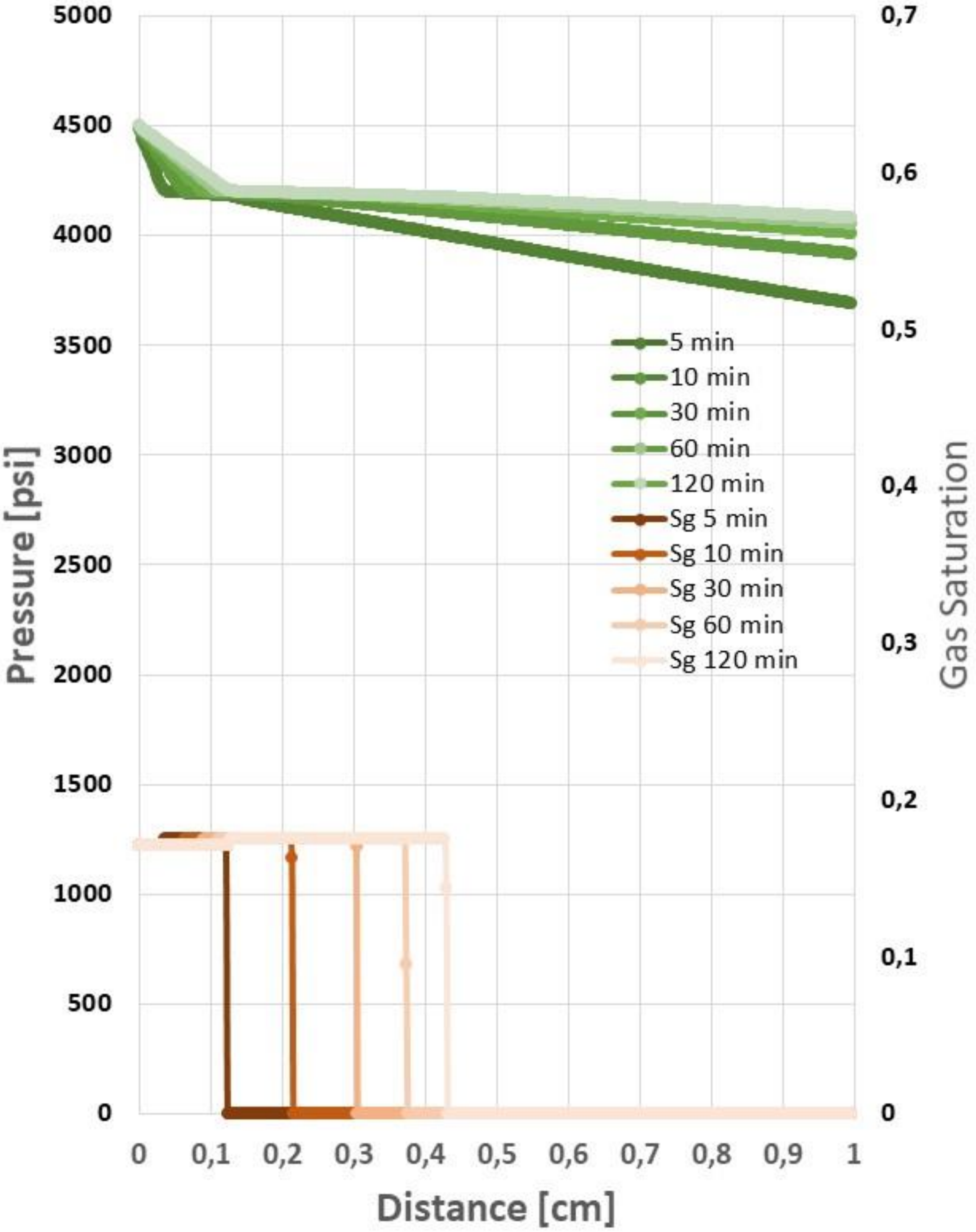

Figure 43: Gas saturation and pressure profiles. One-centimeter zooms over gas phase on simultaneous gas and water invasion simulation; 20 centimeters 100 nD core. Injection pressure 4,500 psi, reservoir pressure 3,000 psi. The shown values were pick at a simulated time of 5, 10, 30, 60 and 120 minutes.

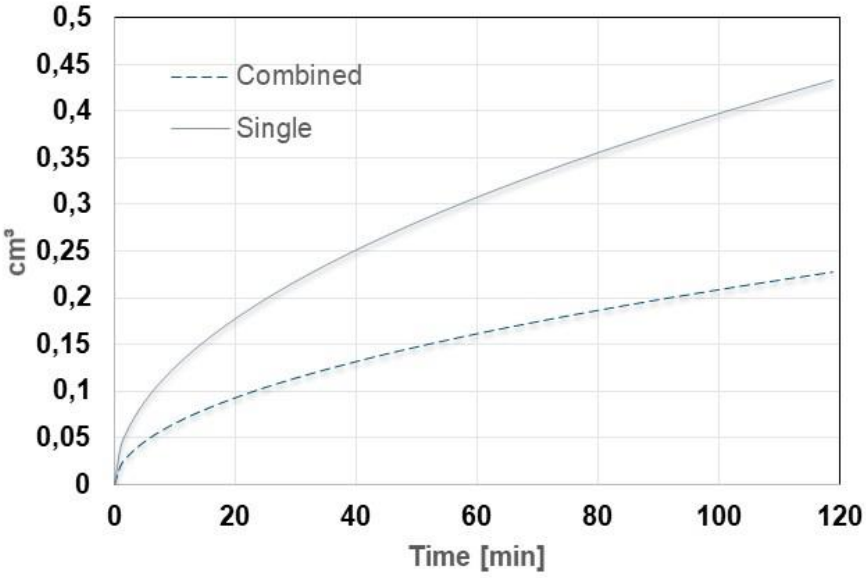

Figure 44: Cumulative volumes. Water cumulative volume comparison between single invasion and combined invasion. Simultaneous gas and water invasion (combined) simulation on 100nd core. Injection pressure 4,500 psi, reservoir pressure 3,000 psi. Volume at reservoir conditions.

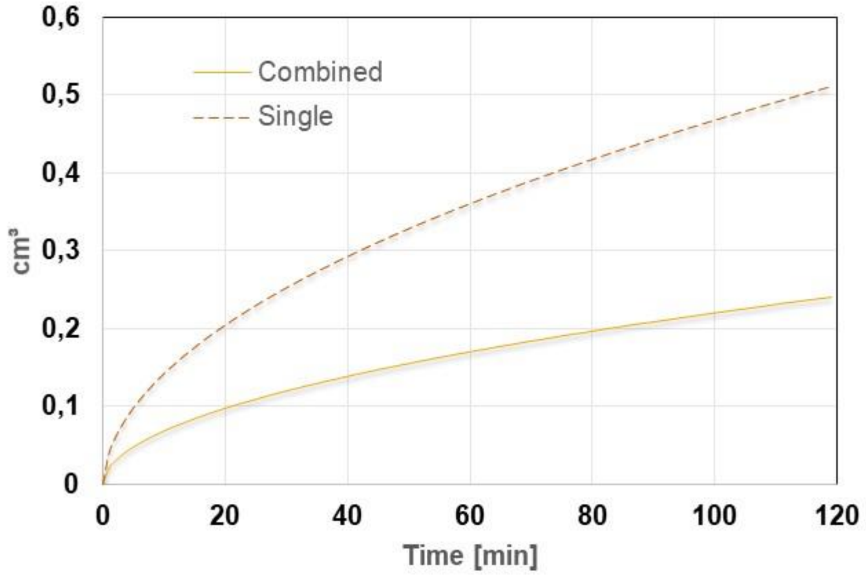

Figure 45: Cumulative volumes. Gas cumulative volume comparison between single invasion and combined invasion. Simultaneous gas and water invasion (combined) simulation on 100nd core. Injection pressure 4,500 psi, reservoir pressure 3,000 psi. Volume at reservoir conditions.

In this simulation the reservoir is invaded at the same time by water and gas generating the pressure distribution on Figure 41. The pressure profile exhibit three regions: the first corresponds to the waterfront effect where the 27% of the injection pressure drop took place, the second expose a minimal injection pressure drop attributable to gas compressibility, and the final region where pressure behavior is attributable to pure oil compressibility performance.

Saturations profiles shown in Figures 42 and 43, reveal a lower invasion velocity for both fluids, reduced between 1.5 to 2 times. The behavior in the saturation profiles could be attributable to the invasion competence between phases, which is materialized in the additional pressure drop one fluid cause to the other.

Ultimately, Figure 44 and 45 show the volume invasion decrease around 50% in the foam injection due to the competition between the two invading phases. The results in this chapter constitute the baseline to validate general leak-off model under reservoir conditions and supports the accepted general leak-off model time dependency (Settari A. , 1985). The obtained results open the path to verify the statements that structure fluid invasion at reservoir conditions, and supply the basis to propose a more accurate reservoir leak-off model.

5.6. SUMMARY

In this chapter, I corroborate the analytical solution for the one-dimensional, one-phase oil invasion at reservoir conditions. Furthermore, I used the simulator to solve two-phase cases: water invasion and gas invasion, and three-phase case: foam invasion. The simulations were performed over the stated reservoir conditions with a constant pressure injection boundary assuming the fluid invades the reservoir in one-dimension, perpendicular to the fracture propagation. The biggest injection pressure drops occurred behind the waterfront in the single water invasion case. The gas moved faster in the single invasion simulation case, and finally the foam case has the smallest invaded volumes over the three scenarios. The square root of time invaded volume leak-off dependency was validated for the three different invasion cases, therefore, other general leak-off model dependencies at reservoir condition will be evaluated in chapter 6.

Chapter 6: Semi-Infinite Core Leak-off Dependencies

In this chapter, I use the numerical model to understand how permeability, delta pressure, gas viscosity, and oil compressibility affect the leak-off rate in semi-infinite rectilinear flow. Some of those parameters were studied in previous chapters but here I focus my effort to validate the listed dependencies under the reservoir boundary conditions embodied in the semi-infinite core simulations. The goal of this chapter is to find the proper dependencies that describe fluid leak-off behavior at reservoir conditions devising new paths that aim future research on this topic.

6.1. PERMEABILITY DEPENDENCIES

The starting point in this chapter will be the approach to permeability dependencies. To conduct the analyses 12 simulation were performed to obtain the required information that depicts an overview of this problem. The data was obtained varying permeability from 10 millidarcy to 100 nanodarcy for the gas and water single invasion cases, and the foam invasion (simultaneous gas and water injection). Figures 46, 47, 48, and 49 show cumulative invaded volume, invasion length, invasion length versus square root of time, and invasion length versus permeability, respectively.

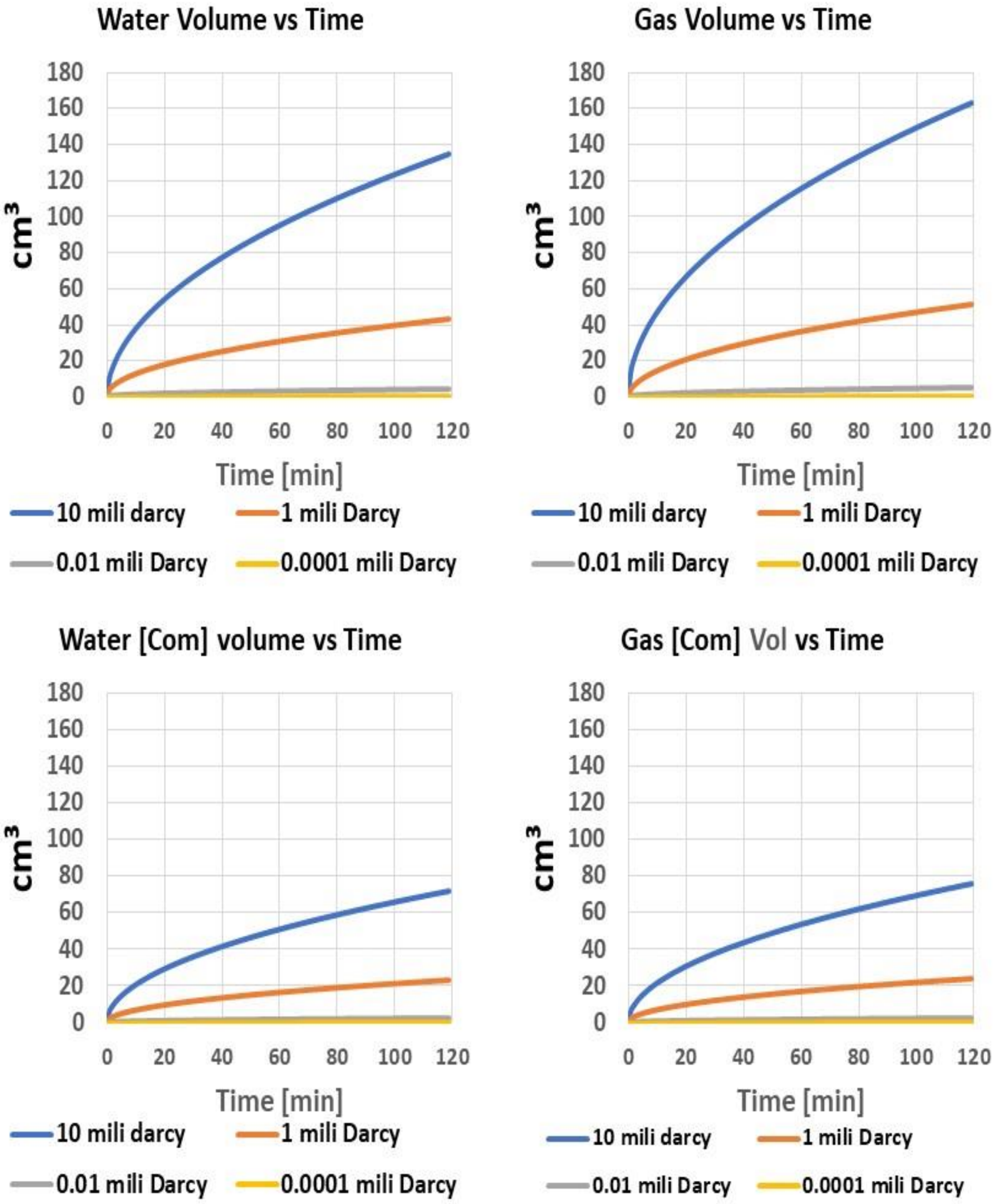

Figure 46: Cumulative volumes versus time plots. Single water invasion (top left), single gas invasion (top right), and simultaneous water and gas invasion (bottom row) were simulated in semi-infinite 10md to 100nd cores with initial pressure of 3,000 psi. The fluids were injected at constant pressure of 4,500 psi along the simulated invasion. The total simulated time was 120 minutes. Volumes at reservoir condition.

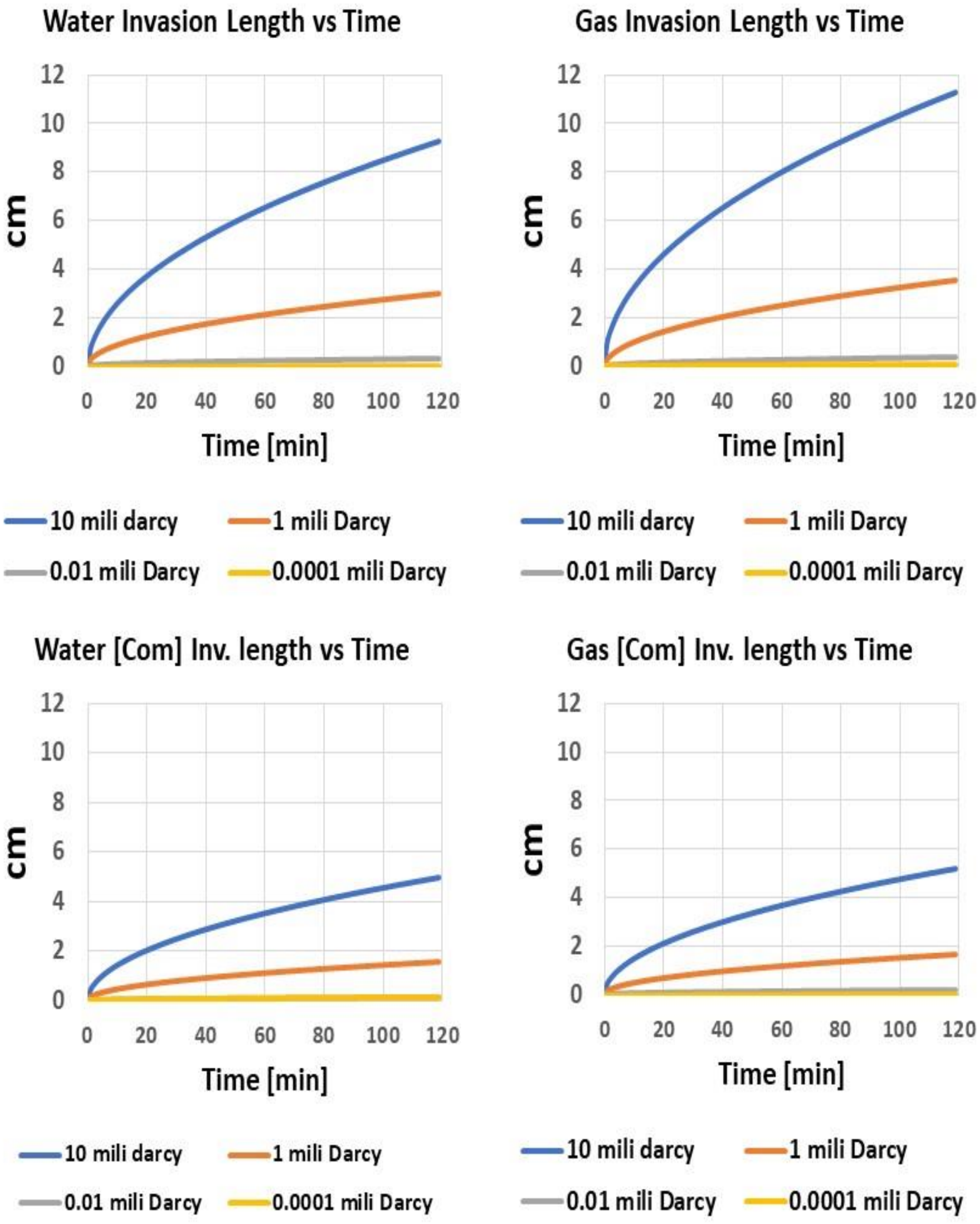

Figure 47: Invasion length versus time plots. Single water invasion (top left), single gas invasion (top right), and simultaneous water and gas invasion (bottom row) were simulated in semi-infinite 10md to 100nd cores with initial pressure of 3,000 psi. The fluids were injected at constant pressure of 4,500 psi along the simulated invasion. The total simulated time was 120 minutes.

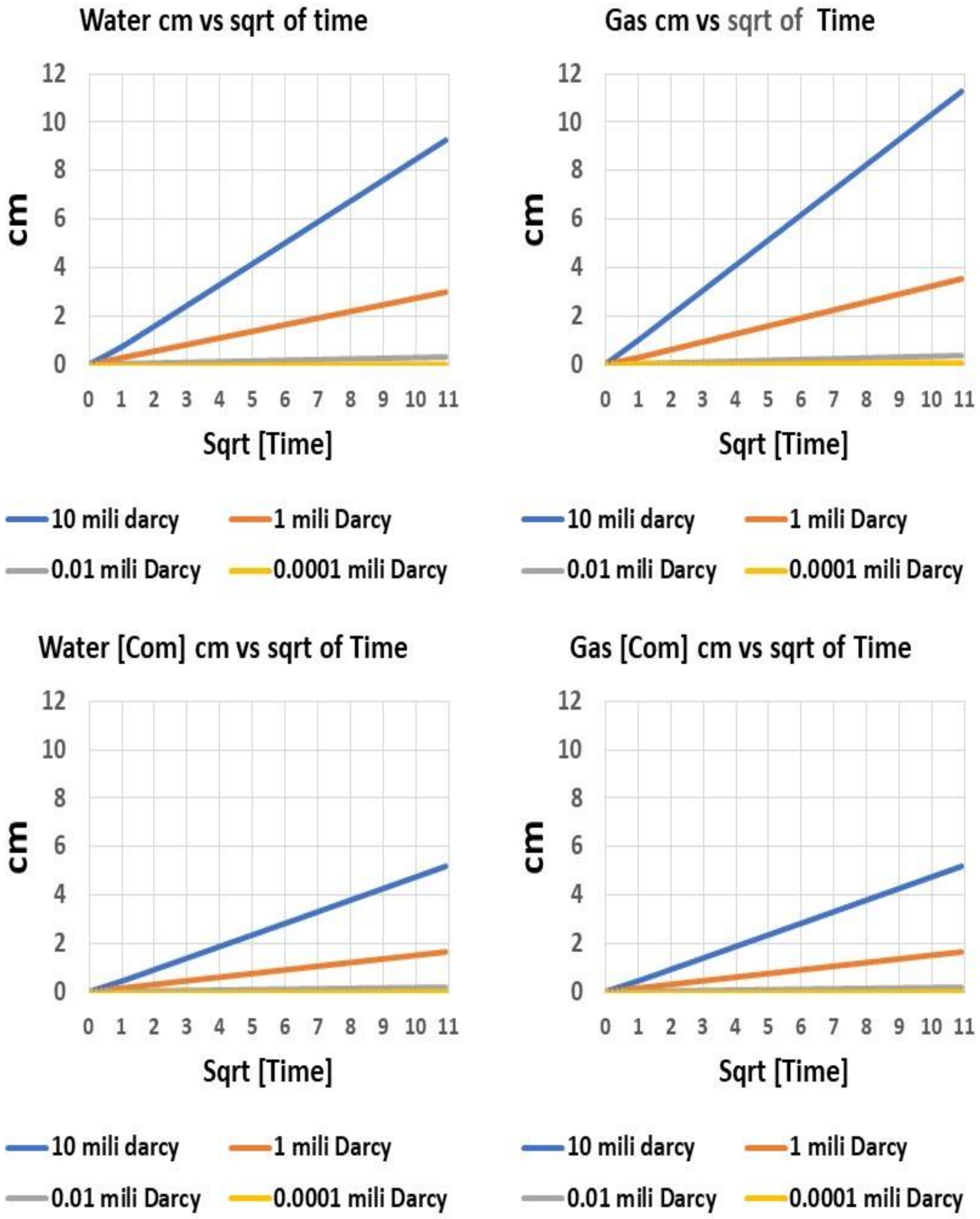

Figure 48: Invasion length vs sqrt of time plot. Single water invasion (top left), single gas invasion (top right), and simultaneous water and gas invasion (bottom row) were simulated in semi-infinite 10md to 100nd cores with initial pressure of 3,000 psi. The fluids were injected at constant pressure of 4,500 psi along the simulated invasion. The total simulated time was 120 minutes.

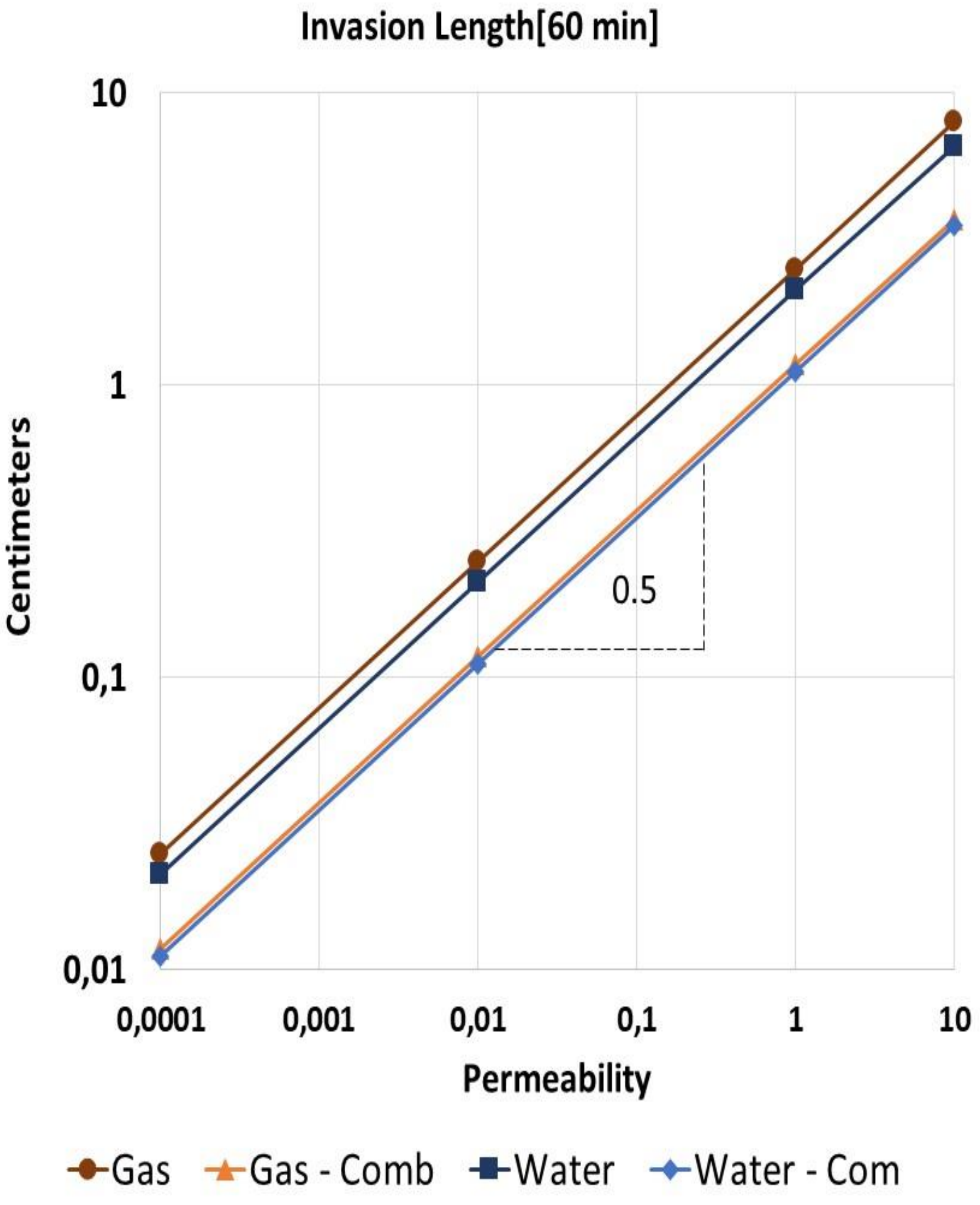

Figure 49: Invasion length versus Permeability plot. Single gas invasion, water invasion, and simultaneous water and gas invasion were simulated in a semi-infinite 10md to 100nd cores with initial pressure of 3,000 psi. The fluids were injected at constant pressure of 4,500 psi along the simulated invasion. The show values were pick at a simulated time of 60 minutes.

The simulated volumes versus time were compared on Figure 46 where square root of time volume dependency predominates in all cases. In contrast to the observed behavior of the gas single invasion in the finite core, the cumulative volume of the invaded gas at the reservoir conditions disagree from the previous observed linear time dependency. In addition, the same effect was seen in the foam case (simultaneous gas and water injection) where the cumulative volume for both phases is almost the same.

In the same way that the volume versus time profiles of Figure 46, the calculated invasion length profiles versus time in Figure 47 keep the square root of time dependency. The square root of time dependency is validated in Figure 48 where invasion length is plotted versus the square root of time. In the three invasion cases: single gas invasion, single water invasion, and foam (combined) a linear tendency is seen at every permeability sensitivity (10md, 1md, 10µd, and 100nd). The results suggest the permeability dependency can also be confirmed using a time dependent property plot.

Finally, Figure 48 shows: invasion length versus permeability at sixty minutes of simulated time in a log-log plot. The plot represents invasion length ratio of change when permeability varies at the same simulated time. Here it is possible to see that the four different profiles share the same slope of 0.5, which indicates permeability has the same square root proportionality independently of the fluid nature. The same dependency was determined in the general leak-off model where the kind of fluid is not considered in the square root of permeability leak-off dependency (Settari A. , 1985).

6.2. PRESSURE DEPENDENCIES

In addition to the permeability effect on the leak-off phenomena, the next fundamental parameter is the pressure dependency between the injection pressure and the reservoir pressure. The invasion length is affected proportionally by the pressure difference applying the square root of pressure difference in concordance with the general leak-off model (Settari A. , 1985). To validate the previous assumption, several simulation sensitivities were executed with the following parameters.

The simulations were run over eighteen scenarios varying pressure difference from 250 psi to 2500 psi; the initial pressure in the reservoir was set constant at 3,000 psi, then the changed parameter was the injection pressure from 3,250 psi, in the first scenario, to 3,500 psi, 4,000 psi, 4,000 psi, 5,000 psi, and finally 5,500 psi. Those pressure sensitivities where run for the three different invasion cases: single gas invasion, single water invasion, and simultaneous gas and water (foam) invasion. Those cases were run using the 100 nanodarcy reservoir baseline parameters and keeping constant the earlier rock-interactions to control the noise related to other variables. Figures 50, 51, 52, 53 and 54 show the cumulative volumes, invasion length, invasion length versus square root of time, invasion length versus pressure, and invasion length versus pressure varying gas viscosity, respectively.

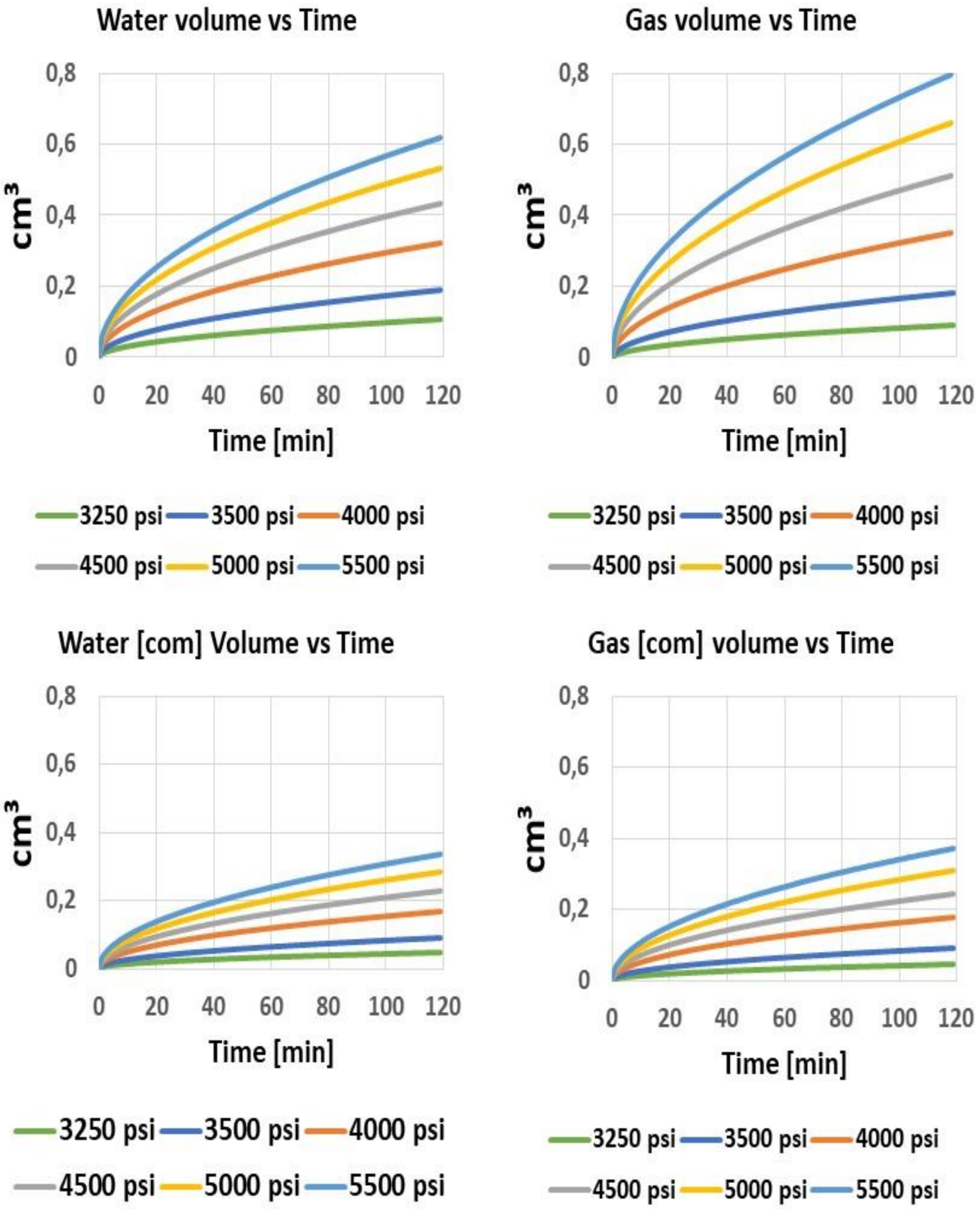

Figure 50: Cumulative volumes versus time plots. Single water invasion (top left), single gas invasion (top right), and simultaneous water and gas invasion (bottom row) were simulated in semi-infinite 100nd core with an initial pressure of 3,000 psi. The fluids were injected at constant pressure varying from 3,250 psi to 5,500 psi along the simulated invasions. The total simulated time was 120 minutes. Volumes at reservoir condition.

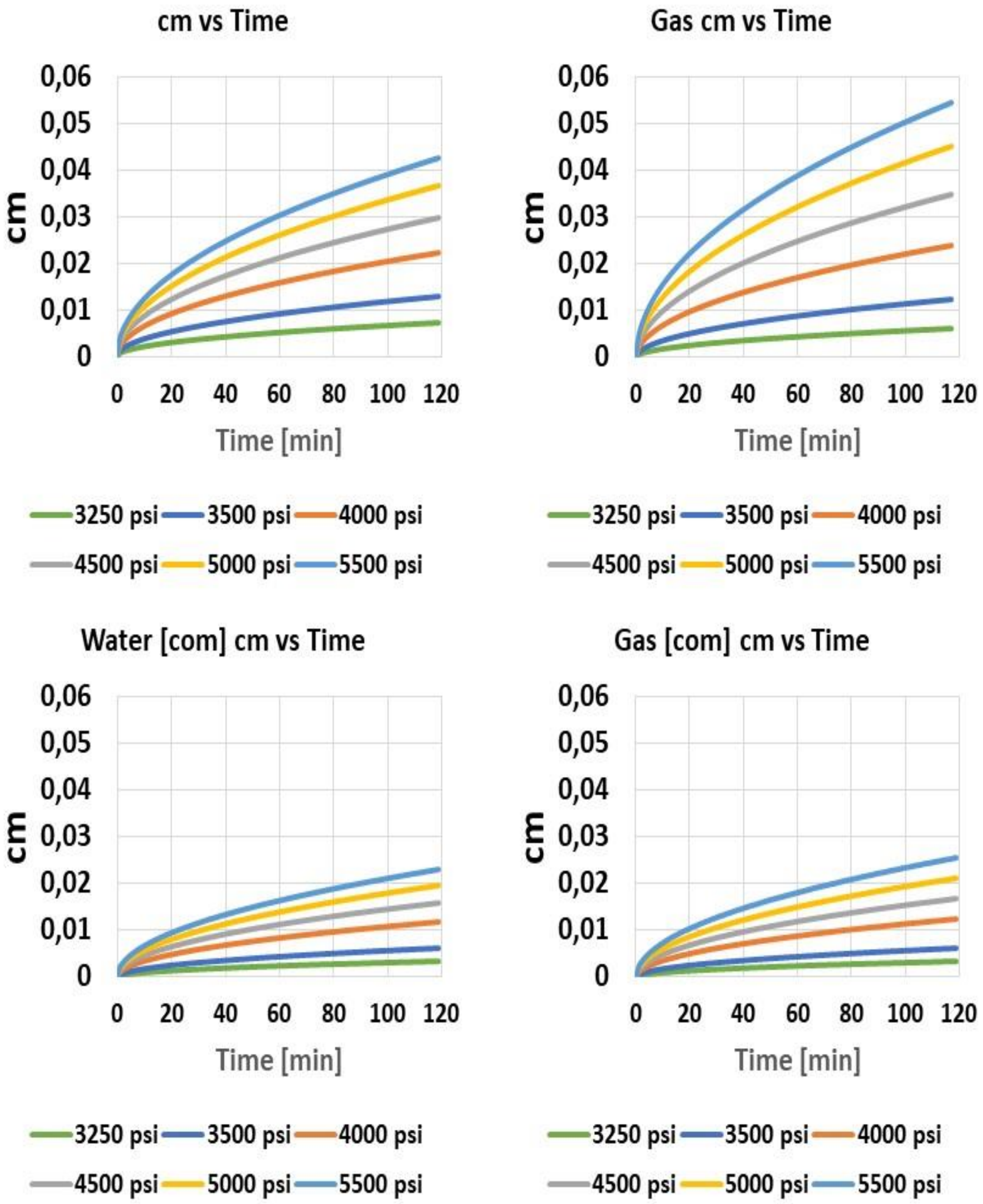

Figure 51: Invasion length versus time plots. Single water invasion (top left), single gas invasion (top right), and simultaneous water and gas invasion (bottom row) were simulated in semi-infinite 100nd core with an initial pressure of 3,000 psi. The fluids were injected at constant pressure varying from 3,250 psi to 5,500 psi along the simulated invasions. The total simulated time was 120 minutes.

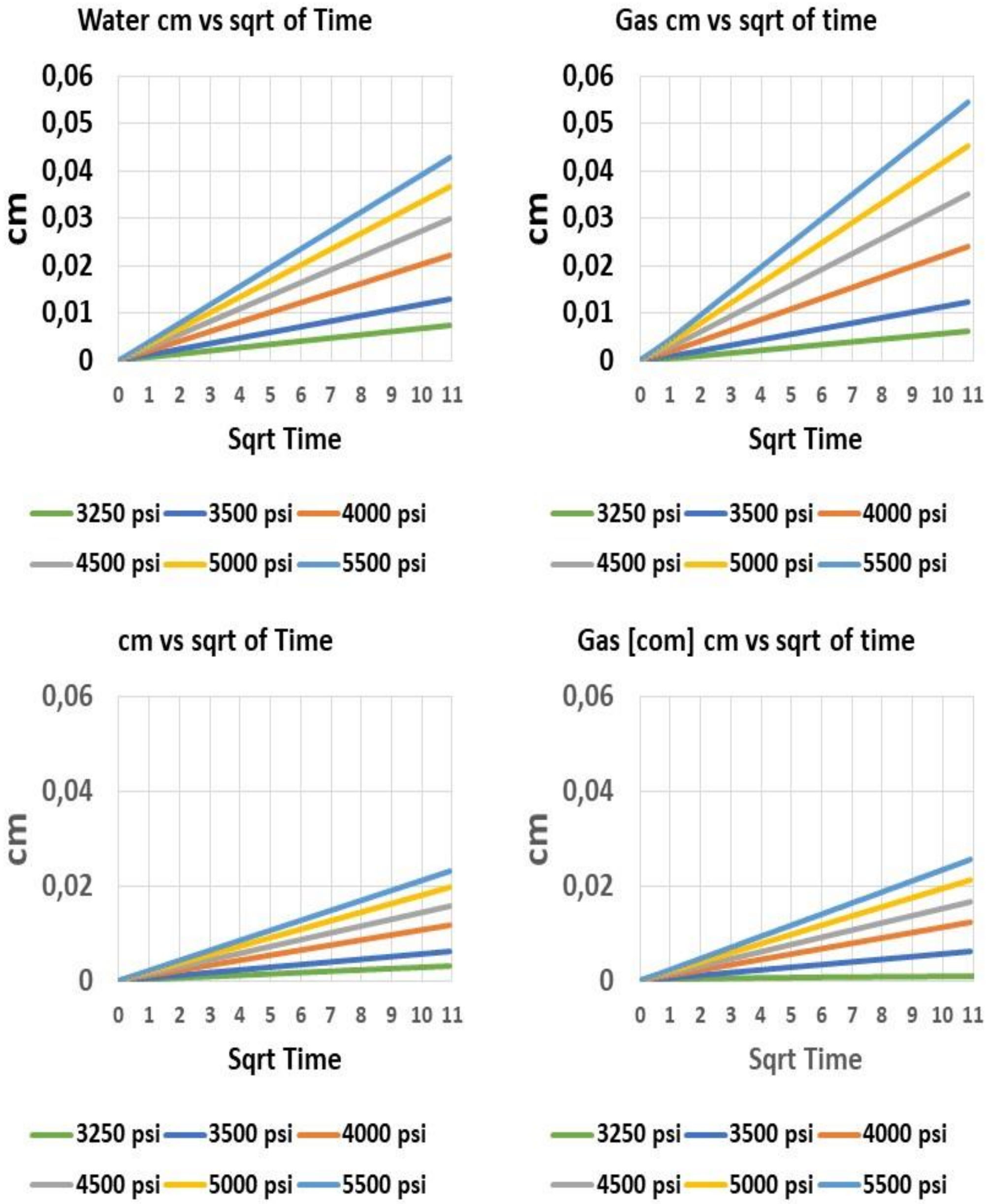
Water cm vs sqrt of Time

Gas cm vs sqrt of time

cm vs sqrt of Time

Gas [com] cm vs sqrt of time

Figure 52: Invasion length versus square root of time plots. Single gas invasion, water invasion, and simultaneous water and gas invasion were simulated in a semi-infinite 100nd core with an initial pressure of 3,000 psi. The fluids were injected at constant pressure varying from 3,250 psi to 4,500 psi along the simulated invasion. The show values were pick at a simulated time of 60 minutes.

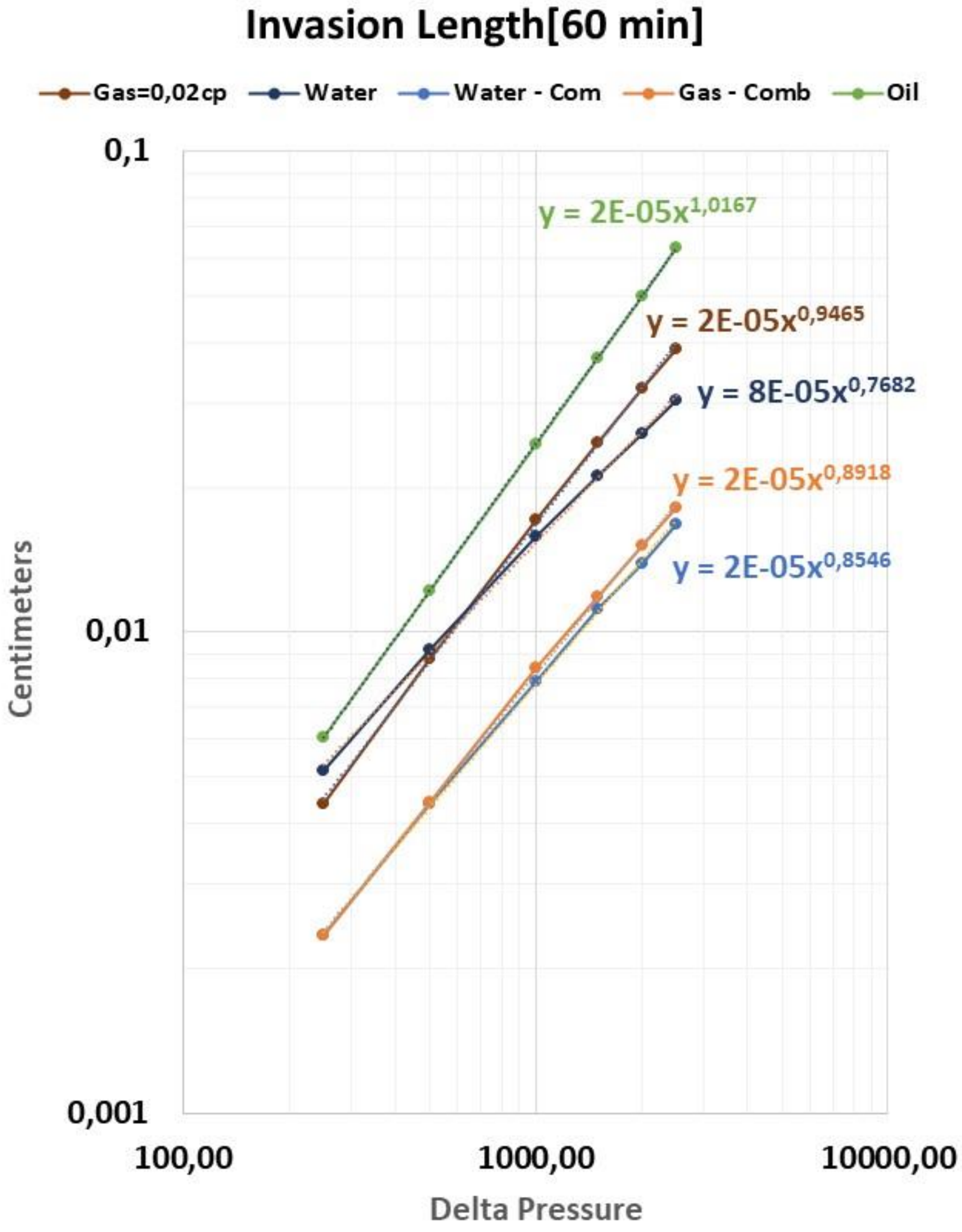

Figure 53: Invasion length versus delta pressure. Oil invasion, Single gas invasion, single water invasion, and simultaneous water and gas invasion were simulated in a semi-infinite 100nd core with 3,000 psi of initial pressure. The fluids were injected at constant delta pressure varying from 3,250 psi to 4,500 psi along the simulated invasion. The show values were pick at a simulated time of 60 minutes.

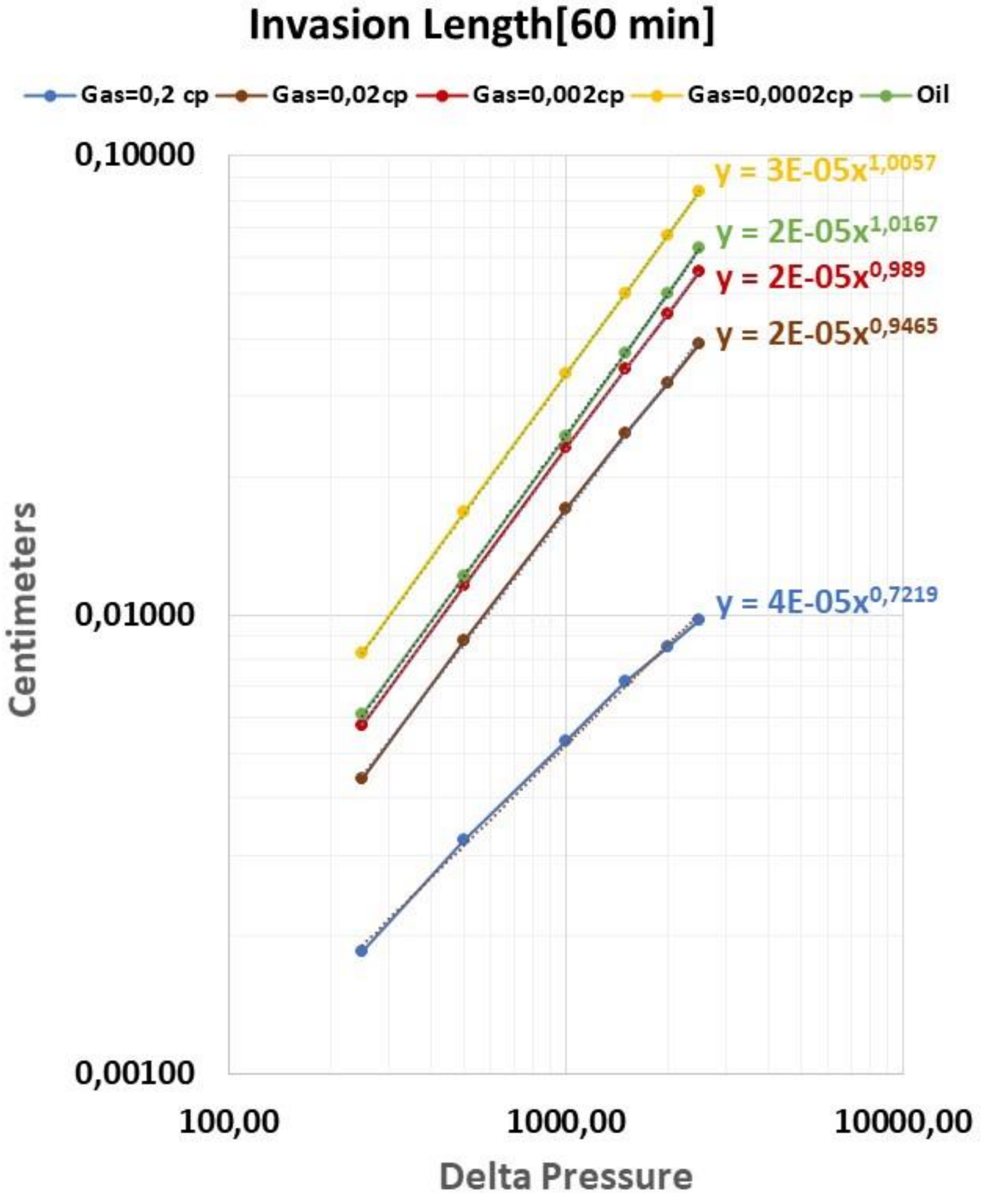

Figure 54: Invasion length versus pressure plot for gas viscosity sensitivity. Gas invasion was simulated in a semi-infinite 100nd core with 3,000 psi of initial pressure, varying gas viscosity form 0.0002 cp to 0.2 cp. The fluid was injected at constant pressure of 3250 psi to 4,500 psi along the simulated invasions. The show values were pick at a simulated time of 60 minutes.

The volume versus time results were plot in Figure 50, and them show a square root of time dependency on every invasion case.

The invasion length presented in the Figure 51 is reciprocals to Figure 40, where is possible to observe that the square root of time behavior also describes the length the fluids invaded into the reservoir, like it was previously seen in the permeability dependency sensitivities.

The invasion length versus square root of time plot confirms in Figure 52 the previous square root of time assumption. This was the starting point to generate an invasion length versus pressure sensitivity plot, like the one generated in previous section to determine the correct permeability dependency.

The invasion length versus pressure log-log plot shown in Figure 53 represent the dependencies for the three invasion cases: Single gas invasion, single water invasion, simultaneous water and gas injection (foam) run at pressure differences from 250 psi to 2500 psi. The invasion length volumes were found at 60 minutes in the simulated time for every case. Additionally to the previous invasion cases, an oil invasion case was run to validate the dependency over a miscible displacement. That case corresponds to the green line in the Figure 53 that shows a linear dependency supported in the close to one exponent. The other tendencies seen in the Figure 53 described a different behavior for every fluid invasion case. In the case of single gas invasion, the shown tendency corresponds to and pseudo-linear dependency due to the power regression exponent presenting a value of 0.94, differing from the expected square root of pressure difference dependency that will be represented by an exponent equal to 0.5 (Settari A. , 1985). On the other hand, in the water invasion scenario the pressure slope tends to be near 0.75 as can be seen in the darker blue line exponent. The most defying case occurred in the foam invasion (gas and water simultaneous injection) where both fluids differ from the previous determined dependencies. Even when the invasion length values are close, the calculated dependencies differed from both determined exponents (water=0.85, gas=0.89).

Contrary to the stated by the general leak-off model (Settari A. , 1985), the fluid type has a deep influence in the leak-off behavior at reservoir conditions like was shown in Figure 53. To obtain a clearer understanding over the fluid invasion process, in the Figure 54 the single gas invasion was analyzed with more detail to identify the gas viscosity effect over the leak-off pressure dependency phenomena. Four simulations were executed varying gas viscosity from 0.0002 cp to 0.2cp, and a final oil invasion simulation were present to contrast the results with a miscible displacement injection.

The results shown in Figure 54 highlighted that the linear tendency is tied to a viscosity reduction. When the fluid tends to be inviscid, it behaves linearly to pressure, like the oil invasion case, showing a pure compressibility pressure dependency supported by the drastic viscosity reduction. Otherwise, when viscosity is augmented to 0.2 cp (100 times the baseline of 0.02cp) the behavior tended to be like water invasion, that reflected a slope of 0.75 in the log-log plot at the same 60 minutes of simulated time.

6.2.1. Single Gas Invasion Viscosity Dependencies

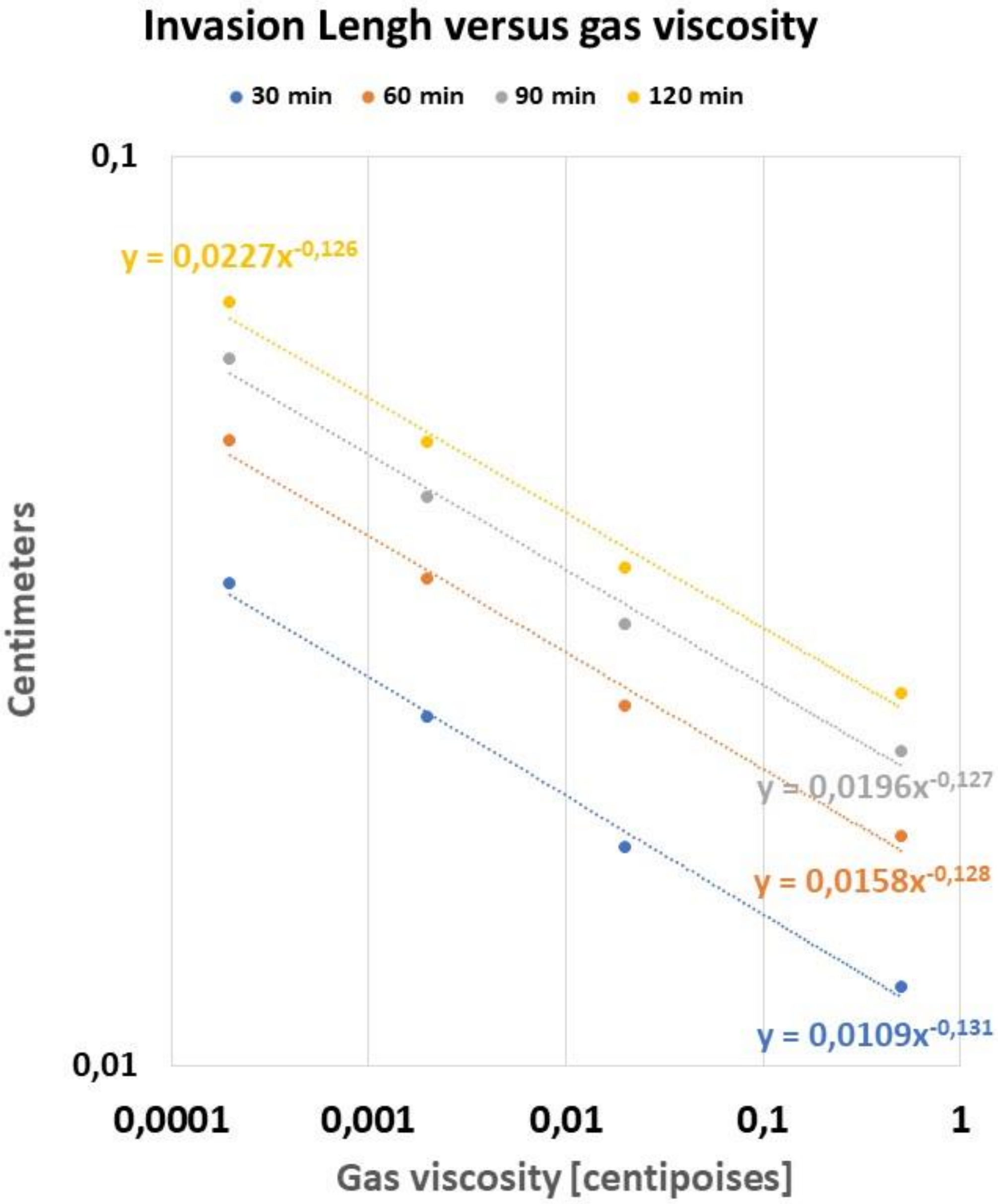

Figure 55: Invasion length versus gas viscosity plot. Gas invasion was simulated in a 100nd reservoir with 3,000 psi of initial pressure varying gas viscosity form 0.0002 cp to 0.5 cp. The fluid was injected at constant pressure of 4,500 psi along the simulated invasion. The shown values were pick at a simulated time of 30, 60, 90 and 120 minutes.

The effect of viscosity in the invasion length was studied specifically in this chapter with the previous simulated gas invasion data. The simulations were run over the 100 nanodarcy reservoir case, with a delta pressure of 1,500 psi (baseline simulation). Invasion length results were plotted at four different times varying the viscosity from 0.002 to 0.2 centipoises. The results shown all the cases follow an average slope of -0.13 in the log-log plot, contradicting the general leak-off model that stated a proportionality of $\mu_f^{-0.5}$.

Using this approach will be possible to simulate gas viscosity sensitivities using the determined power dependency. The using of this dependency will be tested in the section 6.3 with the other determined proportionalities summarizing the main research objective of this work.

6.2.2. Oil Compressibility Dependencies

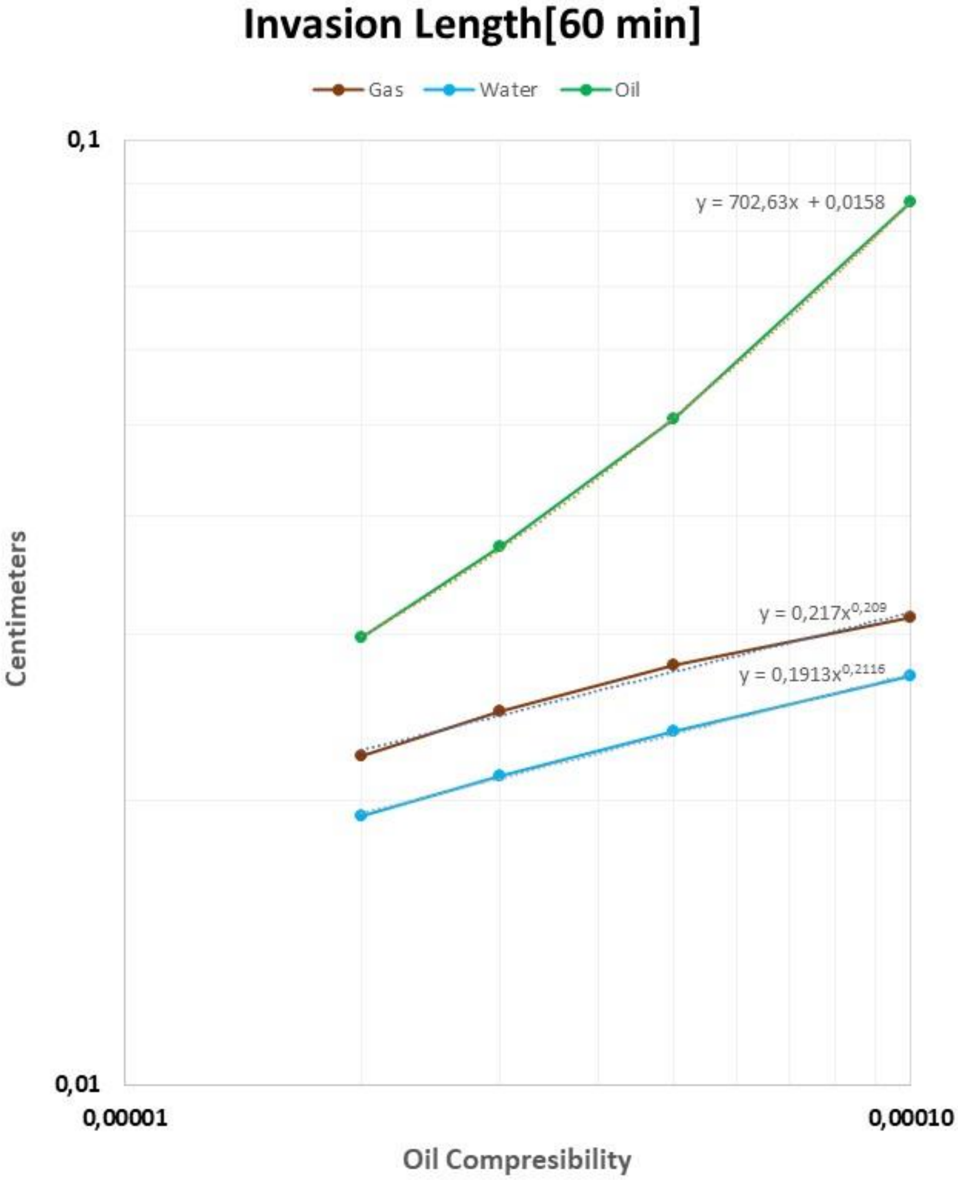

Figure 56: Invasion length versus Oil Compressibility plot. Oil invasion, Single gas invasion and water invasion were simulated in a semi-infinite 100nd core with 3,000 psi of initial pressure. The fluids were injected at constant pressure of 4,500 psi along the simulated invasion. The shown values were pick at a simulated time of 60 minutes.

Oil compressibility is a key factor to analyze the leak-off effect in the reservoir because in this specific case it dominates total compressibility considering established reservoir pressure, temperature condition, and initial 100% oil saturation. The 100 nD reservoir simulation was kept constant just changing the oil compressibility. Other parameters related to simulation remain steady like reservoir initial pressure (3,000 psi) and constant injection pressure (4,500 psi).

Oil compressibility directly affects the diffusivity constant; therefore, the variation range was chosen to keep the reservoir like behavior in the core length (20 centimeters). The selected compressibility values for the 100 nanodarcy reservoir ranged from 0.0002 to 0.001 1/psi because higher values will require longer lengths to fulfill the expected pressure wave propagation.

The plot in Figure 55 shows the dependencies for single gas, and single water leak-off with a comparative case for oil injection leak-off representing the miscible injection displacement. According to the simulation results, both gas and water injection show an average 0.2 slope in the log-log plot of invasion length versus oil compressibility. The previous data shows the compressibility divergence from the general leak-off model, that states invasion length can be scaled using the square root of the compressibility (Settari A. , 1985). An attempt to summarize the found dependencies will be described in the next section where a simplified leak-off dependencies model will be tested.

6.3. SUMMARIZED LEAK-OFF DEPENDENCIES

Ultimately, Table 5 summaries the explored simulated dependencies for semi-infinite core replicating the reservoir conditions. Considering the results, the simulated data shows a differing tendency for pressure, viscosity, and oil compressibility. Using the developed tendencies table will be possible to determine invasion lengths or invaded volumes starting from a single simulated profile varying: time, permeability, pressure, viscosity (single gas case), or oil compressibility (oil, gas, and water singles invasion). The use of this developed dependencies model will reduce simulation time to optimize the simulation process. Finally, the use of the general leak-off must be consider under more specific conditions where the boundaries grant the stated dependencies. To develop a more realistic model, general leak-off should be changed to replicate real reservoir behavior according to the Table 5.

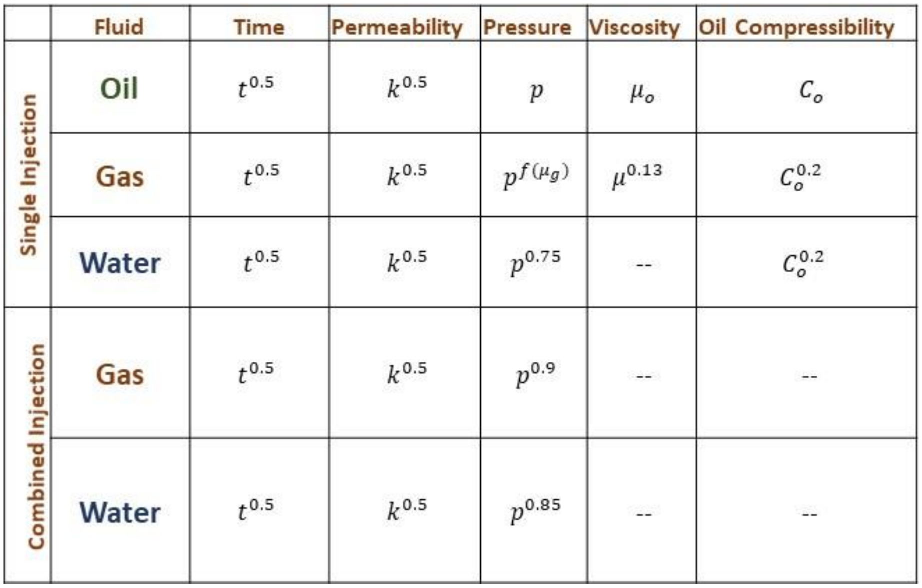

	Fluid	Time	Permeability	Pressure	Viscosity	Oil Compressibility
Single Injection	Oil	$t^{0.5}$	$k^{0.5}$	p	μ_o	C_o
	Gas	$t^{0.5}$	$k^{0.5}$	$p^{f(\mu_g)}$	$\mu^{0.13}$	$C_o^{0.2}$
	Water	$t^{0.5}$	$k^{0.5}$	$p^{0.75}$	--	$C_o^{0.2}$
Combined Injection	Gas	$t^{0.5}$	$k^{0.5}$	$p^{0.9}$	--	--
	Water	$t^{0.5}$	$k^{0.5}$	$p^{0.85}$	--	--

Table 5: Leak-off dependencies for combined (water and gas simultaneously) and single-phase invasion. For every injection case the following dependencies were determined: time, permeability, pressure, gas viscosity and oil compressibility. dependencies.

6.3.1. Single water Dependencies

The previous determined dependencies for single water invasion will be presented in three subsections: permeability, Delta Pressure, and gas viscosity, comparing the calculated value with the proportionality, and the simulated data for every listed case.

6.3.1.1. Permeability

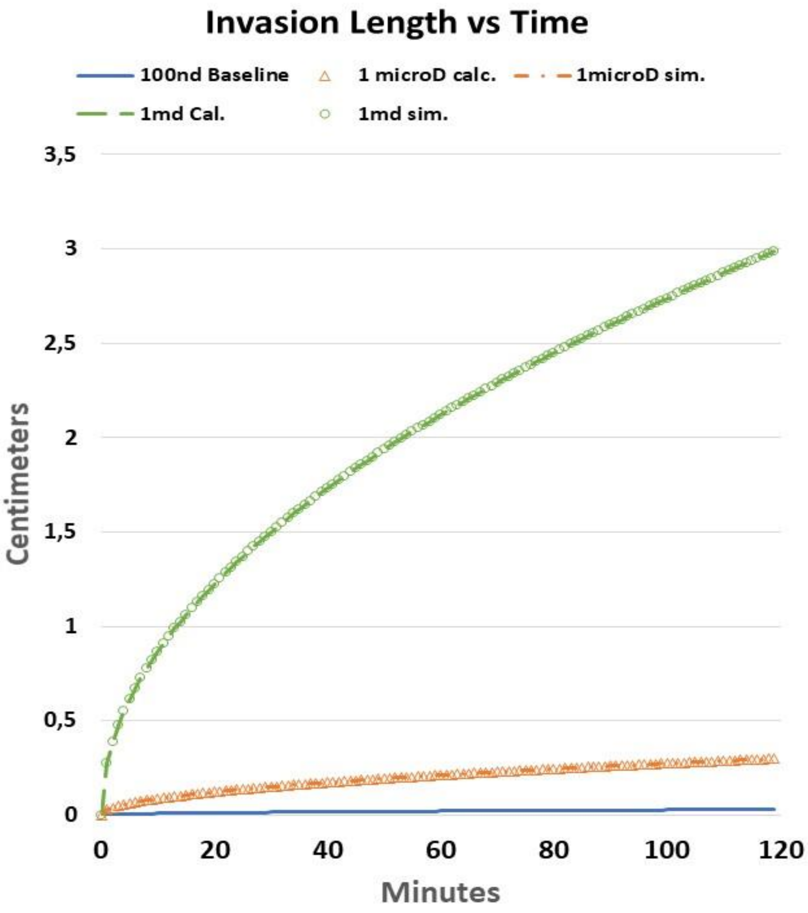

Figure 57: Invasion length versus time plot. Single simulated and calculated (using $k^{0.5}$ dependency) water invasion profiles for 1md, 10µd, and 100nd (baseline case) cores with 3,000 psi of initial pressure. The fluids were injected at constant pressure of 4,500 psi along the simulated invasion. The total simulated versus calculated time was 120 minutes.

6.3.1.2. Pressure

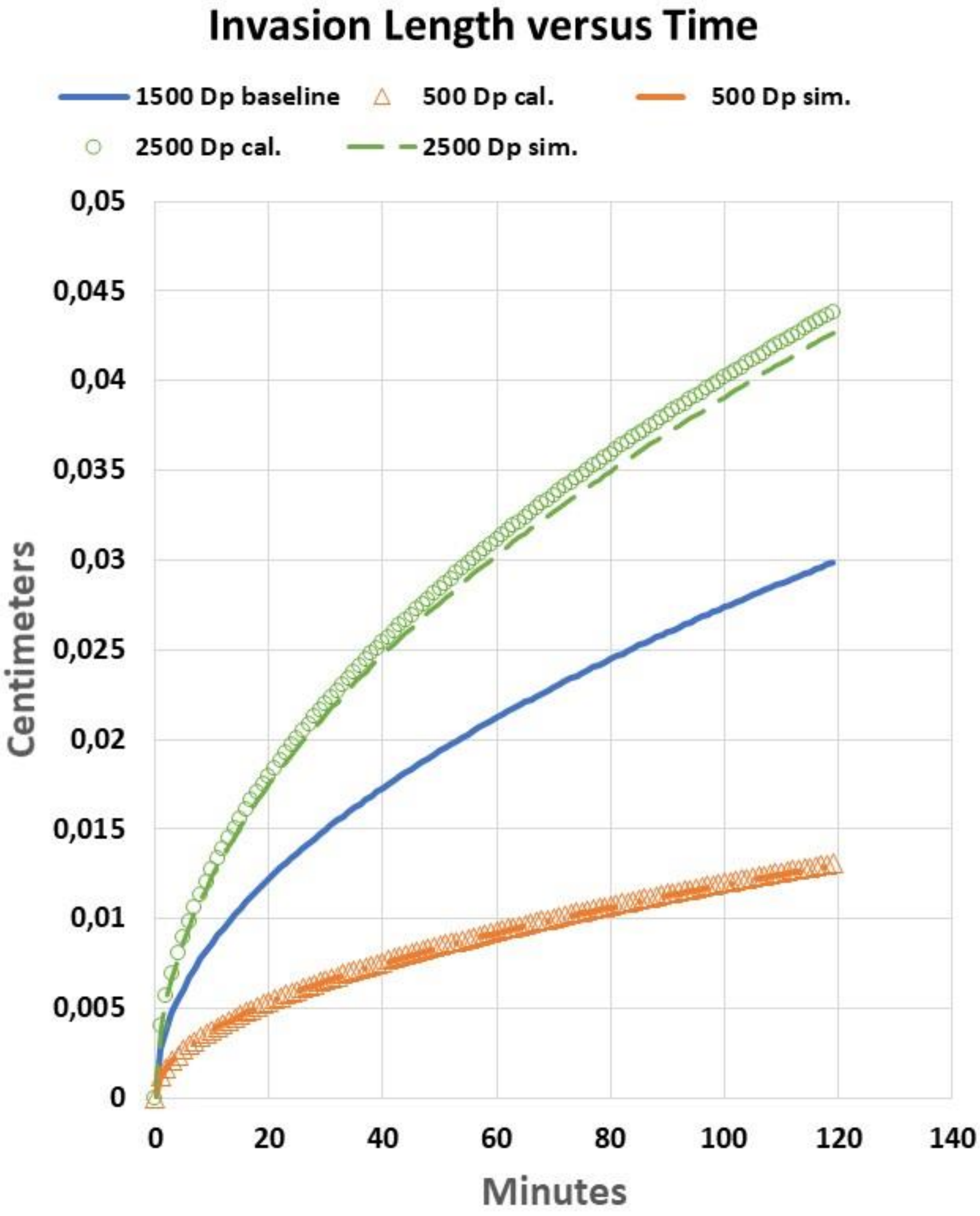

Figure 58: Invasion length versus time plot. Single simulated and calculated (using $p^{0.75}$ dependency) water invasion profiles for 100nd cores with 3,000 psi of initial pressure. The fluids were injected at constant pressures of 3500 psi, 4,500 psi (baseline case), and 5500 psi, along the simulated invasion. The total simulated versus calculated time was 120 minutes.

6.3.1.3. Oil compressibility

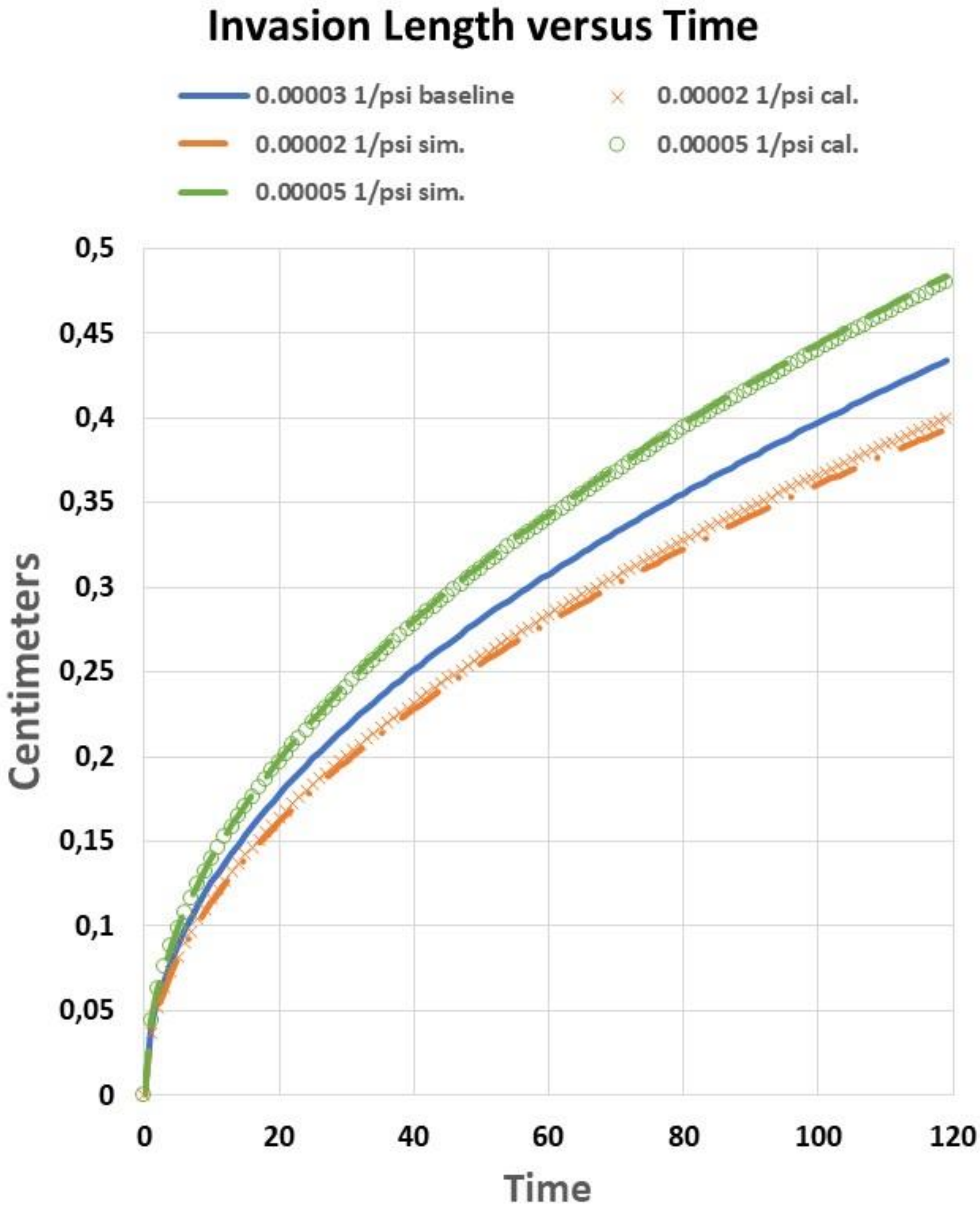

Figure 59: Invasion length versus time plot. Single simulated and calculated (using $C_o^{0.2}$ dependency) water invasion profiles for 100nd cores with 3,000 psi of initial pressure. The fluids were injected at a constant pressures 4,500 psi, for 0.00002, 0.00003 (baseline), and 0.00005 psi^{-1} along the simulated invasion. The total simulated versus calculated time was 120 minutes.

6.3.2. Single Gas Dependencies

The previous determined dependencies for single water invasion will be presented I three subsections: permeability, Delta Pressure, and gas viscosity as follows, comparing the calculated value with the proportionality, and the simulated data for every listed case.

6.3.2.1. Permeability

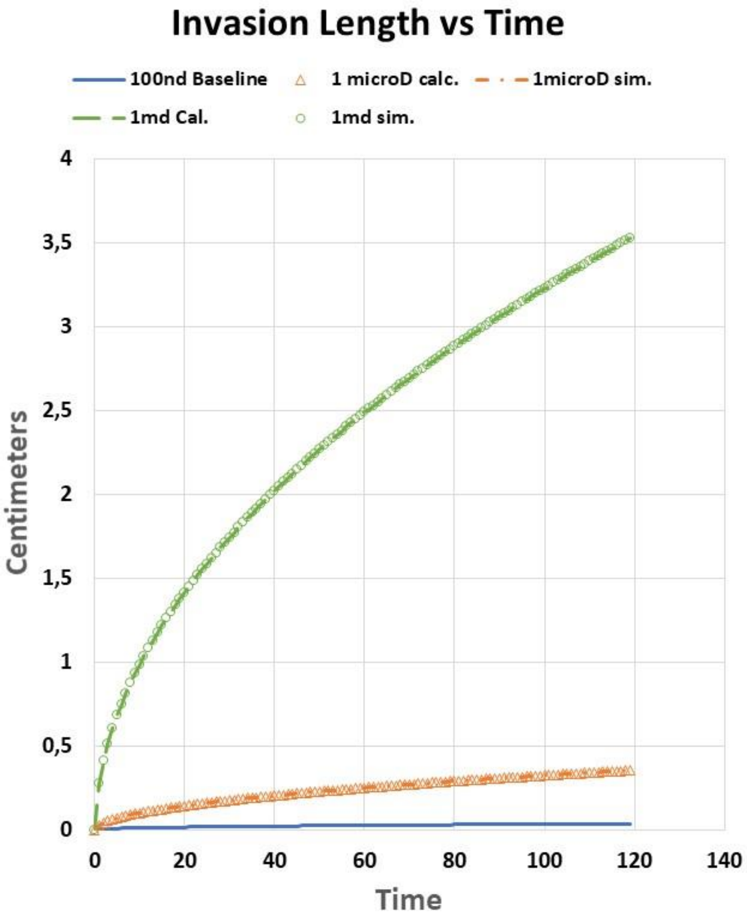

Figure 60: Invasion length versus time plot. Single simulated and calculated (using $k^{0.5}$ dependency) gas invasion profiles for 1md, 10µd, and 100nd (baseline case) cores with 3,000 psi of initial pressure. The fluids were injected at constant pressure of 4,500 psi along the simulated invasion. The total simulated versus calculated time was 120 minutes.

6.3.2.2. Pressure

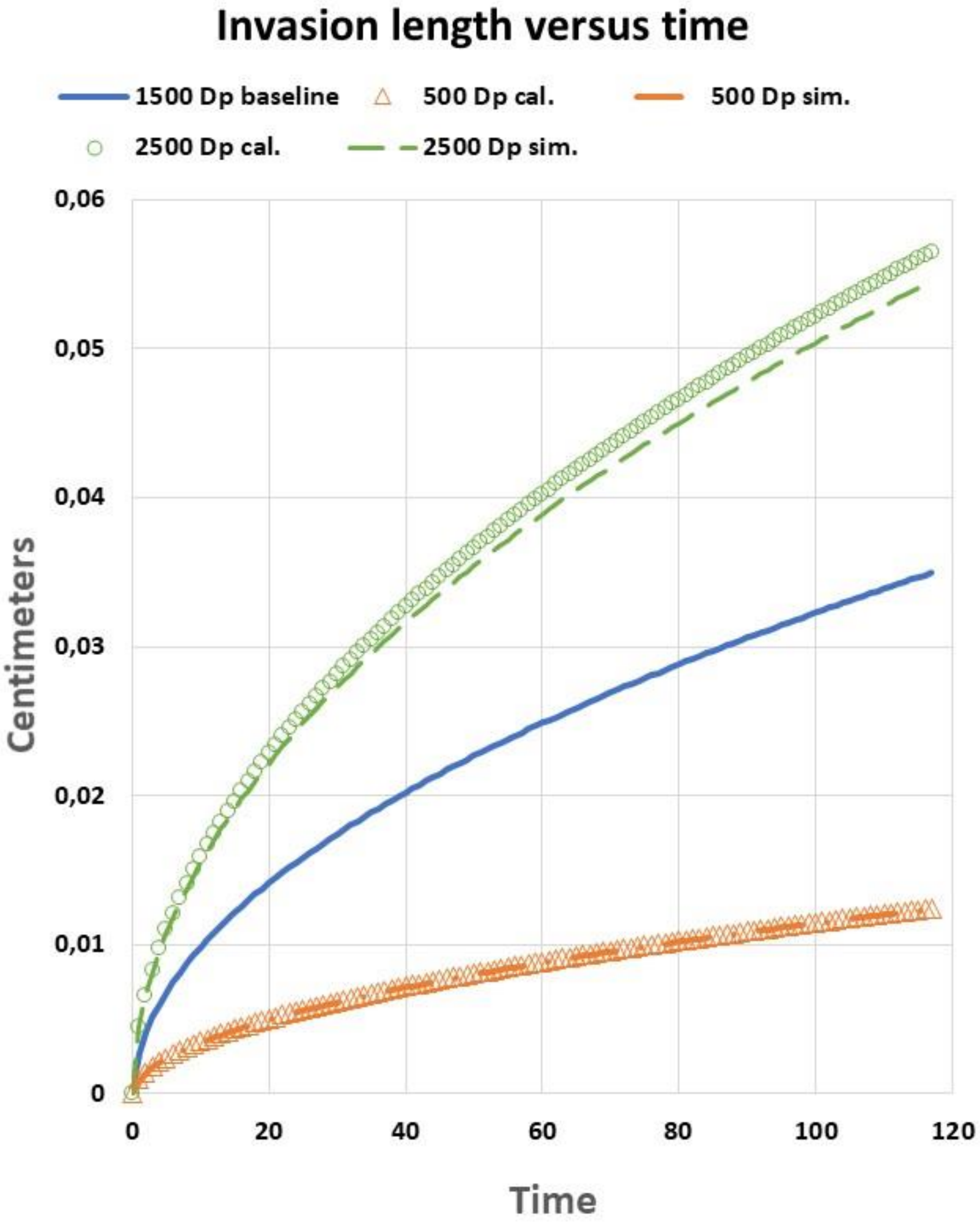

Figure 61: Invasion length versus time plot. Single simulated and calculated (using $p^{0.94}$ dependency) gas invasion profiles for 100nd cores with 3,000 psi of initial pressure. The fluids were injected at constant pressures of 3500 psi, 4,500 psi (baseline case), and 5500 psi, along the simulated invasion. The total simulated versus calculated time was 120 minutes.

6.3.2.3. Viscosity

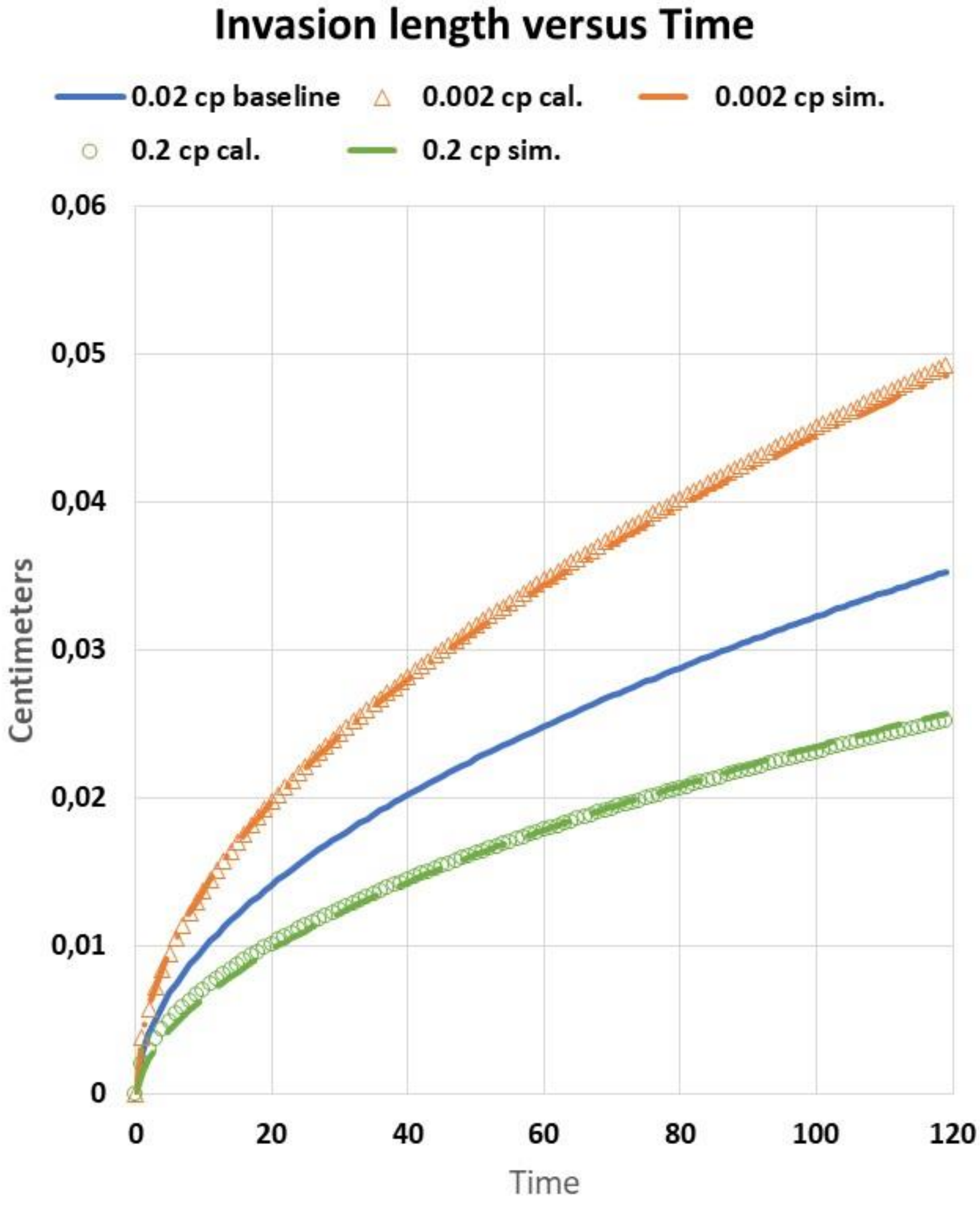

Figure 62: Invasion length versus time plot. Single simulated and calculated (using $\mu_g^{0.13}$ dependency) gas invasion profiles for 100nd cores with 3,000 psi of initial pressure. The fluids were injected at a constant pressures 4,500 psi, for 0.002, 0.02 (baseline), and 0.2 centipoises along the simulated invasion. The total simulated versus calculated time was 120 minutes.

6.3.2.4. Oil compressibility

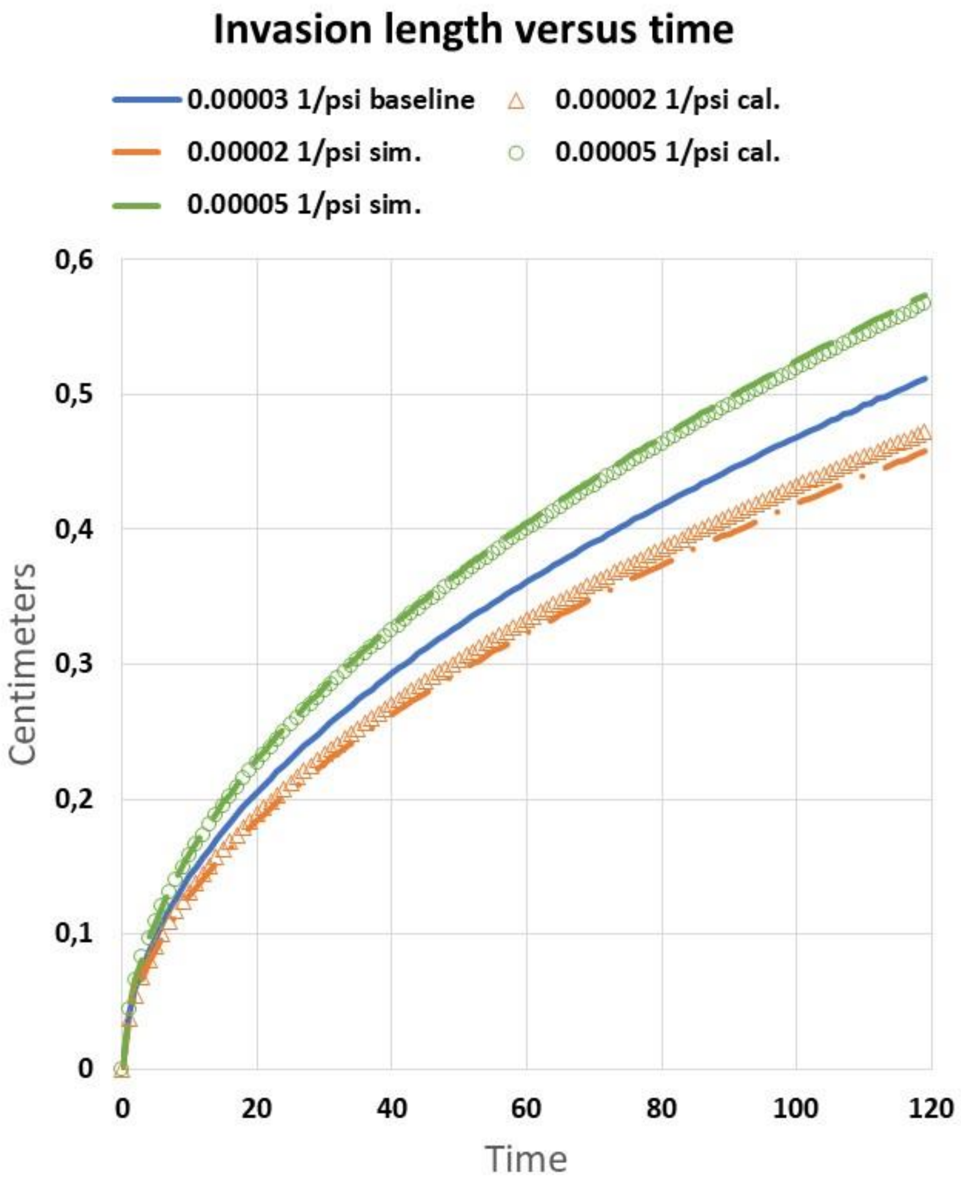

Figure 63: Invasion length versus time plot. Single simulated and calculated (using $C_o^{0.2}$ dependency) gas invasion profiles for 100nd cores with 3,000 psi of initial pressure. The fluids were injected at a constant pressures 4,500 psi, for 0.00002, 0.00003 (baseline), and 0.00005 psi^{-1} along the simulated invasion. The total simulated versus calculated time was 120 minutes.

6.4. SUMMARY

In this chapter, I use the numerical simulation over the three stated invasion cases: water invasion, gas invasion, and foam invasion, to determine leak-off dependencies, and validate general leak-off model applications at reservoir conditions. The dependencies were divided in five groups including: time, permeability, delta pressure, gas viscosity, and oil compressibility. Moreover, the baseline scenarios were used to validate the previous determined dependencies with simulated invasion cases. Finally, the obtained data conclude the general leak-off model differed under some of the established reservoir conditions and is valid only for the square root of time dependency and the square root of permeability.

Chapter 7: Summary, Conclusions and Future Work

7.1. SUMMARY

In this research I study the fluid invasion phenomena in porous media addressing two different scopes. The first section from Chapters 3 and 4 is related to the laboratory test leak-off behavior and the phenomena occurring at laboratory conditions. The second section from Chapters 5 and 6 has a broader approach on reservoir fluid invasion phenomena, and the validation of the previously proposed general leak-off model (Settari A. , 1985).

The laboratory approach started with the key rock-fluid parameters determination. Those parameters included fundamental properties like porosity, permeability, boundary conditions, fluid properties and flow models that suited this porous media problem. The focus of simulation in chapter two was to mimic the experiment of Luo (2020) verifying the matching between simulated data and laboratory results over three different invasion cases: water invasion, gas invasion, and foam invasion. In chapter three I perform permeability sensitivities over the baseline simulated test, trying to understand the effect of permeability reduction from 10 millidarcy in the laboratory core to 100 nanodarcy rock expected in an ultra-low permeability reservoir. The obtained results showed a divergent behavior that differs from the expected square root of permeability, stated in the general leak-off model. Those simulations were performed over the three different invasion cases: water invasion, gas invasion, and foam invasion, varying permeability from 10md to 100nd. The simulations proven the square root of permeability dependency was not achieved at any of the cases over the established boundary conditions.

Finally, in the reservoir simulation approach, the rock and fluid parameters were configurated to simulate fluid leak-off effect at reservoir conditions. In chapter five three different invasion process were performed in a 100 nanodarcy core: gas invasion, single water invasion, and foam invasion (simultaneous gas and water invasion). The obtained results matched the expected square root of time behavior for all fluids, differing form the previous linear behavior seen in the gas invasion case in Chapters 3 and 4. Starting from the baseline scenarios simulated in Chapter 5 and Chapter 6 where I performed some sensitivities to understand the dependencies related to permeability, delta pressure, gas viscosity and oil compressibility, to validate the expected reservoir behavior explored in the general leak-off model. Finally, the sensitivities allow the determination of new corroborated proportionalities and a suggested approach on a more accurate leak-off model over the reservoir conditions.

7.2. CONCLUSIONS

Simulation is a useful tool to mimic laboratory experiments and reproduce fluid behavior in porous media to expand the research over current lab limitations. Once the simulation is matched with real experimental data, new predictions and forecasts can be done with consistency and certainty. The key factor to expand baseline simulation is based on the definition of the experimental parameters that affect the replicated behavior, and the use of corroborated models to obtain the numerical results. In this research was possible to mimic the laboratory test performed by Luo (2020) using a commercial numerical simulator choosing the correct input parameters, and correlation models that support the observed phenomena. Furthermore, the correspondent numerical results were expanded to understand fluid interactions over complex parameters like ultra-low permeabilities, that would take big amount of time to process in a usual fluid displacement laboratory test. The permeability sensitivities simulations show the water invasion can be scaled using $k^{0.75}$, and gas using $k^{1.25}$.

In addition to the laboratory match, I also focus my effort on the understanding of fluid invasion phenomena at reservoir conditions. The reservoir behavior was modelled for three different invasion phenomena: Single gas invasion, single water invasion, and foam invasion (simultaneous gas and water invasion), simulating sensitivities over permeability from low to ultra-low values, delta pressure, gas viscosity, and oil compressibility. The simulated data show: time and permeability dependencies agree with the general leak-off model square root behavior, but differs for delta pressure, gas viscosity, and oil compressibility, all these dependencies are summarized in Table 5.

Ultimately, this research bound a new approach validating proper leak-off dependencies over the established reservoir conditions and the simulation model suggesting key modifications on the general leak-off model interpretation to grant more accurate results, that would optimize fracturing fluid performance.

7.3. FUTURE WORK

- Further understanding of three-dimensional problem that would include new variables affecting the leak-off considering gravity, heterogenous permeability, pore size distribution, and capillary pressure effect.
- Broader approach over pressure propagation along the generated fracture that allows the understanding of injection pressure behavior along the fracture and its impact in leak-off phenomena.
- Simulation of gel like fluids used commonly in hydraulic fracturing operations, involving complex leak-off combined mechanisms, reactions, and new interactions with the reservoir fluids.

References

Baker, L. E. (1988, January 1). Three-Phase Relative Permeability Correlations. *Society of Petroleum Engineers*. doi:10.2118/17369-MS

Barree, R. D., & Mukherjee, H. (1996, January 1). Determination of Pressure Dependent Leakoff and Its Effect on Fracture Geometry. *Society of Petroleum Engineers*. doi:10.2118/36424-MS

Bird, R. (1961). *Transport phenomena [by] R. Byron Bird, Warren E. Stewart [and] Edwin N. Lightfoot.* Wiley.

Calhoun, J. C., & Yuster, S. T. (1946, January 1). A Study of the Flow of Homogeneous Fluids Through Ideal Porous Media. *American Petroleum Institute*, 335-355.

Carslaw, H., & Jaeger, J. (1959). *Conduction of heat in solids, by H. S. Carslaw and J. C. Jaeger* (2d ed.). Clarendon Press.

Christianovich, S. A., Zheltov, Y. P., Barenblatt, G. I., & Maximovich, G. K. (1959, January 1). Theoretical Principles of Hydraulic Fracturing of Oil Strata. *World Petroleum Congress*, 289-296.

Collins, R. E. (1961). Simultaneous Flow of Immiscible Fluids. In R. E. Collins, *Flow of Fluids Through Porous Media* (pp. 108-138). Houston: Reinhold Pub. Corp.

Computer Modeling Group Limited. (2017). *CMG IMEX (Version 2017.10.6504.34460).* Austin, Texas: Center for Petroleum and Geosystems Engineering, University of Texas at Austin.

Corey, A. T. (1956, November 1). Three-Phase Relative Permeability. *Society of Petroleum Engineers*. doi:10.2118/737-G

Crawford, P. B., & Collins, R. E. (1954, August 1). Estimated Effect of Vertical Fractures on Secondary Recovery. *Journal of Petroleum Technology*, 41-45. doi:10.2118/325-G

Crawford, P. B., & Landrum, B. L. (1954, January 1). Estimated Effect of Horizontal Fractures on Production Capacity. *Journal of Petroleum Technology*. doi:10.2118/414-G

Crawford, P. B., & Landrum, B. L. (1955, December 1). Effect of Unsymmetrical Vertical Fractures on Production Capacity. *Petroleum Transactions, 204*, 251-254. doi:10.2118/433-G

Daneshy, A. A., Williams, J. R., & Tinsley, J. M. (1971, January 1). Effect of Treatment Parameters on Geometry of a Hydraulic Fracture. *Society of Petroleum Engineers*. doi:10.2118/3507-MS

Deen, W. (1998). *Analysis of Transport Phenomena.* New York: John Wiley & Sons.

Economides, M., & Nolte, K. (2000). *Reservoir stimulation / editors, Michael J. Economides, Kenneth G. Nolte* (3rd ed.). Sugar Land: J. Wiley.

Gulbis, J. (1984, January 1). Dynamic Fluid-loss Study of Fracturing Fluids. *Petroleum Society of Canada*. doi:10.2118/84-01-02

Guo, B., & Ghalambor, A. (2004). Pressure Stability Analysis for Aerated Mud Drilling Using an Analytical Hydraulics Model. *Society of Petroleum Engineers*.

Guo, B., & Ghalambor, A. (2004, January 1). Pressure Stability Analysis for Aerated Mud Drilling Using an Analytical Hydraulics Model. *Society of Petroleum Engineers*. doi:10.2118/91356-MS

Hall, C. D., & Dollahide, F. E. (1964, May 1). Effects of Fracturing Fluid Velocity on Fluid-Loss Agent Performance. *Journal of Petroleum Technology*, 555-560. doi:10.2118/736-PA

Hall, C. D., & Dollarhide, F. E. (1968, July 1). Performance of Fracturing Fluid Loss Agents Under Dynamic Conditions. *Journal of Petroleum Technology*, 763-769. doi:10.2118/1904-PA

Harrison, E., Kieschnick, W. F., & McGuire, W. J. (1958, July 31). The Mechanics of Fracture Induction and Extension. *Petroleum Transactions, 201*, 252-321. doi:10.2118/318-G

Howard, G. C., & Fast, C. R. (1957, January 1). Optimum Fluid Characteristics for Fracture Extension. *American Petroleum Institute*.

IEA. (2020, March). *Oil 2020.* Retrieved from International Energy Agency: https://www.iea.org/reports/oil-2020

Ilk, D. J. (2011, January 1). Production Analysis in Unconventional Reservoirs - Diagnostics, Challenges, and Methodologies. *Society of Petroleum Engineers*. doi:10.2118/144376-MS

Lake, L. W., Johns, R. T., Rossen, W. R., & Pope, G. A. (2014). *Fundamentals of Enhanced Oil Recovery* (Second ed.). Richardson, Texas: SPE.

Landrum, B. L., & Crawford, P. B. (1957, October 1). Estimated Effect of Horizontal Fractures in Thick Reservoirs on Pattern Conductivity. *Journal of Petroleum Technology*, 50-52. doi:10.2118/601-G

Leverett, M. C. (1941, December 1). Capillary Behavior in Porous Solids. *Society of Petroleum Engineers*. doi:10.2118/941152-G

Luo, X. (2020). *Oil Relative Permeability Reduction from Fracturing Fluid Invasion in Low-permeability Rocks. PhD Dissertation, The University of Texas at Austin.* Austin, Texas.

Mayerhofer, M. J. (1991, January 1). An Experimental and Fundamental Interpretation of Fracturing Filter-Cake Fluid Loss. *Society of Petroleum Engineers*. doi:10.2118/22873-MS

Meng, H. Z., & Brown, K. E. (1987, January 1). Coupling of Production Forecasting, Fracture Geometry Requirements and Treatment Scheduling in the Optimum Hydraulic Fracture Design. *Society of Petroleum Engineers*. doi:10.2118/16435-MS

Muskat, M. (1983). *The flow of homogeneous fluids through porous media / by M. Muskat* (Repr. of 1st ed.). International Human Resources Development Corporation.

Nolte, K. G. (1986, December 1). A General Analysis of Fracturing Pressure Decline with Application to Three Models. *Society of Petroleum Engineers*. doi:10.2118/12941-PA

Settari, A. (1985, August 1). A New General Model of Fluid Loss in Hydraulic Fracturing. *Society of Petroleum Engineers*. doi:10.2118/11625-PA

Settari, A. (1988, January 1). General Model of Fluid Flow (Leakoff) From Fractures Induced in Injection Operations. *Society of Petroleum Engineers*. doi:10.2118/18197-MS

Settari, A., & Cleary, M. P. (1984, July 1). Three-Dimensional Simulation of Hydraulic Fracturing. *Journal of Petroleum Technology*. doi:10.2118/10504-PA

Stone, H. L. (1970, February 1). Probability Model for Estimating Three-Phase Relative Permeability. *Society of Petroleum Engineers*. doi:10.2118/2116-PA

Stone, H. L. (1973, October 1). Estimation of Three-Phase Relative Permeability and Residual Oil Data. *Petroleum Society of Canada*. doi:10.2118/73-04-06

Suo, Y., Rahman, S., & Xu, W. (2018, November 12). Effects of Formation Properties and Treatment Parameters on Hydraulic Fracture Geometry in Poro-Viscoelasticity Shale Gas Reservoirs Using Cohesive Zone Method in a 3D Model. *Society of Petroleum Engineers*. doi:10.2118/192713-MS

Thomas, L. K. (1968, June 1). Threshold Pressure Phenomena in Porous Media. *Society of Petroleum Engineers*. doi:10.2118/1816-PA

Wang, J., & Rahman, S. S. (2016, July 1). Investigation of Water Leakoff Considering the Component Variation and Gas Entrapment in Shale During Hydraulic-Fracturing Stimulation. *Society of Petroleum Engineers*. doi:10.2118/174392-PA

Washburn, E. W. (1921, March). The Dynamics of Capillary Flow. *The Physical Review, XVII* (3), 273-283. doi:10.1103/PhysRev.17.273

Williams, B. B. (1970, January 1). Fluid Loss from Hydraulically Induced Fractures. *Society of Petroleum Engineers*. doi:10.2118/2769-PA

Williams, B., Gidley, J., & Schechter, R. (1979). *Acidizing fundamentals / Bert B. Williams, John L. Gidley, Robert S. Schechter. Henry L. Doherty Memorial Fund of AIME.* New York: Society of Petroleum Engineers of AIME.

Wilsey, L. E., & Bearden, W. G. (1953, August 1). Reservoir Fracturing - A Method of Oil Recovery from Extremely Low Permeability Formations. *Journal of Petroleum Technology*, 21-27. doi:10.2118/317-G

Zeng, F., & Zhao, G. (2008, January 1). The Optimal Hydraulic Fracture Geometry Under Non-Darcy Flow Effects. *Society of Petroleum Engineers*. doi:10.2118/114285-MS